The Design and Prototyping of a Low-Cost & Efficient Ocean Cleanup Robot

Major Qualifying Project

A Major Qualifying Project submitted to the Faculty of WORCESTER POLYTECHNIC INSTITUTE in partial fulfillment of the requirements for the Bachelor of Science.

Authors:
Gabriel Espinosa[1], Danny Ngo[1,2], Sebastian Valle[2], Alexander Wadsworth[1]

Advisors:
Selcuk Guceri[1] & Vincent Aloi[2]

Submitted:
April 25th, 2024

[1] WPI Department of Mechanical and Materials Engineering (MME)

[2] WPI Department of Robotics Engineering (RBE)

Abstract

11 million metric tons of trash enter Earth's oceans each year, contributing to ecosystem loss, wildlife endangerment, and microplastic infiltration within the food supply. Over the past 2 decades, public awareness of the growing threat has increased, resulting in numerous organizations, like The Ocean Cleanup (TOC), seeking to curb the problem with their large-scale sweeping tugboats. However, all current efforts are costly, require large crews, and rely on diesel-powered vessels for collection and transport. The team sought to decarbonize and automate cleanup by developing an efficient robotic platform for open ocean surface trawling. Prototypes of 2 seaworthy, inexpensive, and autonomous-capable robots were developed to tow nets for cleanup in the turbulent open ocean. These robots were designed to operate without human crews and rely on minimal energy and operational costs when compared to existing systems. Future efforts may focus on commercializing the platform by selling oceanic data collected by onboard sensors.

Acknowledgements

The completion of this Major Qualifying Project would not have been possible without the guidance and support of our advisors, Professors Vincent Aloi and Selcuk Guceri. The team would also like to thank Professor Reza Ebadi for his assistance in drag force analysis, and MME department Lab Manager Peter Hefti for his support with equipment and tool usage.

The team would also like to extend our gratitude to Tim Perry of Clear Blue Sea, David Pearson of GreenSea-IQ, and Caitlin Townsend of Net Your Problem for their industry insights during the research phase of this project.

Table of Contents

List of Tables and Figures

Table of Authorship

Section	Authors	Editors
1.1 The Problem	Espinosa	All
1.2 Existing Solutions	Wadsworth	All
1.3 Proposed Solution	Espinosa	All
1.4 Mission Statement & Objectives	Espinosa	All
2.1 The Reality of Ocean Pollution	Espinosa	All
2.2 Types of Ocean Pollution & Affects	Ngo	All
2.3 Addressing the Problem	Valle	All
2.4 Existing Robotic Solutions	Wadsworth	All
3.1 Design Specifications	Espinosa	All
3.2 Thrust Requirements & Drag	Espinosa	All
3.3 Buoyancy, Floatation, & Stability	Espinosa	All
3.4 Structures, Waterproofing & Corrosion Protection	Espinosa	All
3.5 Net Release Mechanism	Wadsworth, Ngo	All
3.6 Net Shape & Optimization	Espinosa	All
3.7 Theoretical System Efficiency	Espinosa	All
3.8 Electronics & Sensors	Wadsworth	All
3.9 Software Design & Communication	Valle	All
4.1 Manufacturing	Wadsworth	All
4.2 Assembly	Espinosa	All
4.3 Troubleshooting	Espinosa, Valle	All
4.4 Validation Experiments & Methodology	Espinosa	All
5.1 Latch Mechanism Force to Fracture	Espinosa	All
5.2 True Buoyancy and Pitch Angle	Espinosa	All
5.3 True Drag Force and Drag Coefficient	Espinosa	All
5.4 Experimental System Efficiency	Espinosa	All
5.5 Discussion of Results	Espinosa	All
6.0 Conclusions	Espinosa	All
7.0 Future Work	Espinosa	All
Appendix A: Net Optimization Code	Wadsworth	All
Appendix B: Robot Operational Code	Valle	All
Appendix C: Interview Notes	Ngo	All
Appendix D: Bill of Materials	Espinosa	All
Appendix E: CAD Part Drawings	Espinosa	All

1.0 Introduction

1.1 The Problem

Ocean plastic pollution is a significant and pressing environmental issue. Vast quantities of plastic waste have accumulated in the world's oceans, with estimates suggesting that there are over 150 million metric tons of plastic currently present [42]. This plastic pollution originates from various sources, including land-based runoff, inadequate landfill management, and maritime activities [28]. The composition of ocean pollution consists of various types of plastics, including bottles, bags, packaging materials, and fishing gear, some of which can be seen in Figure 1.

Figure 1: Plastic pollution in the Pacific Ocean [25].

Ocean plastic pollution has detrimental effects on marine wildlife and ecosystems. Marine animals can ingest or become entangled in plastic debris, leading to injury or death [51]. Plastics can also break down into smaller particles, affecting filter-feeding organisms and potentially entering the human food chain through seafood consumption. The long-term consequences of this pollution include disruption of marine ecosystems, biodiversity loss, and harm to human health through the ingestion of micro-plastics and the toxins they can carry [38].

Numerous initiatives are underway to combat ocean plastic pollution at its source. These include regulations and policies to reduce single-use plastics, promote recycling, and improve waste management on land [50]. Public awareness campaigns, ocean cleanups, and beach cleanups are also common strategies. Innovations in materials, such as biodegradable plastics, aim to reduce plastic's persistence in the environment. Furthermore, the circular economy approach seeks to minimize plastic waste by promoting recycling and reuse.

While fishing nets are a form of plastic waste that enters the oceans, the primary focus of this discussion lies in the broader context of ocean plastic pollution. The choice to emphasize plastics over fishing nets stemmed from an interview with Net Your Problem, a company specializing in fishing net recycling. Fishing nets, though a notable component of marine debris, present a unique set of challenges that distinguishes them from other forms of plastic pollution. These nets are often retrieved from the ocean, either self-reported by fishermen or located through initiatives such as the Ghost Gear Project. However, their condition upon retrieval can vary significantly, with damaged or undesirable nets often precluding recycling [17]. The contamination of nets with marine fouling renders them a challenging material to recycle effectively. Moreover, fishing nets are heavy and are often found entangled on the ocean floor, making automated retrieval technically challenging. The interview underscored the need for heavy machinery, such as excavators, to manage the retrieval, manipulation, and untangling process for nets still equipped with chains and buoys. Full automation, without human intervention, was regarded as infeasible with current technologies. Further details of the interview are detailed in Appendix C-3.

1.2 Existing Solutions

Considering the last decade, robotics has taken an ever more present place in human life, taking specialized forms to solve problems never thought possible. So, as plastic builds up in rivers and oceans, where are the robots to help clean it up? Recently, ocean cleanup robots have been at the forefront of academic research, only significantly entering the commercial sphere in the last 5 years. Successful companies such as Ranmarine Technology and iADYS have taken on the market with their small-scale autonomous robots. These vessels use GPS and machine vision to clean up smaller bodies of water [52][31], primarily collecting macro (>20mm) plastics on the surface. However, some companies have also branched out to clean up micro plastics (<5mm) and oil spills across waterways [36].

While these technologies present a promising next step to cleaning marine plastic, most only operate in marinas, bays, or near industrial sites. These solutions still fail to remove the bulk of waste that has accumulated within open ocean gyres over decades of pollution. As of now, the most effective solution is designed and managed by The Ocean Cleanup (TOC) which has removed over 10 million kilograms of plastic from the Pacific Ocean to date [15]. They utilize a surface trawling, or buoy assisted net sweeping, system suspended between two tugboats to collect floating waste. The suspended net is over 2km long and acts as an artificial coastline for plastic to accumulate while the boats maintain a slow forward speed, seen in Figure 2 below [34].

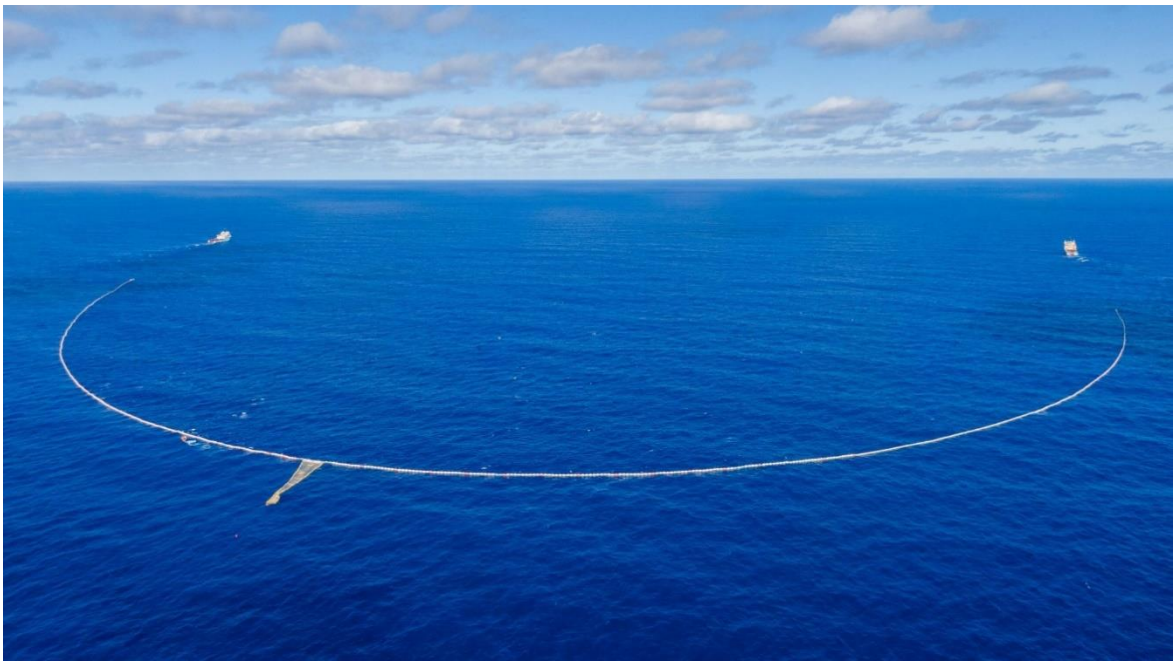

Figure 2: An arial shot of The Ocean Cleanup's System 03 collecting waste in the Great Pacific Garbage Patch halfway between Hawaii and California [35].

1.3 Proposed Solution

There is a distinct difference in the methodology of robotic and human operated ocean cleanup efforts. Robotic surface cleaners often look like a catamaran, where the hollow center is replaced by a conveyor belt or container for skimming trash from the ocean. Larger robot cleaners will store, and sometimes even sort waste within the vessel, while smaller robots generally make frequent trips to a disposal site to empty their collected trash. In contrast, human operated cleanup efforts rely on nets, typically towed from two ends by boats traveling in parallel. These efforts often cover multiple kilometers of ocean surface at a time and rely on humans to constantly monitor wildlife encounters or other problems during collection. While robotic cleanup efforts are efficient in their independence of humans, their capacity and coverage are directly proportional to their size. Thus, a robotic cleaner must be overwhelmingly large and costly to cover the same area as a human-operated cleanup vessel. What if these two strategies were combined?

Over 8 months, the team developed a solution comprised of 2 small robots that operate as a swarm to tug and monitor a surface skimming net for marine plastic collection. These small robots were designed to carry all the sensors necessary to autonomously identify waste and navigate while towing a collection net. They operate with hive-mind style communication to move and target as a single unit, carrying just one net. In deployment, a scaled fleet of cleanup robots would be accompanied by a stationary, manned barge, that can communicate with the robots, store collected waste, and recharge the robots when their batteries are depleted.

1.4 Mission Statement & Objectives

This project is dedicated to the development of a fully operational, autonomous-capable robotic system with the mission of clearing large debris from Earth's oceans. The team's goal was to conduct comprehensive research, design, and prototype a pair of efficient robots for collecting and retaining marine debris via surface trawling. Looking at The Ocean Cleanup's System 003, the team prioritized commercializing, optimizing, and decarbonizing (COD) existing manned cleanup efforts. Objectives to meet this goal are as follows.

- Research existing human and robot operated ocean cleanup systems.
- Develop an electric and autonomous-capable alternative to existing solutions.
- Optimize robot design for high efficiency and low cost.
- Validate design effectiveness and efficiency through open water experimentation.
- Formulate a commercialization strategy for ocean cleanup efforts.

2.0 Background

2.1 The Reality of Ocean Pollution

Of the 430 million metric tons of plastics produced every year, roughly two-thirds are discarded after just a single use. Ultimately, 11 million metric tons, or nearly 4% of discarded plastics end up in water bodies annually [16]. This contributes to the existing 200 million metric tons of plastic already flowing around Earth's oceans and concentrating in patches that can exceed twice the area of Texas, such as the Great Pacific Garbage Patch. A number so large may be difficult to visualize, so imagine the entirety of Manhattan buried roughly one story deep in solid plastic or 11 Empire State buildings worth of trash entering oceans every year. But how exactly is all this waste ending up in the oceans to begin with?

Nearly 80% of marine plastics first start on land and enter rivers or coastlines because of inadequate regulation [42]. Knowing the specific rivers that contribute the most to this pollution is critical to stopping ocean plastics at the source, though the largest emitters are strongly contested. For nearly a decade, scientists have used field data and flow models to map the sources of ocean plastics around the world, with each year yielding more accurate results. In 2017, it was believed that just 10 rivers contributed 91% of all river plastics, or 72% of all ocean trash [23]. Modern studies collect data at hundreds of rivers around the world and have found more complexity in the sources of ocean plastic pollution. It is now believed that nearly 10,000 rivers around the world contribute to roughly 75% of all ocean pollution. Countries in Asia contribute to 80% of all river plastics with just the Philippines accounting for 36% alone. The top 10 highest polluting rivers exist in the Philippines, India, and Malaysia [28]. Figure 3 provides a useful visualization of plastic pollution by country, with Asia and the Americas highlighted as some of the largest contributors.

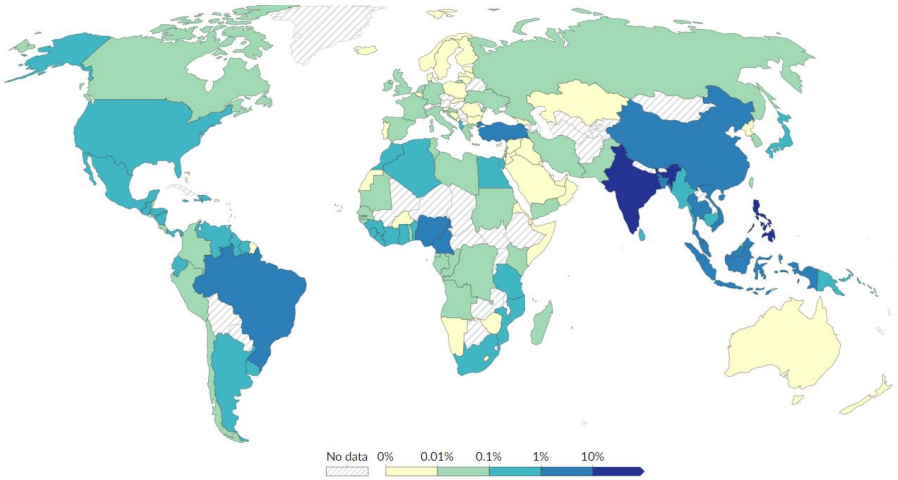

Figure 3: A world map of ocean plastic pollution by country [28].

While Asia single-handedly accounts for 64% of all ocean plastic pollution, the continent comprises 60% of the world's population [23]. This means the problem is not disproportionately caused by any one country or region and is thus the collective responsibility of all. While the emission of plastic waste into the oceans via rivers roughly matches with population distribution, there is a noticeable disparity when accounting for the source of plastic waste. In Figure 4, countries like Germany and the United States, who are shown in Figure 3 as relatively small ocean polluters, are some of the largest plastic waste producers on Earth. Figure 4 also shows India and the Philippines, the largest ocean polluters in the world, as relatively average plastic waste producers. This disparity is a byproduct of the industrialized world's exporting of waste to less developed countries in South America and Southeast Asia. Malaysia and the Philippines import a combined 120,000 tons of trash every month from countries like the US, UK, and Japan [23]. This trash is sold to recycling companies who attempt to salvage waste for its raw materials.

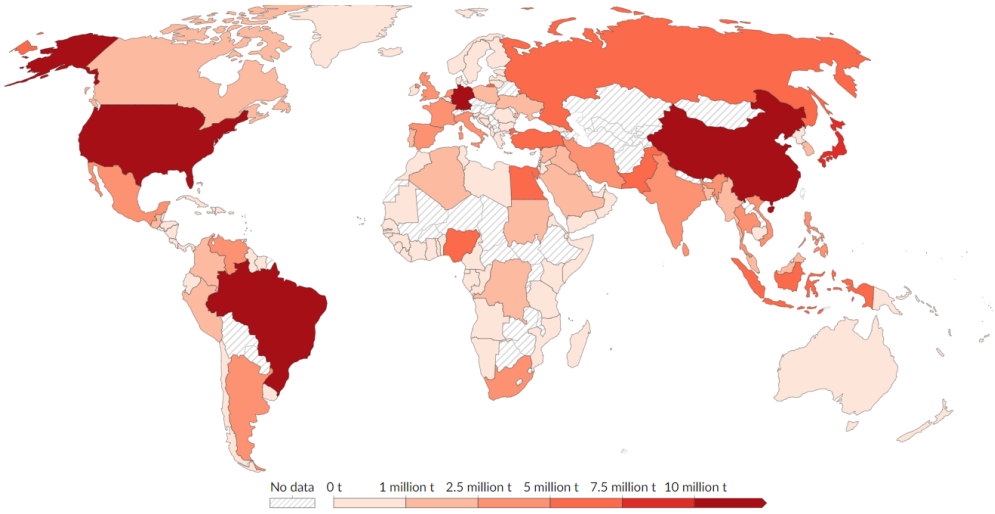

Figure 4: A world map of plastic waste generated by country [28].

Furthermore, the problem of oceanic pollution lies with the mismanagement of plastic waste in addition to its generation. While most industrialized nations heavily regulate the storage and transportation of waste products, less developed countries lack the resources to enforce any policies [16]. This is how plastics piled multiple stories high in industrial scale landfills fall into and accumulate in rivers. The immense volume of plastics entering these waterways poses an obvious risk to ocean environments, but also puts pressure on the ecosystems surrounding rivers and the people that rely on their water to survive. Despite plastic pollution being distributed around the world by population, the responsibility still predominately lies amongst wealthy and industrialized nations. These are the countries who export the byproducts of their immense consumption around the world to be managed within a less expensive and less regulated market.

2.2 Types of Ocean Pollution & Affects

While 80% of all ocean debris starts on land before flowing into rivers, the other 20% is the result of fishing practices [16]. Ghost gear is a term used to describe anything from fishing nets to buoys that drift away from vessels at sea. Ghost gear has a disproportionate impact on ocean wildlife and ecosystems when compared to typical floating plastics [29]. Most nations enforce strict fishing practices within their United Nations defined Exclusive Economic Zones, thus regulating the disposal of fishing gear or collection of anything lost at sea. Following a conversation with a fisherman at Net Your Problem (see Appendix C-3), a non-profit fishing gear recycler, the team found that most commercial fishing nets can cost upwards of $10,000 and weigh thousands of pounds. This large expense is a great incentive for fisherman to recover or report any lost gear, a practice common amongst North American commercial fishing operations. Thus, most ghost gear originates in unregulated international waters or because of illegal fishing. Those fishing illegally will often discard fishing gear while in international waters to disguise their operations after returning to land. Ghost gear is next to impossible to remove from the ocean as the vast majority sinks to the ocean floor, inadvertently trapping marine life along the way [29]. Nets often become tangled around coral reefs, shown in Figure 5, or other ecosystems, requiring both intricate manipulation by human divers and large waterborne machinery to remove the heavy gear [51].

Figure 5: Large fishing net tangled around a coral reef off the coast of Thailand [17].

Despite the immediate and clearly visible impacts of ghost gear or large plastic waste, one of the most dangerous forms of ocean debris is microplastics. As large plastic objects drift through the open ocean, they are exposed to nearly constant daytime ultraviolet (UV) radiation. This radiation is strong enough to bleach and break apart the polymer bonds that comprise plastics [36]. Over years of exposure, large plastics are broken down into microplastics which appear almost like small beads of glass or sand. While microplastics don't visibly pollute oceans and waterways, their presence poses a great risk to marine life and humans alike. These particles are often mistaken for microorganisms such as plankton and consumed by small animals as food, leading to irreparable damage to the creature's digestive system [38]. Microplastics eventually work their way up the food chain until they end up on the plates of the countless people who consume seafood regularly. Microplastics are difficult to track, nearly impossible to collect from the oceans, and can only be stopped by first eliminating the sources of ocean plastics.

Larger plastic debris, comprising most oceanic pollution, poses a considerable threat to marine life even before breaking down into microplastics. Items such as bottle caps, lighters, and balloons, are often mistaken for food by sea turtles, seabirds, and marine mammals, leading to intestinal blockage and starvation [39]. Ghost gear and other fragmented debris can entangle marine life, causing suffocation, or permanent deformities if trapped at a young age. Sea turtles are highly susceptible to entanglement, with netting and monofilament lines frequently found around reef habitats. Bird species like seagulls are at risk when they become ensnared while looking for nesting materials [50]. The vastness and remote nature of oceans makes cleanup efforts challenging and time-intensive, all the while sun exposure quickly breaks down debris into nearly unobtainable microplastics.

2.3 Addressing the Problem

Recognizing the urgency of addressing ocean plastic pollution, governments, organizations, and individuals are implementing a range of strategies to tackle the problem at its source, reducing the overall generation of plastic waste. One crucial approach involves promoting sustainable alternatives to single-use plastics, such as reusable shopping bags, water bottles, and food containers [41]. Effective waste management practices play a critical role in preventing plastic waste from entering waterways and eventually reaching the ocean. This includes expanding recycling infrastructure, implementing waste segregation programs, and educating the public on proper waste disposal methods [50]. To intercept inevitable plastic waste before it reaches the ocean, various capture systems are being deployed along rivers and canals. These include floating barriers, nets, and booms that collect plastic debris as it flows downstream [9].

In addition to preventing new plastic pollution, efforts are underway to clean up the vast number of plastic debris already present in the ocean. Ocean cleanup organizations are developing innovative technologies, such as specialized vessels and underwater drones, to remove plastic waste from marine environments [1]. Public awareness and engagement are essential for driving long-term behavioral changes that can significantly reduce plastic pollution. Educational campaigns, community outreach initiatives, and media engagement are crucial in promoting sustainable practices and fostering a sense of responsibility among individuals and communities [39]. Addressing ocean plastic pollution requires concerted global action. International agreements, such as the Basel Convention and the MARPOL Convention, provide frameworks for regulating the transboundary movement of plastic waste and preventing marine pollution from ships [50].

The ocean plastic pollution crisis demands a comprehensive and multi-pronged approach. By reducing plastic waste generation, capturing waste from land-based sources, clearing existing pollution, and raising awareness, humans can collectively work towards a cleaner and healthier ocean for future generations.

2.4 Existing Robotic Solutions

Within the last decade, many robotic solutions to collect ocean waste have been presented, including autonomous surface vehicles and underwater drones. In addition, human-operated solutions like "The Ocean Cleanup" have gained attention for their efforts to clear floating plastic, though they can be limited by their nonprofit status. To work around funding challenges, some companies have commercialized cleanups with passive data collection. By equipping vessels or robots with sensors like sonar and lidar, hydrographic data of the seafloor can be collected and sold to fund cleanup operations. Organizations developing offshore wind farms, managing fisheries, or monitoring environmental conditions are all invested in the purchase of ocean-based data. This

strategy was highlighted in an interview described in Appendix C-1 with Clean Blue Sea's chief engineer, who shared his experience making a robotic solution to clean harbors in San Diego. The results of these attempts were categorized into three groups. large-scale removers, small-scale skimmers, and seafloor cleaners outlined in Table 1.

Table 1: Summary of existing robotic solutions for marine plastic removal.

Project	Description
Large Scale Removers	
"Circular Explorer" (2019) by OEOO and Holcim	• A 12x8m catamaran-style boat with large deflectors to guide trash to a centralized conveyor belt. • Trash is sorted off the conveyor by hand and collected into transport bags. • Fully powered by onboard solar panels. • Cleaning capacity of 30,000 square meters per hour. • Deployed in Germany and Hong Kong [13].
"Interceptor" (2019) by The Ocean Cleanup	• A stationary vessel with long buoy lines to deflect floating plastic into a conveyor belt. • Autonomously sorts trash into bins with a carrying capacity of $50m^3$. • Human operators unload trash once the system reaches capacity [30].
Small Scale Skimmers	
"Wasteshark" (2023) by Ranmarine	• A 1x1.5m catamaran drone with a central opening to collect floating trash. • Thrusters and onboard sensors drive the system toward plastic waste. • Emptied by hand. • Remotely operated or autonomously collects waste via waypoint planning. • Collects 500kg of waste with an 8-hour battery life [52].
"Aquadrone" (2022) by Clean Sea Solutions	• An approximately 1x2m catamaran drone • Actuated front collector that can expand to 4x the drone's width. • Fully autonomous with 20 hours of battery life • Its range can cover most harbors and uses sensors to adjust its path to collect waste [14].
"Jellyfishbot" (2018) by iADYS	• A modular catamaran robotic platform with modules for collecting macro-plastics, micro-plastics, and oil. • Remote and autonomous control. • Sensor fleet for collecting oceanic data. • There are around 50 systems currently deployed worldwide, with 14 in the US [31][43].
Sea Floor Cleaners	
"Robotic Seabed Cleaning Platform" (2022) by MAELSTROM	• A floating barge with a rectangular moon pool where a 2-ton robot can dive into the water to retrieve pollutants. • The system is controlled by 8 winches for lifting heavy objects and maintaining position in strong currents. • Sonar, camera, and inertial sensors are used to position and identify waste accurately. • Deployed in Venice, plans to extend to the Montpellier coast [37].
"SeaCAT" (2020) by SeaClear	• 4-part robotic system with autonomous and manual control capabilities. • The central vehicle deploys complimentary drones with advanced sensors to scout and collect waste. • The waste is placed in a deployed cage which can be manually retrieved later [2].

Large-scale removers of plastic waste in the ocean rely on the principle of removing as much material at once before unloading. These systems have relatively small collecting devices which still allow them to remove high volumes of plastic in short periods of time, provided there is a high density of trash. With that requirement, large-scale cleaners typically work best around rivers or shorelines, where most plastic enters the oceans and concentrates. Solutions such as the Ocean Cleanup's Interceptor, seen in Figure 6, will sit stationary in rivers and have trash funneled towards a conveyor belt that removes the plastic from the water and into sorting bins for recycling. These machines have collected over 1,000,000 kg of trash from rivers to date and are continuing to be one of the most effective solutions on the market [30]. One Earth One Ocean's (OEOO) Circular Explorer, depicted in Figure 6, operates around the coastlines of Germany and Hong Kong, removing up to four tons of garbage each day [13]. Large-scale removers can be partially autonomous, although still require human assistance with piloting, sorting, wildlife preservation, and dumping waste once full. They are also either slow-moving or stationary, making it difficult to cover large areas.

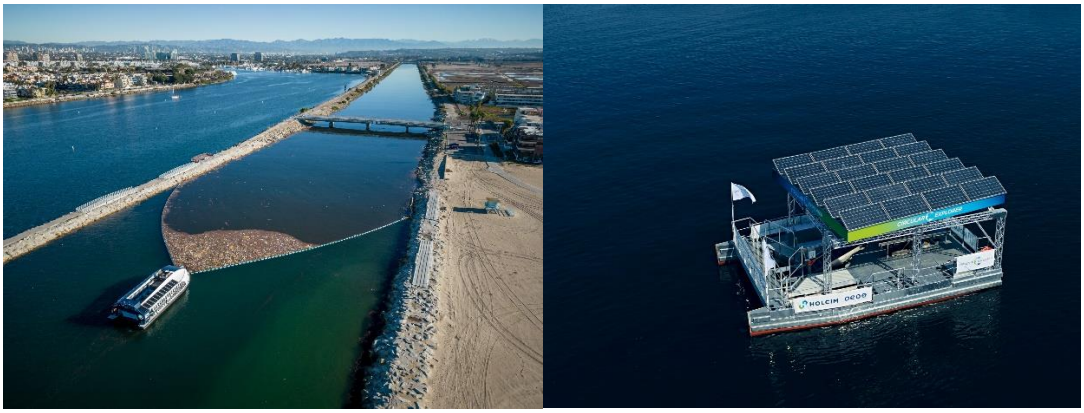

Figure 6: (Left) The Ocean Cleanup's Interceptor 007 cleaning Ballona Creek in Los Angeles, 2022 [30]. (Right) OEOO's Circular Explorer in the Philippines [13].

In contrast to the previous group, small-scale skimmers offer a more versatile platform for collecting waste in different areas, specifically in places with much lower densities of plastic. They are smaller and can typically carry only small amounts of plastic at a time, routinely collecting waste and placing it in a centralized location for human removal. To date, most of these solutions operate in tight urban waterways or in bays and marinas to catch trash before it reaches larger bodies of water. For example, Clean Sea Solution's Aquadrone operates autonomously around private docks in Norway to collect floating waste [14]. Similarly, Wasteshark from Ranmarine Technologies can collect 500kg of waste per day, assuming an operation time of 8 hours, targeting tight spaces that other reclamation devices can't reach [52]. Some cleaners are also modular, designed to collect more than just macroplastics; the French company iADYS offers multiple configurations of their product, Jellyfishbot, to clean up

macro/micro plastics and even oil [31]. The robots shown in Figure 7 incorporate a much higher level of autonomy because they can detect, collect, and remove trash from the water on their own. Their size makes them significantly cheaper to manufacture and operate while also being adaptable to different environments.

Figure 7: (Left) Clean Sea Solution's Aquadrone ready for deployment in Oslo [14]. (Middle) Three Wasteshark systems collecting trash in an urban river [52]. (Right) Jellyfishbot with a full net of reclaimed waste [31].

Seafloor cleaners are a more experimental group of heavily specialized robotic solutions. They typically contain a central hub that controls a smaller mechanism to dive below the water's surface and pick up sunken waste. Since these systems are more complex, there is significantly less active development of their technology, leading to prototypes being developed in just the past few years. Notable progress came from SeaClear, who successfully demonstrated their fully autonomous 4-part system to identify, locate, and collect waste on the Croatian sea floor in October 2023. In their demonstration, they collected a few pieces of litter that were intentionally placed in the water for the test [19]. Moreover, European university and industry collaboration MAELSTROM developed a barge with a heavy-duty diving unit to remove waste from the sea floor near Venice [37]. The larger size and robust nature of the devices shown in Figure 8 make them best suited for removing heavier objects from the sea floor, like tires and discarded fishing nets.

Figure 8: (Left) SeaCat by SeaClear during a system's test [19]. (Right) MAELSTROM's Seabed Cleaning Platform docked in a venetian harbor [37].

All the discussed robotic solutions are steps in the right direction to remove the 11 million tons of plastic entering the ocean each year. However, current available technologies stay along coastlines and lack the capacity to collect waste at the scale of ocean-wide pollution. The most effective solution at this time is System 003, operated by The Ocean Cleanup (TOC), which uses a 2.2km long net to funnel and capture waste in the middle of the ocean. This entirely human-operated effort yields the highest amount of plastic captured per extraction, on the order of 10,000kg, dwarfing the 500kg capacity of smaller-scale robots [34]. Despite their slow operating speed, The Ocean Cleanup covers significantly more area than large-scale robots at over 6 million square meters per hour compared to the 30,000 square meters per hour of the Circular Explorer [34][13]. Reports from The Ocean Cleanup claim a fleet of about 60 System 003's are necessary to remove 90% of ocean plastic by 2040 [32]. However, each TOC System 003 depends on 3 large diesel-powered tugboats and crews of at least 45 people to operate. Scaling this program 60-fold would require enormous capital costs, operational expenses, and further contribute to climate change via fossil fuel emissions. An autonomous robotic solution capable of matching System 003 capacity could drastically cut costs, improve efficiency, and decarbonize the sector. Commercializing cleanup efforts with passive data collection would also allow for rapid growth and profitability of operations.

3.0 Design

3.1 Design Specifications

In designing a more efficient method of surface trawling than traditional tugboats, like used by The Ocean Cleanup, optimization of all components is essential. The robots were designed for stability in harsh seas, maneuverability, towing capacity, drag reduction, and a sensor fleet for autonomous capabilities. The following design specifications were outlined to guide the production of the robot pair.

1. Streamline the hull shape for a drag coefficient of less than 0.5.
2. Design the hull to reduce the possibility of tipping or rolling in harsh waves.
3. Implement features and thruster placement for responsive turning and stability.
4. Use sealing techniques and mechanisms to prevent water from entering the primary electronics cavity.
5. Chose materials to reduce the chance of galvanic and saltwater corrosion.
6. Balance volume and weight for a net positive buoyancy at the robot midline.
7. Optimize the shape and size of the towed net to maximize yield while minimizing induced instability.
8. Develop a mechanized system to hold and release the net from towing, capable of withstanding the applied load of collected trash.
9. Allow for onboard sensors to aid in autonomous and commercial capabilities.
10. Minimize cost and manufacturing complexity.

Minimizing the drag coefficient of the hull was essential in maximizing the effective thrust applied to the water by the propellers, increasing payload capacity and top speed. The coefficient value of 0.5 was chosen as a rough benchmark for this first prototype of the design, comparable to the drag coefficient of a bullet or sphere [45]. Though efficient when traveling parallel to their streamlined profile, low drag coefficient shapes can become unstable in turning maneuvers. Thus, some tradeoffs in drag reduction were expected when designing for stability in harsh ocean conditions.

As with any aquatic based electrical device, protecting valuable and delicate electronics from water was of upmost importance. The team made use of waterproof devices like motors and accommodated waterproofing features when applicable. Keeping the internal volume of the robot free of water was also critical in maintaining positive buoyancy under harsh operating conditions. While less serious during the relatively short operational period of the built prototypes, protecting frame components from corrosion is important to longevity of structural integrity [49]. Galvanic corrosion between materials, saltwater corrosion from the environment, and UV corrosion from the sun all influenced the material choices throughout the robot's development. In a similar vein, cost savings and weight reduction were made a priority when designing for manufacturing simplicity and commercial viability.

3.2 Thrust Requirements & Drag

To determine the best motors for propulsion, the team first had to calculate the amount of thrust needed to move the robots at a defined speed and how many motors would be required. Finding the total thrust needed to move each robot first involved estimating the drag experienced by the system. The Ocean Cleanup found that a speed of 1.5knots, or about 0.77m/s, was most effective [34] when sweeping trash from waterways. All the following calculations assume a system velocity (v) of 0.77m/s. To minimize the effective drag on the robot, the hull was designed to mimic that of a symmetrical airfoil, or a teardrop. This would lead to a theoretical drag coefficient (C) of only 0.05 for the central hull [45], a rough profile of the design is pictured in Figure 9 below. However, it is important to note that the drag coefficient of a shape can vary depending on the Reynolds number of the fluid. Under the same speed conditions, a symmetric airfoil in water could expect to exhibit a drag coefficient closer to 0.5 or 1, the low end of which is used in the following theoretical calculations.

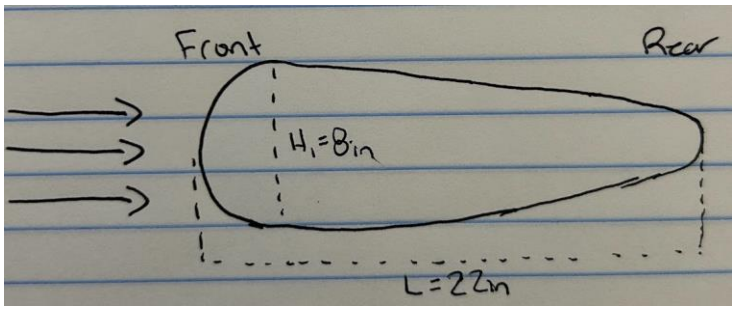

Figure 9: Side profile sketch of the robot's central hull.

The hull's overall length or chord was decided to be less than 24in to reduce the cost of materials. For a 24in hull or greater, the stock material used for cutting the side plates would have to be at least 48in, making each side plate far more expensive. The cord ratio of an airfoil defines the ratio between the thickness (H) and cord (L) which affects the airflow and drag experienced by a wing. While a lower cord ratio, around 0.275, is most advantageous in minimizing drag [21], the robot hull shown in Figure 9 exhibits a cord ratio of 0.37 due to its larger front bow. The enlarged front face of the robot shifts the center of buoyancy forward, allowing it to stay on the surface above waves rather than diving through waves like a classic airfoil shape. Though increasing the drag experienced by the hull, the team also found the larger internal capacity better for wire management and electronics distribution. The width of each robot hull was made 18in to match the traditionally square footprints of most other marine surface robots. This gave the robot an effective wet area (A), perpendicular to the path of motion, of 0.04645m^2, assuming a hull that is only half submerged. Despite the robots being designed for open ocean conditions, all experimentation was conducted in fresh water, and thus the density (ρ) of fresh water, 1000kg/m^3, was used in the following drag force calculations.

$$F_{drag} = \frac{1}{2} C\rho A v^2$$

$$\boldsymbol{F_{drag-hull}} = \frac{1}{2} \times 0.5 \times 1000 \frac{kg}{m^3} \times 0.04645 m^2 \times (0.77 \frac{m}{s})^2 = \boldsymbol{6.89N}$$

While the shape of the robots generated some drag that must be overcome by the thrusters, most of the drag experienced by the robots comes from towing the trash-filled net. The shape of the robot bodies was streamlined to focus most of the applied thrust on towing capacity. On land, towing capacity is generally a function of mass, while in water towing capacity is more a function of an object's geometry and resultant drag. Given the surface trawling functionality of the robots, all trash collected can be considered weightless by their floating nature. But, tugging oddly shaped trash through the water can be equated to towing a wall, generating considerable drag for the robots to overcome [6]. For these calculations, the system was assumed to be towing a net with a 3m span between robots and a 0.32m depth. An affective area of 0.32m^2 was used given a net at 30% capacity, in conjunction with a drag coefficient of 1.28 for a flat plate. The below calculation determines the drag experienced by the net in towing.

$$\boldsymbol{F_{drag-net}} = \frac{1}{2} \times 1.28 \times 1000 \frac{kg}{m^3} \times 0.32 m^2 \times (0.77 \frac{m}{s})^2 = \boldsymbol{121.43N}$$

Assuming the resultant drag force acts at the center of the net, each robot would experience half the total force acting as tension at their back centers. Thus, the drag force experienced by each robot totals to **67.61N**, which should match the propelled thrust to maintain a constant velocity of 0.77m/s.

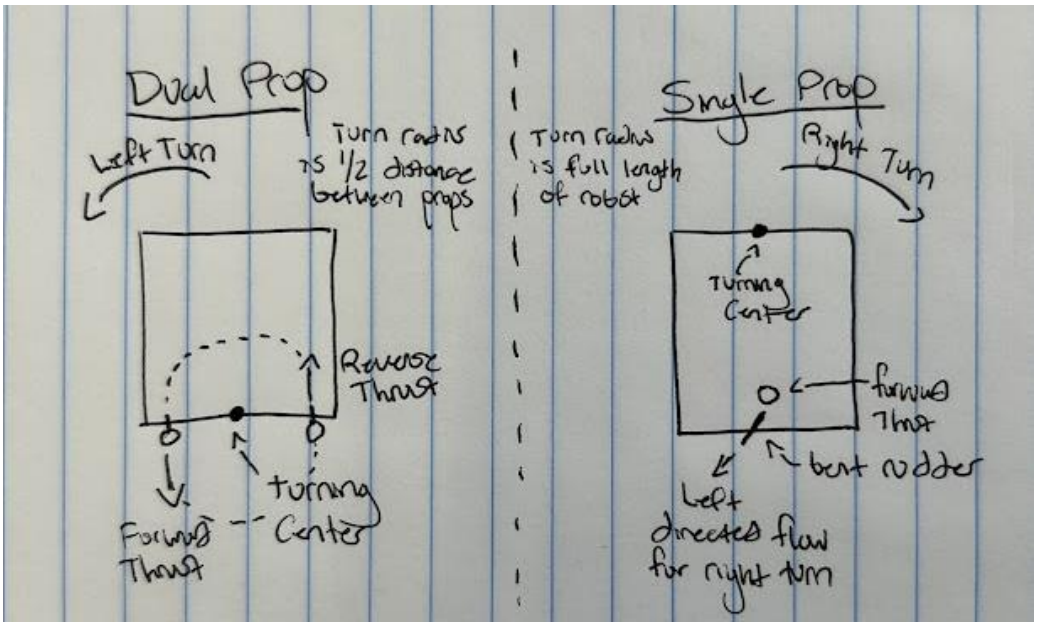

Figure 10: Comparison between dual propeller and single propeller maneuverability.

The primary options for propulsion were either dual motors, one on either side of the robot, or a single central motor with an articulated rudder for turning. Dual motor watercraft offer far superior maneuverability than a rudder where turn radius is dependent on speed [4]. Given the low relative speeds of the robots during collection, having dual propellers that can reverse directions for turning allows for course correction with essentially zero turn radius as shown in Figure 10. While having a single larger motor is less expensive than dual motors, achieving desired performance would be much more demanding on a single motor. Brushless DC motor efficiency does not peak at its highest speed, to achieve the desired speed of 0.77m/s, a single motor would have to operate at its highest power and near lowest efficiency [18]. In contrast, dual motors share the system load and can operate at near half power and peak efficiency. The combination of improved maneuverability and lower power requirements justifies the increased cost of dual motors and simplifies the design by eliminating the need for an articulated rudder. The 5-blade brushless Hobby Hawk underwater thruster, shown in Figure 11 below, was chosen to provide thrust to the robots. Each motor can provide a theoretical maximum thrust of 68.67N when powered with 24volts [24]. Given the limitations of the robot's battery, the motors were run at just 12volts, yielding half the thrust for each motor. Thus, requiring two motors per robot to achieve the necessary 67.61N of thrust to overcome drag at 0.77m/s. One clockwise turning and one counterclockwise turning propeller were purchased for each robot to provide appropriate directional control.

Figure 11: Hobby Hawk 1080W 5-blade DC brushless waterproof thruster [24].

3.3 Buoyancy, Floatation, & Stability

Looking next at the buoyancy and floatation of the robots, many decisions regarding hull shape, capacity, and stability were made to further optimize performance. Early in the design process, a weight limit of around 23kg (~50lbs) was established by the team to keep the robots easily portable by any human operators. It was also decided that the robots should float at their symmetric midline, keeping half of the robot underwater and half above water. With a completely submerged robot, water pressure would become a considerable factor and a completely above-surface robot would require large excess structures for floatation. Thus, the midline was chosen as an ideal waterline and provided favorable drag reducing fluid flow around the robots when in motion. To float 23kg of mass, the submerged volume must provide 23kg of positive buoyancy. Given the symmetric geometry of the hull, a robot's total volume must provide 46kg of positive buoyancy to float 23kg at the axis of symmetry. With the dimensions previously discussed in Section 3.2, the hull has a total volume of 0.0301m^3, providing a total submerged buoyant force of 30.1kg using the following equation.

$$F_b = \rho g V$$

$$F_{b-hull} = 1000\frac{kg}{m^3} \times 9.81\frac{m}{s^2} \times 0.0301m^3 = \mathbf{294.85}\boldsymbol{N}\ or\ \mathbf{30.1}\boldsymbol{kg}$$

It is important to note the final geometry of the hull profile is shown on the left in Figure 12. While ideal for minimizing drag, placing thrusters along the back (right) of the hull and the tight radius complicates sealing of the internal hull cavity. As a result, the back of the hull, where the thrusters mount, was left outside of the enclosed space leaving a volume profile shown on the right in Figure 12. Further details about this decision are explained in Section 3.4 following.

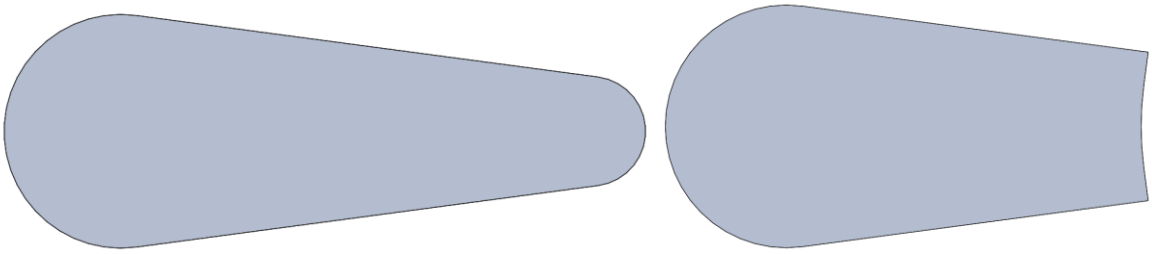

Figure 12: Complete hull profile (left) and profile of contained hull cavity (right).

While the robot hull provides enough positive buoyancy to float on its own, floating at the midline would require an additional 16kg of buoyant potential. Rather than simply increasing the size of the robot's central hull, the team found it more advantageous to add additional hulls, or pontoons, to either side of the central hull. The low density, high strength, and corrosion resistance of PVC makes it a great choice for

aquatic floatation. Reversing the buoyancy equation from before to calculate the volume and diameter needed for each PVC pipe yields the following.

$$V = \frac{F_b}{\rho g} \; where: F_{b-pontoon} = 78.5N \; or \; 8kg$$

$$V = \frac{78.5N}{1000\frac{kg}{m^3} \times 9.81\frac{m}{s^2}} = \mathbf{0.008}\boldsymbol{m^3}$$

For a round pipe of 30in length, the pipe diameter required is $D = \sqrt{\frac{4 \times 488in^3}{\pi \times 30in}} = \mathbf{4.55}\boldsymbol{in}$

Nominal 4in schedule 40 PVC has a true outside diameter of 4.5in. With 2 pontoons of 30in long 4in PVC, an additional 16kg of positive buoyancy is provided to the robot when accounting for the small volume increase provided by the PVC end caps. Thus, a central hull between two PVC pontoons provides enough positive buoyancy to float a 23kg robot at its symmetric midline. Though important for buoyancy, the additional pontoons are also critical to the stability of the robot in harsh ocean conditions. While single hull ships are incredibly common across the world's seas, they are prone to rolling and harsh movements in large waves [22]. Catamarans solve this problem by distributing the buoyant force across a larger surface area to resist rolling, compared to a monohull where the center of buoyancy is directly below the center of gravity, shown in Figure 13 below.

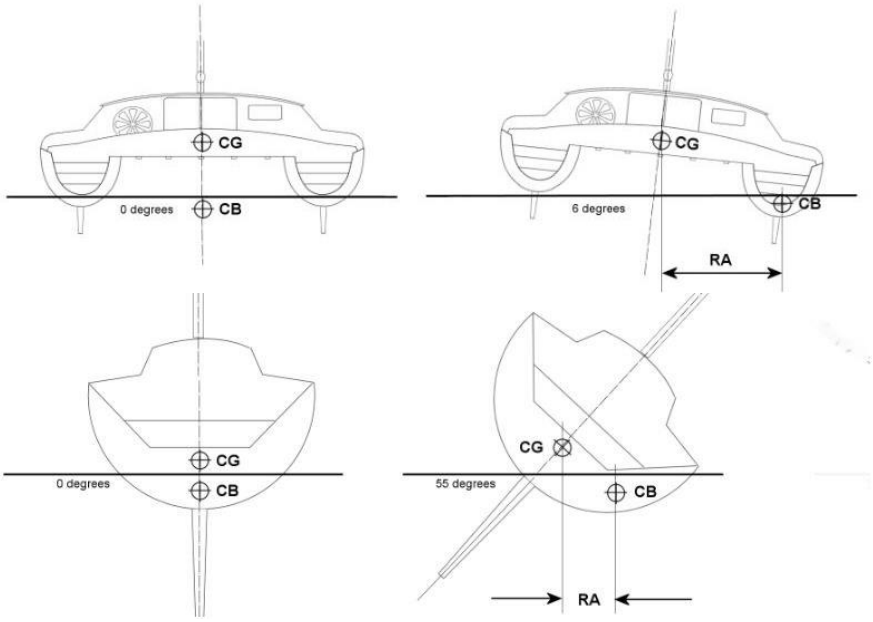

Figure 13: Catamaran (top) vs. monohull (bottom) roll dynamics [22].

A trimaran, or 3 hull ship, further increases the benefits of a catamaran by distributing the buoyant force across a greater wet surface area, resisting tipping, and rolling forces. Thus, the team decided to move forward with a 3-hull robot design for the benefits of stability and increased buoyancy. Though, one drawback that comes from a thin and streamed design is difficulty maneuvering through the water. Straight-line movement was optimized with the hull design of each robot, but little surface area extends into the water to provide resistance in turning operations [5]. Surfboards, which are similarly designed for ocean surface movement, have fins located on their backs to improve turning ability and to prevent sliding laterally across surface waves. 2 fins modeled with the same characteristic shape were added to the side hull pontoons of each robot to provide lateral resistance and improve turning maneuverability. A visual of the robot design can be seen in Figure 14 below.

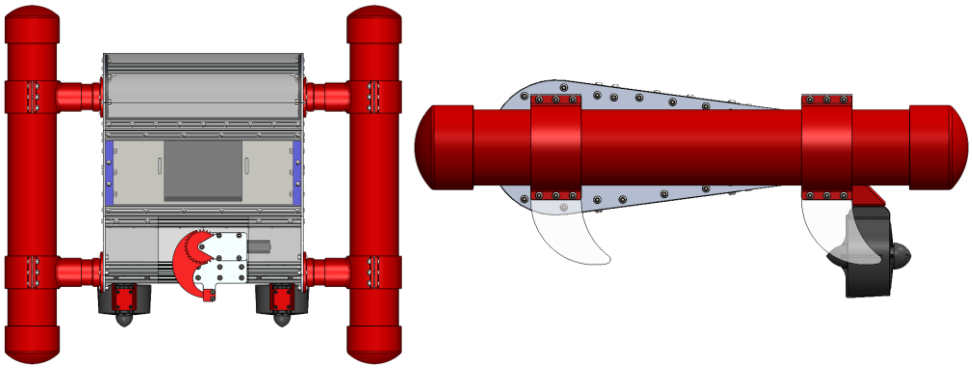

Figure 14: Top view of robot 3-hull design (left) and side view of stabilizing fins (right).

The final Solidworks model of the robot had a mass of 23.92kg and a theoretical buoyant potential of 53.54kg based on its total enclosed volume. Additional design elements are discussed in the following sections.

3.4 Structures, Waterproofing & Corrosion Protection

While optimizing the shape and design of the robot was an essential priority for the team, it was equally important to ensure structural design elements could endure the unforgiving ocean environment. The robot's primary hull is made of two flat 3/16in 5052 aluminum plates separated by 1in 80/20 aluminum extrusion. 1/32in ultra-flexible polycarbonate was then bent around the two metal plates and bolted to the 80/20 to create an enclosed central cavity. In pulling the polycarbonate in tension, waterproof butyl tape lining the black and red brackets in Figure 15 were compressed. Under compression, the tape expands to fill the gaps between the polycarbonate and aluminum plates, creating a permanent watertight seal [11]. The blue brackets on the top of the hull feature threaded inserts to allow for a removable polycarbonate hatch to access internal electronics. When bolted down, this hatch compresses a rubber gasket, sealing the insides from any water intrusion.

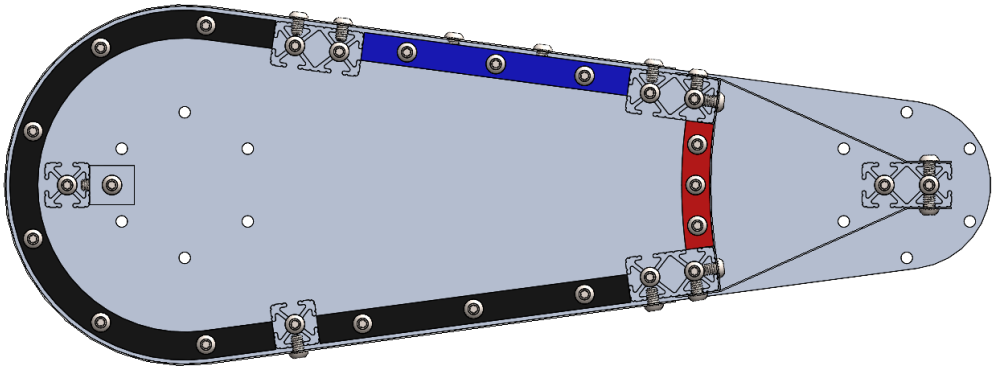

Figure 15: Side profile of the robot's central hull, each color sealing bracket represents a different polycarbonate panel.

Given that most existing ocean-based robots use a single injection molded hull to minimize seams and leaks, this plated style of construction is unconventional. Injection molding services require complex machined molds that increase manufacturing time and cost, leading the team to adopt the plated design described [26]. Aluminum and polycarbonate were chosen as the primary body components of the central hull for their high corrosion resistance and low relative weight. The colored brackets used for waterproofing were made of 3D-printed ABS plastic, a rigid and high strength material resistant to corrosion. The placement of the brackets next to 80/20 extrusion was intended to prevent rotation of the extrusion and create a sturdy hull frame. The front-most 80/20 extrusion, intended for sensor mounting, relied on a secondary angle bracket to prevent rotation, as seen in Figure 16. The back-most 80/20 extrusion lies outside the watertight central cavity, creating a sharp angle at the back red sealing bracket for turbulent drag inducing eddies to form. To continue the streamlined profile of the robot without encasing the thrusters, secondary polycarbonate "aero panels" were added to the robot's back, allowing a smooth path for fluid flow.

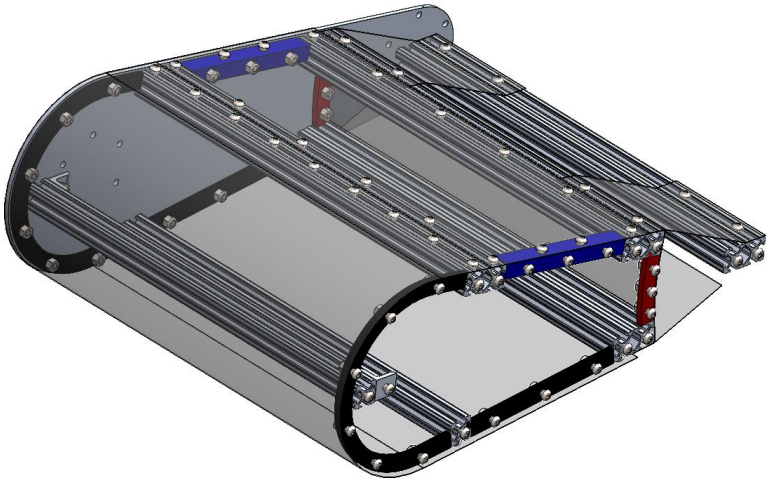

Figure 16: 3D view of the robot central hull with one side plate removed.

In addition to the main body of the robot, the secondary PVC hulls required rigid attachments to the central hull for effective floatation and stabilization. To hold the 4in PVC in place, saddle-style clamps were 3D-printed using ABS. Each clamp featured an internal hole that could fit a standard 2in schedule 40 ABS pipe which then interfaced with a 3D-printed flange that was bolted to central hull side panel. The assembly is pictured below in Figure 17, showing the interactions between the various parts. The 3D-printed ABS components were glued to the purchased ABS pipe using ABS weld, forming a single assembly of the 3 components on the left. All PVC and ABS plastic components regularly exposed to water were painted with red Rust-Oleum spray paint, providing protection from UV and saltwater corrosion. The paint also acts as a marine fouling deterrent, preventing organic growth on the outside of the robot over time. Red was chosen to comply with US Coast Guard regulations for high visibility identification of unmanned marine vessels [12].

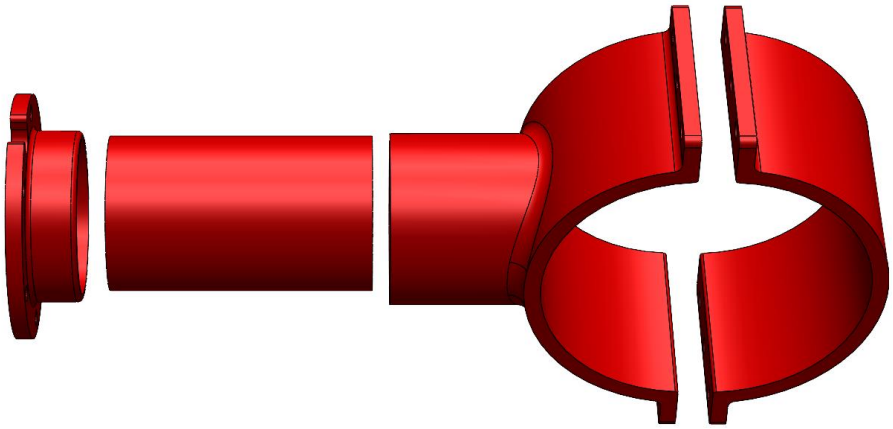

Figure 17: ABS pipe clamp assembly featuring a flange, pipe, saddle mount, and clamp.

In the design of the thruster mounting brackets, two primary factors were accounted for, strength to resist the thrust of the motors and their depth in the water. If the propellers are mounted too close to the robot's waterline, air can be sucked through the blades, drastically decreasing efficiency, and potentially cause overheating [40]. In most boating applications with outboard motors, it is recommended that the top of the propeller blades sit at least 3in below the waterline. Thus, the motor bracket shown on the left in Figure 18 positions the top of the propeller roughly 3.5in below the waterline for optimal efficiency. Assuming a rigid robot hull, under the propulsive load of the thruster, the mounting bracket is prone to fracture from the bending moment applied to it. To ensure the ABS plastic brackets could withstand the theoretical load of 35N from each motor, a Solidworks static analysis was conducted. Given a solid ABS shear strength of 28MPa [3] and applying a safety factor of 5 to account for 3D-printer infill, a maximum allowed stress would be just 5.6MPa. The resultant simulation shown on the right in Figure 18 indicates a maximum stress of 1.65MPa located at the bracket-robot interface. Though relatively high, this maximum shear stress yields a safety factor of nearly 17, validating the bracket's ability to support the thrusters under load.

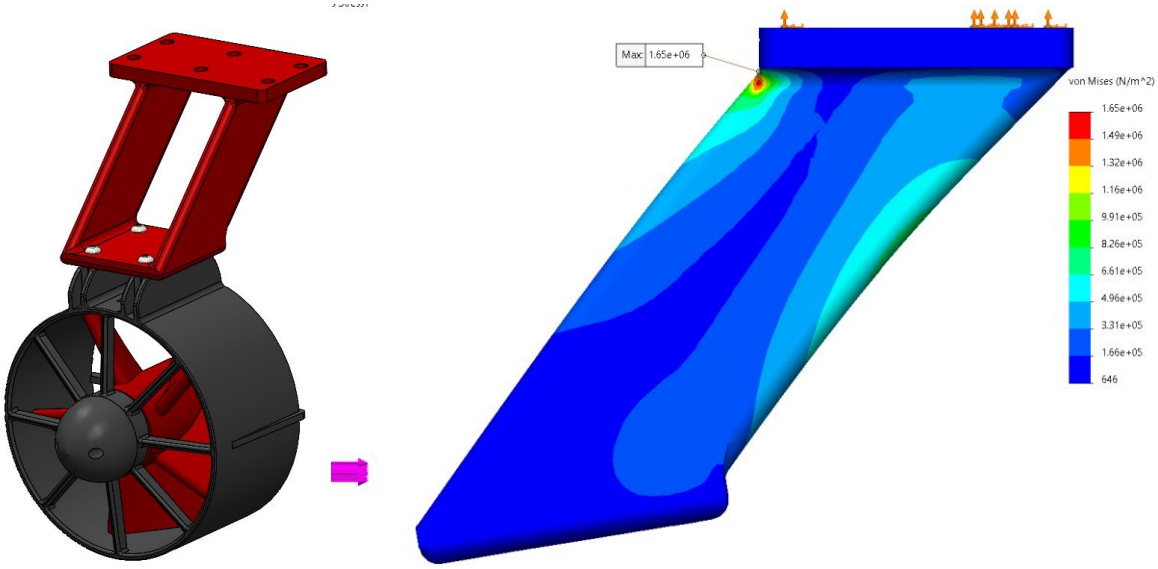

Figure 18: Bracket with mounted thruster (left) and Solidworks stress analysis (right).

Galvanic corrosion is the process of electrochemical bonding and oxidation of two different metals in the presence of electrical current and when in direct contact [20]. Though uncommon in a non-electrically charged environment, under exposure to salt-water and direct sunlight, galvanic corrosion is accelerated between differing metals. Given the use of exposed stainless-steel fasteners throughout the robot chassis, isolating the bolts from the aluminum frame was essential to prevent aggressive galvanic corrosion. This was done through careful planning of bolt placement and use of rubber washers. Most steel bolts are only in contact with polycarbonate or ABS, and others are shielded from aluminum by a thin layer of plastic. All bolts that directly mount to the outer aluminum plates first pass through rubber washers that compress to both prevent corrosion and aid in waterproofing. Wherever rubber washers couldn't be used for waterproofing holes, such as in mounting the ABS pipe flanges, rubber gasket material was cut to size and compressed between the plate and flange.

3.5 Net Release Mechanism

During the research and design phase of the project, it became apparent that the robots needed a mechanized net release system. For full system autonomy to be achieved, the emptying of a full net would also require seamless autonomous design. An automated hand-off between the robots and an external trash collector was beyond the scope of the current project phase. This led the to team to only design and build an actuated latch mechanism to withstand the applied drag-induced loads of the net and trash. Similar release mechanisms are used by The Ocean Cleanup as an emergency measure in case of net entanglement or wildlife entrapment [34].

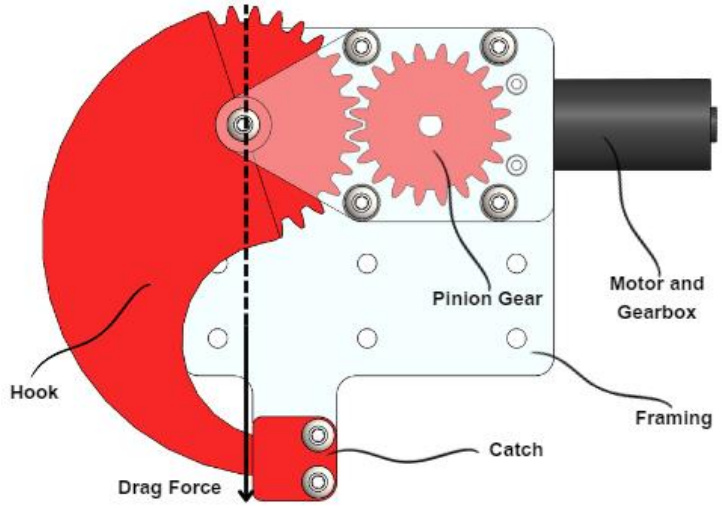

Figure 19: A labeled diagram of the net release mechanism.

Figure 19 depicts the final design for the net latch mechanism, specifically the different components and their interactions. The mechanism consists of a driving motor and gearbox directly connected to a pinion that spins a geared hook into a catch for locking a net in place. The team chose to use Greartisan 12V Self-Locking Motor for their documented use in prior projects and their worm-drive gearbox which prevents the mechanism from opening without actuation. Since the motor is not waterproof and is located outside the hull in a fully submerged position, a watertight enclosure was designed to prevent flooding the motor. The enclosure was manufactured in two pieces, shown in Figure 20, made through stereolithography (SLA) of an ABS-like resin to prevent water from seeping through the material. The two parts of the enclosure were first screwed together, then bonded using an ABS welding adhesive with the motor positioned inside. The top of the part was then sealed against the aluminum plate with butyl tape and fixed in placed by eight bolts compressing the enclosure, gearbox, and framing together.

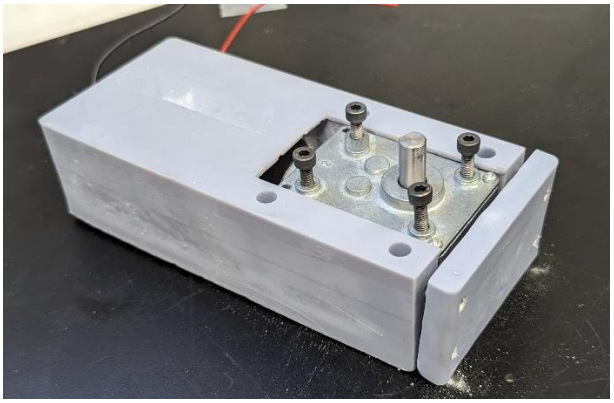

Figure 20: Assembly of the net release motor prior to chemical welding and sealing.

The net latch mechanism was designed to withstand the required load from the net's drag. The frame was made of ⅛th inch thick 5052 aluminum for its low-cost, rigid, and durable properties. In contrast, the hook and pinion gear were 3D printed out of ABS plastic due to its high impact and corrosion resistance as well as its relatively low yield stress, ensuring their fracture before any damage could be done to the robot frame. Additionally, the line of action of the drag force was positioned as closely to the hook's center of rotation, seen in Figure 19, reducing reactive forces and the chance of breaking gear teeth.

The last concern for the system was to calculate the breaking force of the hook, given the robot was fixed in place. For this calculation, the weakest rectangular cross section was found after performing an experiment to measure the breaking force of the system; further details can be found in Section 4.4. Below are the equations for calculating the breaking force, assuming the hook is made of solid ABS plastic with a shear strength of 29.8MPa [3].

$$F = \sigma_{UTS} \cdot A, \text{ where } \sigma_{UTS} = 29.8\,MPa \;\&\; A = 193.548\,mm^2$$

$$F_{max} = 29.8\,MPa \cdot 193.548\,mm^2$$

$$F_{max} = 5767.7\,N$$

The theoretical breaking force of 5767.7N is significantly higher than the expected drag force of 67.61N and the robot's maximum thrust of 68.67N. As a result, any applied drag from accumulated trash in the net would not exceed the breaking force of the latch mechanism, before it prevents the robots from moving forward.

3.6 Net Shape & Optimization

When towing, the two robots were designed to drive in parallel, maintaining a set distance apart that influences the shape of the net. A rope suspended from two points and freely hanging under gravity will naturally form a catenary curve, based on the length and separation of the rope [8]. A net being towed from two points forms a shape that can be approximated as a catenary curve, with drag force taking the place of gravity. The shape of the net's curvature influences the angle at which rope tension, resulting from drag, acts on the back of the robot. Over time, the tension in the net will pull the robots closer together, the scale of which being a factor of tension angle. Using onboard GPS systems, the robots will have to correct their position by making slight turns to stay on course with a set distance between them. An ideal system would see tension acting parallel to the straight-line path of motion. The further the angle from parallel, the more distance each robot must cover in course corrections to maintain separation distance. While greater separation between robots leads to more energy wasted on course corrections, it also yields a large sweep area and thus higher total trash collection potential. Thus, the team found it necessary to optimize the length of the net and separation of the robots to maximize trash collection potential while minimizing energy losses required for parallel pathing. The following equation defines the collection energy efficiency of the robot system.

$$\frac{Energy\ Used}{Trash\ Collected}\left(\frac{J}{kg}\right) = \frac{Energy\ Used\ Over\ a\ Distance\ \left(\frac{J}{km}\right)}{Surface\ Trash\ Density\ \left(\frac{kg}{km^2}\right) \times Sweep\ Width\ (km)}$$

A unitless multiplication factor in the numerator known as "effective distance" was then added to account for the required correction distance at a given tension angle. The variable represents the effective distance covered by a robot to travel just 1 unit of straight-line distance. Figure 21 below illustrates the path of a robot with corrections, with theta representing the angle of the rope relative to the robot's path and the angle at which a robot is pulled inwards.

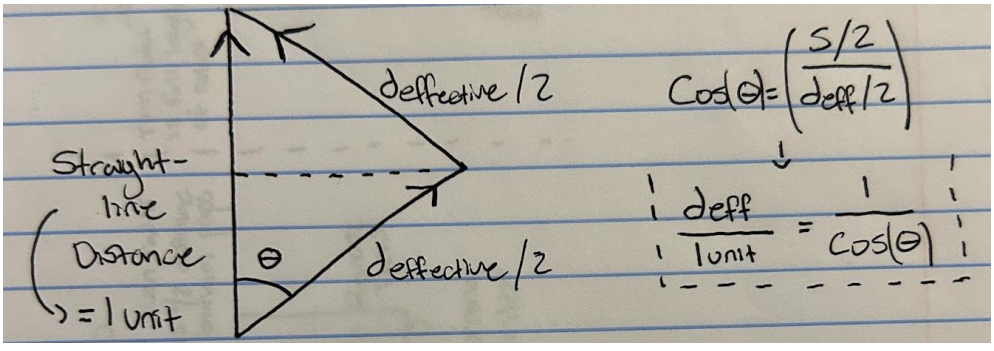

Figure 21: Effective robot travel distance compared to straight-line distance.

This multiplication factor, being greater than 1, scales the energy used per effective distance traveled to account for robot pathing maneuvers. The factor was further modified into the “separation parameter” by dividing by the “sweep width” or robot separation. The resulting efficiency equation yields the following.

$$\frac{Energy\ Used}{Trash\ Collected}\left(\frac{J}{kg}\right) = \frac{Energy\ Used\ \left(\frac{J}{km}\right)}{Surface\ Trash\ Density\ \left(\frac{kg}{km^2}\right)} \times \frac{1}{\cos(\theta) \times Sweep\ Width\ (km)}$$

The last term of the equation, or separation parameter, is dependent on the distance between the robots and the angle at which the net applies tension to each robot. The tension angle is itself a function of robot separation distance and the total length of the net, requiring an iterative or numerical solution. A python script, included in Appendix A, was written to graphically represent the separation parameter as a function of separation distance for various total net lengths. The closer the separation parameter to 0, the more effective the robots are at collecting trash with minimal inefficiencies from pathing corrections. The resulting graph is shown in Figure 22, where an ideal net length of 11m and a robot separation of 8.7m was found to yield the lowest separation parameter of 0.137m^{-1}. The graphical trend implies that an even longer net could result in increased efficiency, further proven by The Ocean Cleanup [34]. However, the purchased net had a maximum rope span of only 11m and was thus used at its fullest.

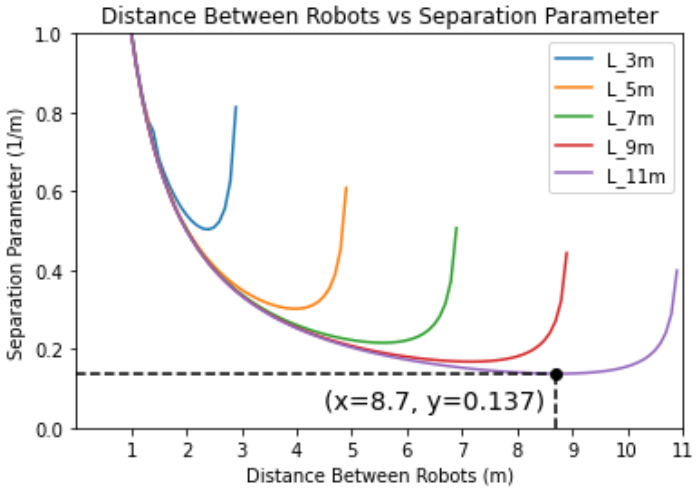

Figure 22: Separation parameter as a function of robot distance for various net lengths.

An 11m long tow rope mounted to the back of two robots separated by 8.7m would result in a catenary curve shown in Figure 23, applying tension to the back of each robot 33.08deg from their path of travel. Though the robots are being pulled inwards at a relatively steep angle, the sweep distance had a much larger effect on collection efficiency. These findings show that the additional energy required to maintain a specific separation distance when being pulled inwards is relatively miniscule.

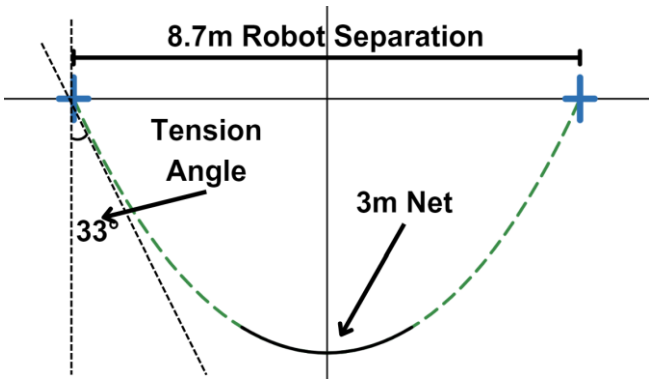

Figure 23: Graphical representation of net catenary curve and applied tension angle.

Though the total length of the rope spans 11m in length, the actual net portion of the towed rope is only 3m in length and 1m in depth. Figure 23 shows the net in solid black and the extending ropes in green dashed lines. The entire 11m rope length is held on the water's surface using 25 buoys, each with a positive buoyancy of 0.2kg. The buoys on the surface sweep ocean trash to the central 3m net for retainment. To collect neutrally buoyant trash that floats slightly below the ocean surface, the net extends an additional 1m below the surface. To maintain a c-shaped side profile of the net, conducive to scooping trash, the bottom of the net was weighed down. The team laced segments of steel chain, totaling 2.5kg, within the bottom row of the net to force it into an open state when being towed.

3.7 Theoretical System Efficiency

For comparison purposes, the team decided to use the joules of energy consumed for every kilogram of trash collected as a baseline for efficiency. The lower the energy consumed to collect trash, the more efficient the system is at its intended purpose, cleaning the oceans. Referring to the equation used in Section 3.6, the following was used for comparing the efficiency of The Ocean Cleanup with that of the robots developed for this MQP.

$$\frac{Energy\ Used}{Trash\ Collected}\left(\frac{J}{kg}\right) = \frac{Energy\ Used\ \left(\frac{J}{km}\right)}{Surface\ Trash\ Density\ \left(\frac{kg}{km^2}\right)} \times Seperation\ Parameter\ (\frac{1}{km})$$

For a towed rope length of 11m and a robot separation of 8.7m, the resultant separation parameter is 0.137m^{-1} or 137km^{-1}. Research conducted by The Ocean Cleanup found that the density of trash in the Pacific Ocean ranges from 100kg/km^2 to 10kg/km^2 depending on proximity to the Great Pacific Garbage Patch [47]. For the purposes of these calculations, 50kg/km^2 was used as the assumed density of trash on the Pacific Ocean surface. When powered with 12volts and drawing a maximum loaded current of 45amps, each Hobby Hawk thruster theoretically consumes 540watts of

power. Assuming this maximum power consumption is required for travel at the predefined 0.77m/s, the system of 4 thrusters and 2 robots consumes 2805kJ/km.

$$MQP\ Theoretical\ Efficiency = \frac{2{,}805{,}000\ \left(\frac{J}{km}\right)}{50\ \left(\frac{kg}{km^2}\right)} \times 137\ \left(\frac{1}{km}\right) = \mathbf{7685}\,\frac{\boldsymbol{kJ}}{\boldsymbol{kg}}$$

To compare this value to that of The Ocean Cleanup System 003, the team had to determine the energy usage and separation of their tugboats during operation. The Ocean Cleanup makes use of 3 Maersk tugboats, Tender and Trader which pull the net, and an additional Trader model command ship [34]. Each ship uses the same 13,872 horsepower or 10.2MW diesel engine [27], traveling at 0.77m/s, each ship consumes 13,347kJ for every kilometer traveled. While towing a 2.2km long net, the tugboats maintain a roughly 1km separation, or sweep distance [34]. The following equation yields the energy used by The Ocean Cleanup for every kilogram of trash collected.

$$The\ Ocean\ Cleanup\ Theoretical\ Efficiency = \frac{39{,}740{,}000\ \left(\frac{J}{km}\right)}{50\left(\frac{kg}{km^2}\right) \times 1km} = \mathbf{794.8}\,\frac{\boldsymbol{kJ}}{\boldsymbol{kg}}$$

This comparison proves the importance of scale in designing ocean cleanup efforts. The much smaller electric robots developed for this project, towing a 0.011km long net, consume **9.67** times more energy for each kilogram of trash collected than the tugboats of The Ocean Cleanup (TOC), towing a 2.2km long net. Where the robots developed here lack scaled efficiency, they make up for in operational and capital cost savings. Though donated to TOC by Maersk, tugboats of similar capacity to the Maersk Trader sell for roughly $3.5million a piece [48] and require crews of at least 15 people for regular operations [27]. While operational costs are more difficult to accurately calculate, to operate their System 003, TOC must pay for at least a 45-person crew and diesel fuel. In comparison, the MQP robots developed here are autonomous-capable and thus require little to no regular operational crew. Additionally, each robot can generate 36W of power with a back-mounted solar panel, assuming an industry standard solar potential of roughly 300W/m^2 [46]. The self-sufficiency of a robotic ocean cleanup platform drastically minimizes operational costs when compared to human-operated counterparts. At a low production scale, each pair of robots is worth roughly $2000. To equal the trash collecting capacity of TOC, 115 robot pairs are required, totaling $230,000 in capital expenses. A 2,000 ton-capacity command barge used for transporting the robots and storing collected trash would cost an additional $4 million to match TOC capabilities [10]. Thus, overall capital for a robotic platform would total **$4.23million** (not accounting for economies of scale), compared to TOC's capital worth of **$10.5million**. Operational cost savings further benefit the use of a robotic alternative to ocean cleanup efforts.

3.8 Electronics & Sensors

To make the system autonomous-capable, each robot was equipped with a sensor fleet to get basic information from its surroundings; Figure 24 below shows the locations of each sensor. For navigation, each robot uses a camera for object identification, and an integrated IMU/GPS to monitor system heading and spatial coordinates. A wide FOV camera was mounted close to the inner edge of system to capture the surrounding environment and direct trash between the robots. Due to the metallic structure of the robot, no GPS signals could penetrate the hull and reach the IMU's integrated GPS antenna. To solve this, a waterproof external GPS receiver with a gain 28dB was mounted on top of the robot where it could receive data from satellites. A sonar sensor was mounted on the bottom of each robot, perpendicular to the waterline for collecting depth measurements up to 7.5 meters. The sonar sensors were intended to improve the commercial viability of the system through the sale of oceanic data. Ocean mapping capabilities are common practice amongst similar on-the-market harbor cleanup robots. Lastly, two water sensors were added to each robot, one at the lowest point in the hull and the other directly under the electronics plate. These sensors give a true Boolean output in the presence of water, allowing the controller to know the location of leaks if they occur.

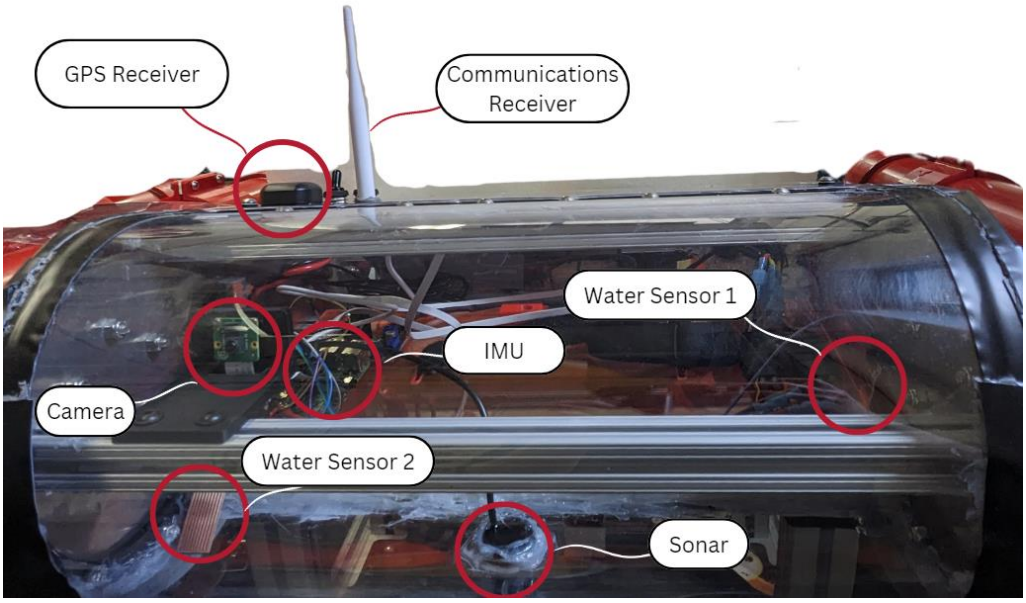

Figure 24: Photo of a robot with all mounted sensors labelled.

All onboard systems are powered by a 216Wh, 12V lead-acid battery located in the center of the electronics plate. Though unconventional, lead-acid was chosen over more power-dense lithium-ion batteries due to lithium's violent reactive capabilities with water [33]. With an initial prototype, perfect waterproofing was not a guarantee, so a safer power system was chosen. The battery was also positioned low and central within

the robot's frame, lowering the center of gravity, and creating a roll-resistant stable hull. This battery was connected to a power distribution panel (PDP) through external switches and a 30A fuse to protect all electronics in case of short-circuiting or overloading. The PDP powers all high current components (i.e. communications receiver, thruster ESCs, and the net release motor controller) directly while all logic level components are given 5V through a voltage regulator. A full wiring diagram of all components can be found in Figure 25.

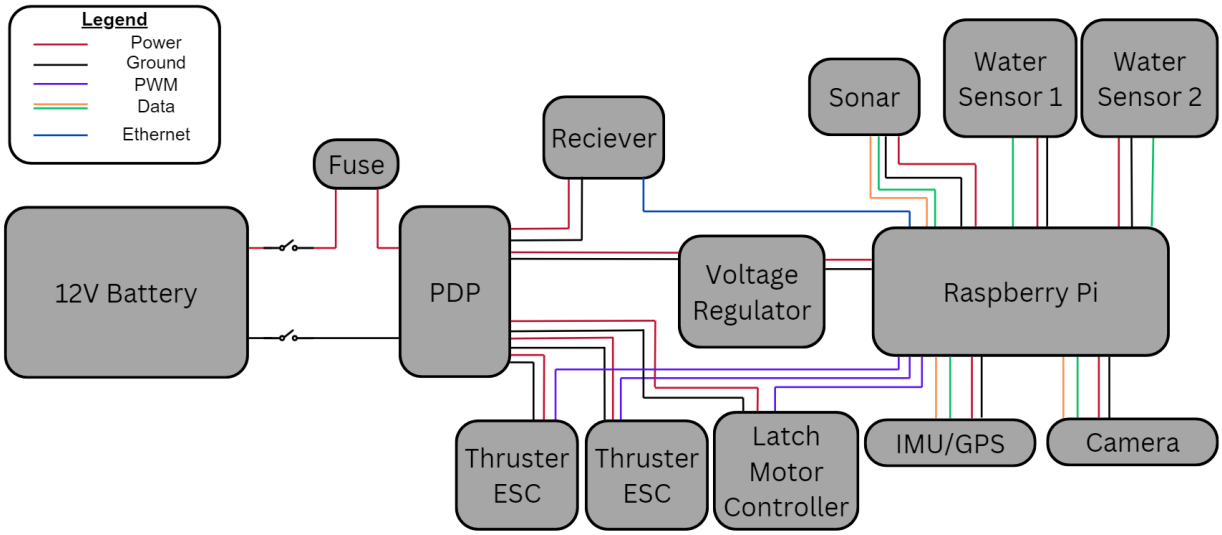

Figure 25: Complete wiring diagram of a single robot and all its components labelled. A legend for different wire purposes is included in the top left corner.

To control the robots while they are active in a large body of water, a long-distance communication network was developed to have an onshore control center with an endpoint on each robot. This control center contains a Wi-Fi router configured as an access point (AP) for the local network, directly tethered to two long range wireless ethernet bridges and a laptop with control software. The local network operates at a standard 2.4GHz frequency for short distance communication while the wireless ethernet bridges operate between 902-928MHz for strong penetration and diffraction capabilities. The lower frequency of the wireless bridges allows for an outdoor transmission range up to 2600 feet if unobstructed. For protocol purposes, one robot was declared the master, which broadcasts its Wi-Fi through one ethernet bridge to the AP, where the other robot and the controller can access it. The endpoints on each robot were tethered to the Raspberry Pi directly through an ethernet cable. A detailed diagram of the communication network is shown below in Figure 26.

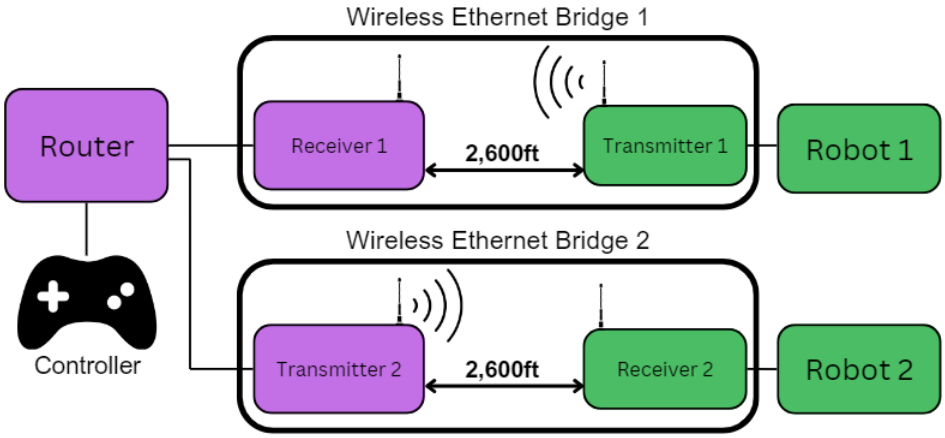

Figure 26: Diagram of the system's communication network with onshore control center components colored purple and onboard systems colored green.

3.9 Software Design & Communication

The first step in designing a robot program architecture was choosing the appropriate operating system. At the start of the project, the team was in talks with engineers at Greensea IQ about utilizing their OPENSEA software. This operating system is designed for ocean-based robotic applications, providing simple integration of navigation and control systems. Unfortunately, the company was unable to allocate the resources to this project at the time of request, forcing the team to investigate other options. After an evaluation of alternatives, an open-source variant of Raspbian Bookworm, called OpenPlotter, was adopted. OpenPlotter is designed for maritime applications and integrates control systems such as SignalK and PyPilot [54]. These integral subsystems facilitate access to a global boat registry and offer a suite of limited autonomous navigation protocols.

With the scope of this phase 1 project limited to teleoperated control, system operations make use of a master-follower framework. An operator first engages with Robot 1 via RealVNC, a remote desktop application. After establishing a connection, the operator can activate a master program, found in Appendix B-1, that initializes all subsidiary scripts. This communication and control design streamlines user engagement and guarantees the seamless functionality of the operating system. Each sensor on the robot is controlled via designated Python scripts designed for their specific task, found in Appendices B-2, B-4, and B-6. Each script extracts and refines data from a sensor, employing a series of filters to improve accuracy by removing noise. The refined data is subsequently committed to a file for reading. An auxiliary script, like in Appendix B-5, is then charged with retrieving this data and disseminating it to a designated MQTT topic. Each topic reflects a different control parameter, encompassing a robot's directional orientation, real-time GPS coordinates, and metrics from aquatic sensors [7].

Inter-system communication utilizes a MQTT server with the Mosquitto protocol housed within Robot 1. MQTT, an acronym for Message Queuing Telemetry Transport, is a streamlined communication protocol for devices with limited bandwidth, elevated latency, or unreliable network conditions [53]. The implementation of MQTT is critical in ensuring the quick exchange of information between system elements. The human-machine interface is actualized through the input of navigational commands into the console of Robot 1 by the system operator. These instructions are subsequently transmitted to Robot 2, which is synced to the movement directives and locational data transmitted from Robot 1. Then, Robot 2 executes the commands given by the operator to Robot 1, lending precise control over both robot trajectories as a single system.

4.0 Prototyping & Testing

4.1 Manufacturing

Due to the highly custom nature of the robots' design, the team manufactured most parts in house with the tools available at WPI. Harsh ocean environments required most parts to be corrosion resistant to prevent degradation, limiting options for material choice. Moreover, the need to manufacture complex geometries such as the saddle clamps and motor brackets led the team to 3D print parts via Fused Deposition Modelling (FDM) with ABS plastic. Access to multiple 3D printing labs on campus and the relatively low cost of ABS filament at $20 per kilogram added to the benefits of this manufacturing process. Watertight parts were printed via SLA which guarantees near-zero porosity through the required curing process. Any gaps left between parts during assembly were sealed using butyl tape and silicone caulking.

FDM printing with ABS plastic across multiple printers came with a significant number of challenges. Parts made in open air printers have problems with warping, where the corners of the print pull up from the bed resulting in a print failure or loss of geometrical accuracy. To resolve this issue, the team made use of heat enclosures around the printers, seen in Figure 27. These prevented uneven cooling and shrinkage of layers that cause warping. Maintaining dimensional accuracy on the saddle clamp parts proved difficult, accommodating frictional fits along perpendicular axes, preventing them from being printed on the XY plane. To solve this, the dimension of the fit not on the XY plane was exaggerated to account for layer sag.

Figure 27: Examples of heat enclosures used to prevent warping of 3D printed parts. A standard off-the-shelf Creality printer enclosure (left) and an improvised enclosure around a personal 3D printer (right).

The robot aluminum side plates presented the most challenging process to manufacture in-house. The unique streamlined shape of the robot hull required complex contours and internal hole features. These complexities require CNC routing, a process unavailable on the WPI campus, requiring outsourced machining. The team evaluated quotes from different manufacturers, eventually ordering the parts from Xometry due to their low cost and quick lead time. Once received, the plates were deburred with sandpaper and verified for accuracy by attaching complementary parts to confirm fit.

Lastly, the team purchased three, 3-foot lengths of single 80/20 extrusion stock, and collected three lengths of double wide stock from WPI ME department storage. An automatic horizontal bandsaw was programmed to cut the extrusion to 17 $\frac{15}{16}$ inches, half of the stock material accounting for an ⅛th inch blade. The ends of each cross brace were then tapped with ¼-20 threads for mounting to the frame.

4.2 Assembly

After manufacturing 3D-printed parts, assembly of the secondary hulls began. This involved using ABS cement in a ventilated room to press the flange, pipe, and saddle clamp, pictured in Figure 28, together. Then the parts were left to cure for 24 hours, forming a solid ABS body. The two PVC secondary hulls were assembled in the same ventilated space by cementing the PVC end caps to the 30in pipe. Once all the saltwater-exposed plastic parts shown in Figure 28 were assembled, they were coated with corrosion resistant paint, as mentioned previously.

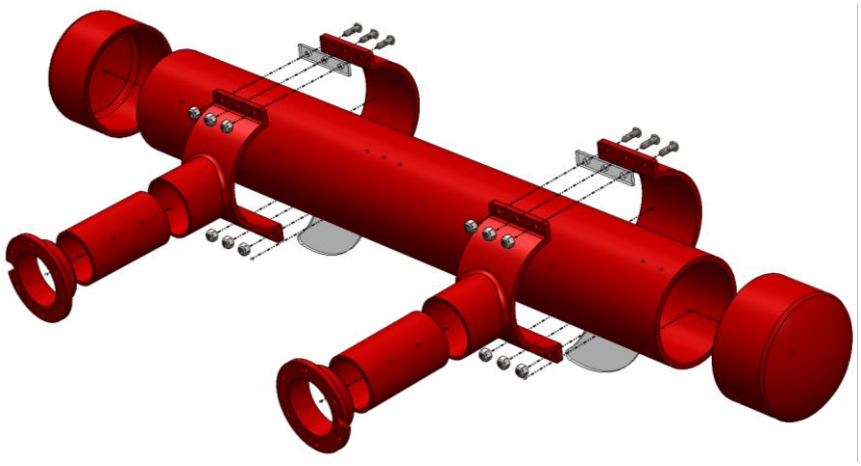

Figure 28: Secondary hull subassembly with stabilizing fins.

In tandem with the cementing and painting of plastic components, the central hull side plates were outfitted with the ABS brackets used for waterproofing the internal cavity. As seen in Figure 29, all brackets were bolted to the aluminum side plates, using rubber washers on the outsides of each plate to protect against water intrusion and corrosion. Once each plate assembly was complete, they were attached together using

18in 80/20 extrusion that slots between the sealing brackets and bolts to each side plate. It was important to first attach all 80/20 rails to just one plate, so 80/20 slot nuts could be placed inside each piece of extrusion. To keep the frame watertight, the nut rails are inaccessible after sealing. Thus, each rail had to hold the correct number of slot nuts to for polycarbonate panels attachment before the second plate was attached. Lastly, the mounting features for the secondary hull were attached, using rubber gaskets to waterproof between the ABS and aluminum plate interface. This completes the structural framing for the central hull, shown on the right in Figure 29.

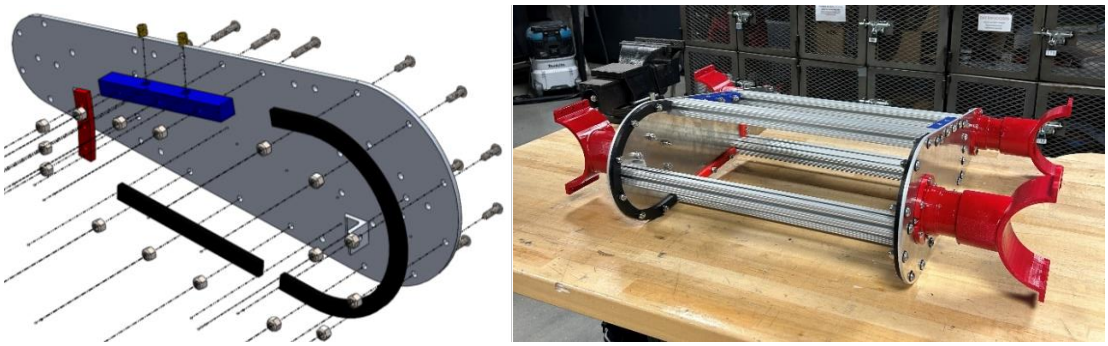

Figure 29: Assembly method of central hull side plate with sealing brackets (left) and complete hull structural assembly (right).

Once the central hull was complete, the polycarbonate panels were attached to create a watertight and buoyant central cavity. This was done by lining colored ABS sealing brackets with butyl tape, a waterproofing adhesive liner with the consistency of clay. The butyl tape was kneaded into the corners between the aluminum plate and brackets to easily conform to the curved surface. Another layer of liner was added along the length of each 80/20 aluminum extrusion, on either side of the bolt channels. Then each polycarbonate plate was carefully placed onto the butyl tape, ensuring the bolt pattern aligned with extrusion slots. Once alignment was ensured and nuts were properly configured below bolt holes, each plate was bolted down one row at a time, shown in Figure 30. At this stage, it was important to apply compression evenly across a row, tightening every bolt in small increments. After all bolts were tightened, the butyl tape compressed by roughly 50%, allowing the polycarbonate plate to rest flush against the curved aluminum surface. Given the intended watertight nature of the internal cavity, once attached, the front, bottom, and back polycarbonate panels could not be removed without damaging the butyl tape. Thus, the top hatch of the robot was intended to securely seal the robot when bolted down and be easily detached for access to electronics. This was done by lining the hatch opening with a rubber gasket that only adheres to surfaces on one side. Then, secondary PVC pipe hulls were inserted into their respective mounts and clamped in place, seen in Figure 30, along with the fin stabilizers.

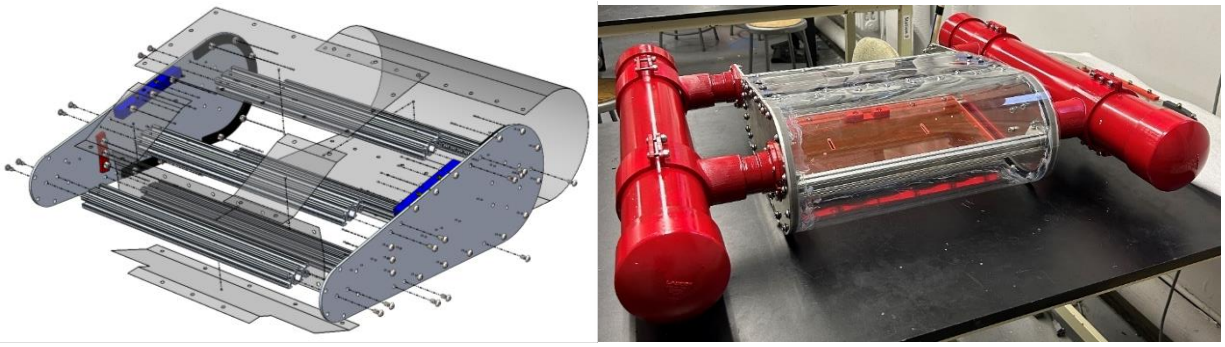

Figure 30: Assembly method for robot central hull with polycarbonate panels (left) and fully assembled robot with all 3 hulls and sealed central cavity (right)

Following the assembly of the robot body, secondary components such as thrusters and the latch mechanism were attached. Importantly, a stand was manufactured to support the robots at their structural elements, 10in above ground, to prevent the robot from resting its weight on the thrusters. The latch mechanism shown on the left in Figure 31 was assembled independently then bolted to the back exposed 80/20 extrusion. Two holes were then drilled into the back polycarbonate sealing panel to install grommets, or wire ports. These ports clamped to either side of the panel with O-rings to prevent leaking and were tightened around the 3 motor wires, as shown on the right in Figure 31. Finally, the previously discussed “aero panels” meant to streamline the unsealed back of the robot, were secured to the 80/20 extrusion, completing assembly.

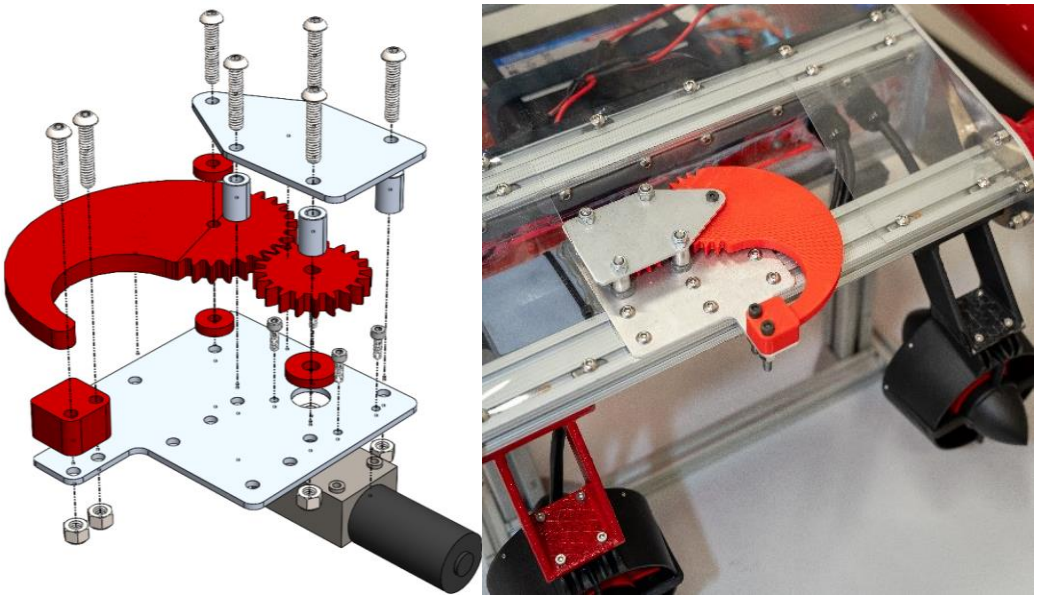

Figure 31: Assembly method for automatic net latching mechanism (left) and back of robot with attached latch mechanism, thrusters, wire ports, and aero panels (right).

4.3 Troubleshooting

Despite following best practices in sealing the central hull, leaks still occurred. After placing the first robot in the WPI pool, the team noticed a slow trickle of water into the central hull from the bottom of the panels. Initially, this problem was solved by using gel-like silicone caulking to fill in any gaps too small to see. The caulking was used to generously line all inside seams of the robot. Though a seemingly sound idea, further testing saw the same leak locations and rate as before adding the caulk. Upon further analysis, the team concluded that the ultra-flexible polycarbonate was slightly pulled away from the butyl tape when under pressure. This became evident during a pool test where the robot would only begin leaking once a team member applied pressure to the polycarbonate hull. Though, the leaks remained slow, further indicating imperceivable gaps being created between the polycarbonate and butyl tape. It is important to emphasize the hardshell design standard amongst aquatic ROVs, which prevents material flexure from breaking seals. Again, this route was not taken by the team as it would have been unaffordable. With the current plated design, the adhesive butyl tape was pulled in tension to resist flexure, its weakest support direction. To solve the leak problem, a secondary source of adhesion was used to resist flexure via compression. This was done by folding 2in segments of Flex Tape, a more adhesive butyl tape composite, over the exterior seam between the polycarbonate and aluminum plate. This compressive application was intended to prevent the panels from flexing at their seams while still allowing flexibility along non-sealing surfaces, shown in Figure 32. After the addition of Flex Tape, leaking was no longer observed during pool testing, even under near-complete forced submersion of the hull's front.

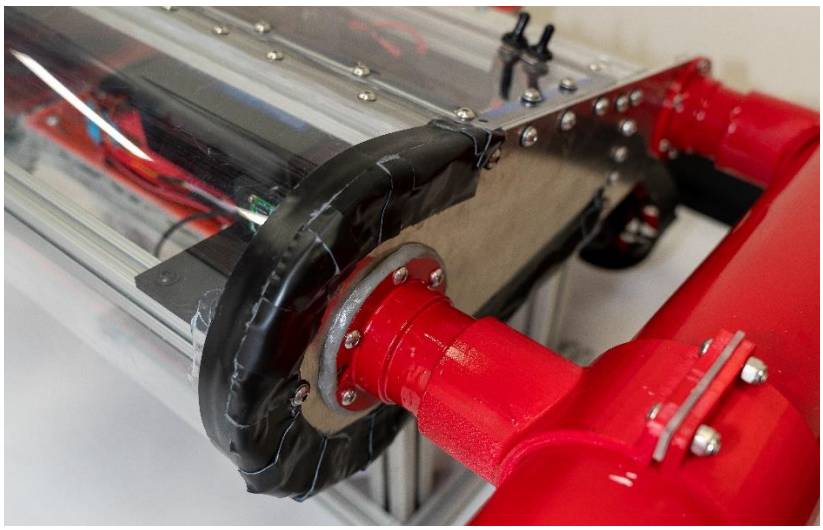

Figure 32: Flex Tape along the outside polycarbonate-aluminum panel interface.

Once leaking issues were resolved, the team felt confident installing electronics for continued testing. The circuitry network described in Section 3.8 was then mounted atop the central acrylic electronics plate, raised slightly above the hull's bottom to rest

on structural 80/20 extrusion. The thruster and latch mechanism motor controllers, along with the Wi-Fi receiver, required 12v to operate. The sonar, water sensors, and GPS IMU alternatively used 5v supplied from the Raspberry Pi, itself receiving 5v from a 12v-5v stepdown voltage regulator. Relying on the Raspberry Pi for sensor power distribution puts unnecessary current load on the CPU. The limited voltage output ports on the Raspberry Pi were also limiting in sensor choice, requiring that both water sensors draw power from the same port. Though never causing immediate problems with the existing prototype, future iterations should consider alternative and more robust power distribution and voltage regulation methods. With little specifications for system current draw, the team was unsure of how to best protect against circuit overload without limiting operational abilities. Though 10A fuses could operate the robot in air, the added load of water on the thrusters immediately blew the fuse. This led to the adoption of 30A fuses, allowing complete operation while protecting the 40A ESCs from overload.

The initial decision to adopt a custom, open-source variant of Raspbian Bookworm—tailored specifically for maritime applications—was not without its complexities. While OpenPlotter offered pre-integration with marine systems, the team faced the challenge of fine-tuning it to the necessary requirements. Customizing the OS involved navigating dependencies, ensuring compatibility with chosen hardware components, and optimizing resource allocation. For example, configuring device drivers for GPS modules and interfacing with GPIO pins on the Raspberry Pi demanded attention to detail in electronics layout and software design.

Implementing system teleoperation control required seamless communication between Robot 1 (master) and Robot 2 (follower). This required minimizing latency while propagating commands between the two robots. The team encountered challenges related to network delays, especially when transmitting real-time movement instructions. To mitigate this, techniques such as predictive command buffering, adaptive message prioritization, and asynchronous data synchronization were utilized.

The system relied on an array of sensors—GPS, water sensors, and compass modules—to provide accurate situational awareness. However, some sensor data was inherently noisy due to environmental factors (waves, electromagnetic interference, etc.). Kalman filters and sensor fusion algorithms were used to find meaning throughout potentially noisy data. For instance, combining GPS coordinates with compass headings required fusion techniques to suppress outliers and enhance accuracy.

4.4 Validation Experiments & Methodology

Given the rather short developmental period allowed by MQPs, the team made many assumptions throughout the design of the two robots. Experimentally testing theoretical calculations was important to validate the design assumptions made. For example, it was assumed that the robots would float at their symmetric midline and maintain that position while in motion. Underwater thrusters force watercraft to pitch upwards when in motion, causing inefficiencies in the process. The actual waterline of the robot was tested experimentally by floating the robot in still pool water and measuring the position relative to horizontal. The pitch of the robot while in motion was tested using the onboard gyroscopes, assuming the natural position as level. Results for the currently described experiments and those that follow can be found in Section 5.

To compare theoretical drag force and efficiency calculations with reality, both static thrust and horizontal terminal velocity were required. Static thrust was measured using a deflection-based force gauge, attaching one end of the gauge to a static surface and the other end to the robot's back. Once secured, the robot was driven forward at full power, held in place by the static force gauge while a pulling force measurement was obtained. Terminal, or peak velocity, of the robots was measured during an open water test at the local Lake Quinsigamond, along with other motion-based measurements like pitch and tow angle. Velocity was measured by first having a robot reach top speed, assumed after roughly 30 seconds of straight-line driving. Then, without slowing down, the robot would cross a known distance while being recorded from a camera perpendicular to the path. The known distance was used to scale the recorded video appropriately while the recorded time was used to calculate velocity. Velocity was used to determine the robot drag coefficient and to determine system energy efficiency.

Lastly, the breaking force of the net latching mechanism was determined in a similar manner to static thrust. An extra latch gear, pinion gear, and latch catch were printed with the intention of breaking them to determine where along the 3D-printed parts, and at what force the parts would break. This test was intended to simulate the net becoming overloaded or caught, tugging backwards on the robots. The latch mounting plate was detached from the robot and secured with a table-mounted vise. To simulate the back-drive resistance of the worm gear motor, the motor was replaced with a bolt to lock the pinion gear in place. Then, a deflection-based force gauge was secured to the latch gear and pulled directly backwards, mimicking the tension of the net. Force was applied until one of the 3 plastic components broke, measuring the peak force applied at the time of fracture.

5.0 Results

5.1 Latch Mechanism Force to Fracture

With the methodology described in Section 4.4, the latch gear mechanism was tested for force to fracture. This test was meant not only to find the force value, but also determine which part would break first. Though the team expected the gear teeth to be the weakest member, the tail end of the latch gear, close to the site of applied force, broke first. As pictured in Figure 33, the latch gear fractured roughly 1.5in from its tip, near the line of action. With a 3D-printed wall thickness of 1.2mm and 60% infill density, the tip of the gear was mostly solid plastic. The point of fracture is likely where the infill begins to bear most of the load, and where less wall material is present.

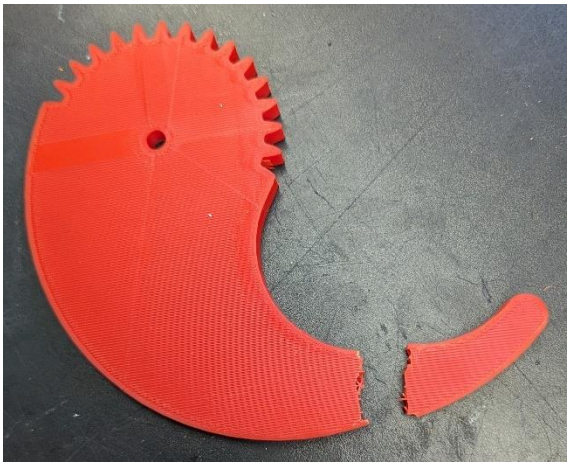

Figure 33: Fracture point of latch gear.

At the time of fracture, the gauge measured a peak force of about 302N, much less than the theoretical breaking force of 5768N, calculated in Section 3.5. The theoretical breaking force was calculated after the experiment was conducted to understand where along the gear stress would peak. At the same fracture point, the theoretical breaking force is much higher due to the assumed solid ABS plastic cross section. Importantly, the true breaking force of about 300N far exceeds the theoretical maximum thrust of the robot, 68N under no load. This means the robots would be restrained from moving forward long before the latch mechanism breaks under stress.

5.2 True Buoyancy and Pitch Angle

Based on the Solidworks model of the robot and as discussed in Section 3.3, the theoretical buoyant potential of the robot is 53.54kg given its total enclosed volume. This means that a 53.54kg robot would float with the top of the robot level with the waterline. With a vertically symmetric hull, to keep half of the robot above water, the robot had to weigh at most 26.77kg. Given applied Solidworks material properties, the total weight of the robot was estimated to be 23.92kg, 2.85kg less than maximum. In

theory, this would make the robot float just above the midline of the hull, assuming the cumulative buoyant force acts at the robot's center of mass. As pictured in Figure 34, a solid body version of the robot was created in Solidworks to determine the geometric center of buoyancy. Though the buoyant force and weight were assumed to act at the same point, the center of buoyancy (blue) lies 2.73in in front of the center of mass (red). This means the robots would pitch upwards above the horizontal dashed midline at the front of the hull, a characteristic further exaggerated when in motion.

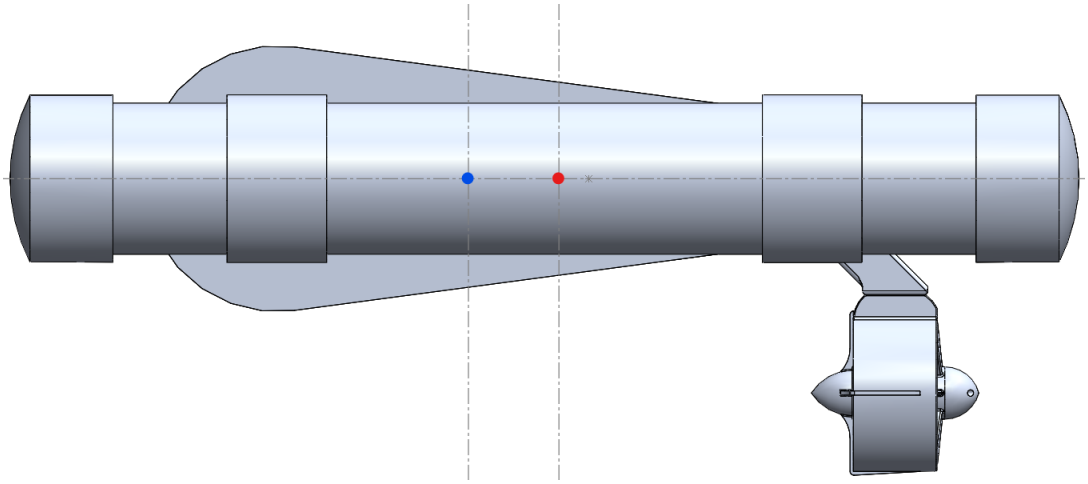

Figure 34: Robot center of buoyancy pictured at blue dot, and center of mass at red dot.

The true weight of the robot, as measured on a standard scale, was **25.25kg**, only 1.33kg heavier than predicted and still 1.52kg less than half the buoyant potential. In static water, the upwards pitch of the robot was clearly visible with the back of the robot dipped further into the water while the front rose out above the midline. The left of Figure 35 below shows the midline measurement of the robot. Translated into the CAD model shown on the right, the robot's true waterline, shown in blue, is **3.63deg** from the midline, shown in black. This upwards pitch impacts overall drag and system performance accounted for in the following section.

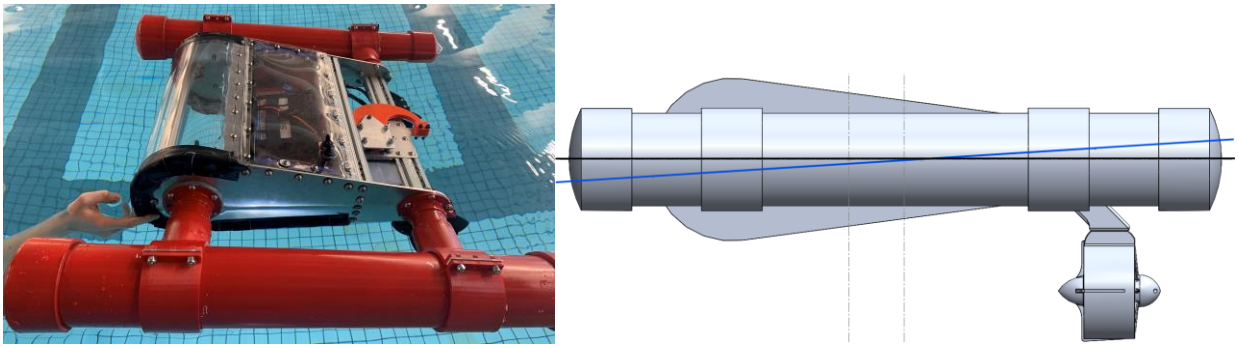

Figure 35: Waterline float test of robot (left) and CAD model of waterline angle (right).

During an open water test at Lake Quinsigamond on Wednesday April 17th, 2024, the robots were stress tested to validate specific design parameters. As mentioned, the robot statically rests in the water 3.63deg from horizontal, with the back of the robot dipped further into the water. When the robot travelled forward, it had the tendency to pitch further upwards, a phenomenon that occurs with any back-driven small aquatic craft. During the open water test, the robot pitched upwards by 6.93deg from its static waterline, or 10.56deg from theoretical horizontal. The theoretical waterline is shown in black in Figure 36, the true static waterline is shown in blue, and the dynamic waterline in red. Given the downwards pitch of the robot's back when static, the thrusters are naturally tilted down slightly. When powered, the thrust is not only applied horizontally but also vertically, further pitching the robot upwards while in motion.

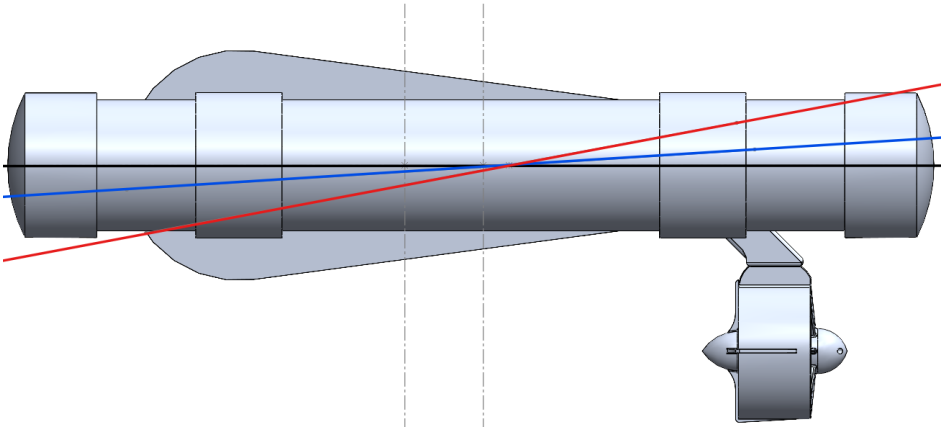

Figure 36: Robot theoretical, static, and dynamic waterlines based on test conditions.

Though some upwards pitch was expected when in motion, the greater the pitch angle, the more the robot's drag profile is affected. As seen by the dynamic waterline shown as red in Figure 36, most of the robot's secondary PVC hull was out of the water when moving. This could negatively affect the robot's stability and drag reducing characteristics when in harsh ocean conditions. Ideally, the robot's thrust is applied parallel to the waterline to minimize pitch and keep most of the robot's surface area and weight distributed across the water. Figure 37 below shows a real example of the dynamic waterline during an open water velocity experiment.

Figure 37: Robot floating in the water while in motion during an open water experiment.

5.3 True Drag Force and Drag Coefficient

Given the significance of energy efficiency in validating the robot design's effectiveness, reducing drag and optimizing performance was important. Section 4.4 details the two experiments conducted to obtain static and dynamic thrust values for the robots, allowing a simple comparison with theoretical calculations. During a pool test, a single robot had a measured static thrust of **45.8N**, compared to a theoretical thrust of 65.8N at full power. Static force can also be calculated using the following equation, where density is 1000kg/m^3 and $A_{thruster}$ represents the area of both 4.5in diameter thrusters.

$$F_{static} = \rho \times A_{thruster} \times v_{water}^2$$

The equation can be rearranged to solve for the exit velocity of the water passing through the thrusters, given the known static thrust of 45.8N.

$$v_{water} = \sqrt{\frac{45.8N}{1000\frac{kg}{m^3} \times 0.020522m^2}} = 1.494m/s$$

With this known exit velocity of the water from both thrusters, the dynamic thrust force of each robot can be calculated using the following equation, where v_{robot} is the steady state velocity of the robot.

$$F_{dyn\,amic} = \rho \times A_{thruster} \times v_{water} \times (v_{water} - v_{robot})$$

During the open water experiment, the robot was timed and recorded driving between two points of known distance, after first accelerating for 30 seconds. After 30 seconds, the robot was assumed to be traveling at constant velocity. The two known points were measured to be 95m apart, taking the robot 130 seconds to travel the distance. This yielded a robot velocity of **0.731m/s** when operating the motors at 12v and half power. Below, the dynamic thrust of the robot is calculated using this velocity.

$$F_{dyn\,amic} = 1000\frac{kg}{m^3} \times 0.020522m^2 \times 1.494\frac{m}{s} \times \left(1.494\frac{m}{s} - 0.731\frac{m}{s}\right) = \boldsymbol{23.39N}$$

When a moving object reaches constant speed, thrust force is equal to drag force and acceleration is zero. Assuming the robot was at constant velocity, 23.39N represents the drag force experienced by the robot. This is nearly 4 times higher than the calculated 6.89N of drag force the designed robots were expected to experience. This large difference between theoretical and experimental drag force likely comes from the additional drag of the secondary hulls and motors that were previously ignored. Additionally, the design robot was expected to have a wetted area of 0.04645m^2 while the actual robot's static pitch of 3.63deg yields a wetted area of 0.043972m^2.

With these values in mind, the true drag coefficient of each robot is calculated below using the true wetted area, velocity of the robot, and calculated drag.

$$F_{drag-hull} = \frac{1}{2} C \rho A v^2$$

$$C = \frac{2 \times 23.39N}{1000 \frac{kg}{m^3} \times 0.043972 m^2 \times (0.731 \frac{m}{s})^2} = \mathbf{1.99}$$

Like the comparison between experimental and theoretical drag, the experimental drag coefficient is nearly 4 times greater than the theoretical value of 0.5 used previously. Though a drag coefficient of 2 is relatively high, it is rather insignificant considering the low speeds, current, and wave conditions experienced during testing. Drag had little impact on the overall performance of the robot during open water testing and the overall thrust of 45.8N is nearly double the experienced drag of 23.39N. This means the two robots have a combined 44.82N of additional thrust that is applied directly to towing the net. Essentially, the robots will continue operating at 0.731m/s until enough trash fills the net to induce 44.82N of drag. To calculate a more comprehensive and accurate dynamic drag coefficient for the robots, computer simulations of fluid flow would be required.

5.4 Experimental System Efficiency

A theoretical power draw of 540W per motor, or 1080W per robot, yields a theoretical robot thrust of 68.67N when the motors are supplied with 12 volts. To conserve battery life during experimental demonstrations, the thrusters were only ever run at half-power. A PWM signal of 1200 resulted in only 21.24W of power being drawn, according to motor characteristic data collected by another WPI MQP team [44]. These power conditions are responsible for the 45.8N of static thrust and 0.731m/s velocity measured in the previous section. With 4 thrusters each consuming 21.24W of power and providing thrust to travel at 0.731m/s, the system consumes 116.22kJ per kilometer traveled. Assuming the same trash density of 50kg/km^2 and separation parameter of 137/km described in Section 3.7, the following is the true system energy usage.

$$MQP\ Experimental\ Efficiency = \frac{116{,}220\ \left(\frac{J}{km}\right)}{50\ \left(\frac{kg}{km^2}\right)} \times 137\ \left(\frac{1}{km}\right) = \mathbf{318.44} \frac{\boldsymbol{kJ}}{\boldsymbol{kg}}$$

An experimental energy usage of 318.44kJ/kg is 24 times less than the theoretical 7685kJ/kg calculated previously. The experimental value is also less than h half the 794.8kJ/kg used by The Ocean Cleanup. While these values are lower than anticipated, full system functionality would utilize 24-volt supply, requiring more power. The unexpectedly low energy usage can be attributed to battery conservation.

5.5 Discussion of Results

The series of validation experiments conducted sheds light on the design viability of the constructed robotic system. Though the unconventional plated robot design created more seams to waterproof than traditional plastic hulls, frequent pool testing allowed for simple solution development. After significant sealing additions to the primary robot hull, no further leaking occurred during at least 10 subsequent water tests. However, the team still found it essential to include onboard water sensors as an extra security feature to prevent possible electronics damage. The metal-plated design also acted as a faraday cage, preventing long range communication systems from penetrating the hull. This proved especially challenging in receiving GPS signals on the Raspberry Pi-mounted IMU, requiring the addition of a GPS antenna mounted on the outside of the robot's hatch panel. Additionally, a long-range Wi-Fi communication antenna was also mounted to the outside of the hatch panel to extend range for open water experimentation. Though functional for its desired purpose as a first prototype, the plated hull design led to significant difficulties with waterproofing and communication.

Figure 38: Tandem robot operation during Lake Quinsigamond open water test.

During the open water test at Lake Quinsigamond, the robot's pitch angle and speed were measured while the performance of the two-robot surface trawling system was evaluated. Though trash could not be added to the water for testing purposes, the team was satisfied with the robot's ability to tow the net and maintain system functionality, shown in Figure 38. Though, the calculated drag coefficient and measured pitch angle certainly led to increased inefficiencies during operation. Overall, the measured speed of 0.73m/s fell just short of the 0.77m/s designed speed, an inconsequential difference for an initial prototype. As mentioned, all robot systems were operating at near-half power, to conserve battery life. During the open water test, the greatest difficulty experienced was battery life and power output. Lead-acid batteries have a rather low power density and cannot maintain peak load conditions for extended periods. This led to inconsistencies in performance and even momentary system brownouts after just 2 hours of operation. Limiting power to the motors also made it challenging to overcome currents in the lake, reducing speeds and towing capacity.

6.0 Conclusions

From its inception, this project was intended to prove the viability of a commercial, optimized, and decarbonized swarm-style robotic platform for ocean cleanup efforts. Throughout the development of the prototype robots, comparisons were made to two primary industry counterparts. Blue Robotics and their Blue ROV is an aquatic robot of similar size and multi-functionality to the MQP cleanup robots. Comparing basic metrics between Blue ROV and MQP ROV gives a benchmark of how the team's robot likens to industry standards. Table 2 below gives a breakdown of some basic metrics, showing the greater cost efficiency and towing capacity of the MQP ROV when compared to the Blue ROV counterpart.

Table 2: Comparison of benchmark metrics between Blue ROV and MQP ROV.

Comparison	MQP ROV	Blue ROV
Weight	25kg	12kg
Cost	$1000	$4500
Thrust	45.8N	9N

As the primary surface trawling system of focus for the team's commercialization, optimization, and decarbonization (COD) efforts, the team primarily compared with The Ocean Cleanup's (TOC) System 003. Previously discussed in Section 3.7, the large-scale operations of TOC are advantageous in energy efficiency, consuming a tenth the energy for every kilogram of trash collected when compared to a single MQP ROV pair. TOC operates 3 tugboats with a total carrying capacity of around 1800 tons and a capital cost of roughly $10.5 million. To match this capacity, the MQP design developed would require 115 robot pairs at a cost of $230,000, and a 2000 ton carrying barge at a cost of $4 million. Though consuming more energy, the swarm-style autonomous cleanup method requires less than half the capital investment of traditional surface trawling systems used by TOC, shown in Figure 39. Operational savings are also expected given the autonomous nature of the robotic cleanup fleet.

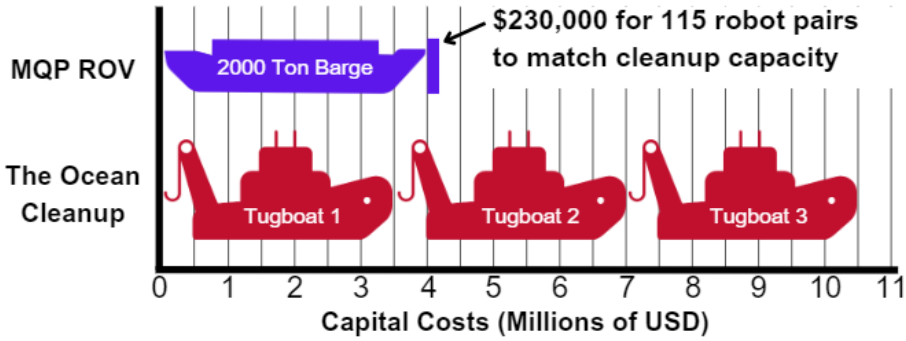

Figure 39: The Ocean Cleanup and MQP ROV capital cost comparison.

The inclusion of onboard sonar and the capacity for additional sensors allows the robots to act as passive data collectors while cleaning the oceans. The National Oceanic and Atmospheric Administration (NOAA), offshore wind companies, along with many other commercial enterprises buy oceanographic data for research and development. While most ocean cleanup companies rely entirely on donations for funding, the commercially viable MQP system permits rapid scaling and growth of cleanup efforts. Since each robot essentially acts as a wave-surfing robotic tugboat, their design versatility allows them to take on additional towing-based applications. One alternative would make use of the robots to skim oil or other pollutants off the surface of water using a specialized skimmer instead of a net. This would take humans out of potentially hazardous environments and provide a more customized cleanup platform. Though designed for open-ocean environments, the robot pairs could also be deployed at smaller scale as automated sweepers in ports or harbors.

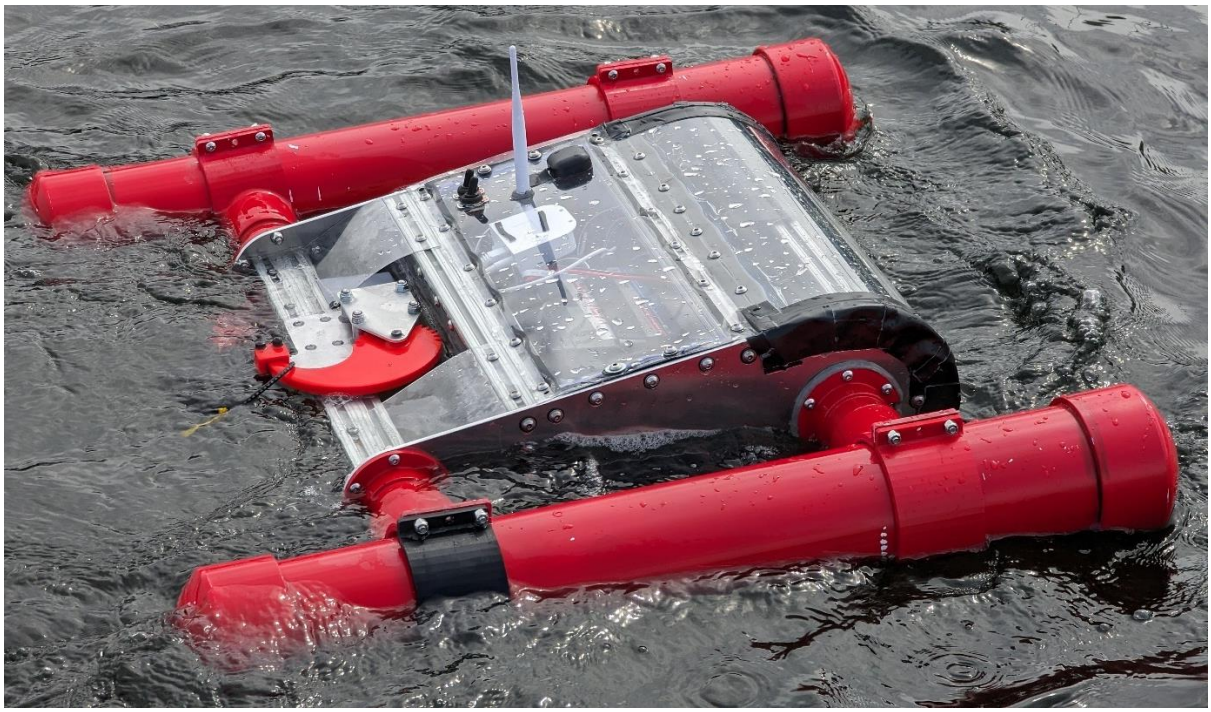

Figure 40: MQP ROV in motion during the Lake Quinsigamond open water test.

In conclusion, the robot designs and prototypes developed as a part of this MQP open the door to a new application for water-based robotics. The goal of the project was to commercialize, optimize, and decarbonize existing surface trawling ocean cleanup systems. In just 8 months, the team is proud to have accomplished and validated their goals through the development of a novel robotic ocean cleanup system. Future work on this project, discussed in the following section, will seek to continue optimization and autonomous control implementation.

7.0 Future Work

As the development of this project continues into future years, specific areas should be prioritized to improve upon the current robot design and functionality. The current robot prototypes were structurally sound and consistently met design requirements, leading the next phase of this project to focus on autonomous control. Though the robots were equipped with all the sensors necessary for full autonomy, the timeframe of the current MQP only allowed for the development of teleoperation code. In following years, more time can be spent on the design and implementation of full autonomous system infrastructure. This should allow the robots to easily communicate with each other to maintain separation distance, direction, and pathing maneuvers. Further design for swarm-style communication and coordination should also be considered. To best implement these features, it is recommended that a higher resolution camera be installed, allowing use of computer vision for target identification and tracking.

A limiting factor during the first year of development was the use of a 12-volt lead acid battery. With waterproofing issues solved, it is now safe to install a higher power density lithium-ion battery. A 24-volt lithium-ion battery of similar size to the current battery would allow each robot to utilize more thrust, having the power to overcome strong currents and increase towing capacity. Lithium-ion batteries can also increase battery life to nearly 12 hours and improve overall performance. In addition to battery upgrades, immediate improvements should also include replacing the latch gear motor. The installed worm-drive motor was not intended for water-based applications and implemented sealing techniques were not reliable over extended periods in the water. Replacing this motor with a waterproof servo or DC-motor would improve reliability and increase functionality.

While less important to immediate system upgrades, an improved cost model would benefit the robot's commercialization strategy. Accounting for economies of scale in the mass production of the robot and estimating operational costs should be considered. Conducting a failure analysis on the swarm functionality of a large-scale cleanup operation could also prove advantageous in developing a commercial model. This model should also include a detailed energy usage breakdown and make considerations for renewable energy charging via an onboard solar array.

After commercialization improvements, slight design upgrades, and autonomous implementation, a refined and production-ready model should be created. An ideal production model would replace the metal plated central hull with a uniform injection-molded plastic hull. This design was forgone during the current prototype phase due to the capital cost of an injection mold. Though, at production-scale, these capital costs would be countered by mass-production cost savings. A uniform plastic hull design would reduce leak potential and allow for a more drag mitigating custom shape.

To improve the reliability of autonomous control implementation and drag reduction, the team further recommends the use of ProteusDS software. This software provides advanced dynamic ocean models and performance characterization of vessels in designed ocean conditions. Though expensive, modeling the hull shape in a dynamic solver can help visualize real-world behavior at sea. Commercial-scale fleet design and swarm autonomy would benefit from these additional design considerations. s

Finally, what would a perfect version of a robotic replacement to The Ocean Cleanup's System 003 look like? A 2000-ton barge equipped with cranes and loaded with 115 robot pairs travels out to sea. A small crew large enough to operate the barge and oversee the robot operations lives on the barge during assignment. Once the barge reaches its desired cleanup location, the ship cuts engine power and/or drops anchor to hold position. At this time, the fleet of robots is deployed into the water. Each of the 115 robot pairs is given a designated collecting area and a designed sweep path. The robot latch mechanism is equipped with pressure sensors to measure the tension in the net, corresponding to the weight of trash collected. Once a robot pair reaches capacity, it automatically navigates back to the barge to be emptied. The robots position themselves so a mechanized crane can reach down to the latch mechanism. Once aligned with the latch mechanism, the robot and crane coordinate a transfer. This allows the barge cranes to automatically remove the net from the back of each robot, emptying the trash contents onto the barge. Then the system resets and the robots proceed with cleaning their designated paths. Most cleaning operations occur at night when waters are calmer, allowing onboard solar panels to charge the robots during the day. Once the barge reaches capacity and trash is secured, the robots are brought back aboard, and the barge returns to land for proper waste disposal.

Humans serve a unique position on our planet as stewards of the land, and it will take creative solutions to undo the environmental disaster at hand. A hopeful picture of the future is one where all can enjoy the beauty our Earth has to offer. Let's all do our part in cleaning the world of our waste.

References

[1] “About,” *The Ocean Cleanup*. Available: https://theoceancleanup.com/about/.

[2] “About the Project - SEACLEAR,” *SEACLEAR*, 2024. Available: https://seaclear-project.eu/about-main/about-seaclear.

[3] “ABS Plastic,” *Curbell Plastics*, 2023. Available: https://www.curbellplastics.com/materials/plastics/abs/

[4] “Advantages of Adding Twin Outboards to Your Boat,” *Blazer - High Performance Boats*, Mar. 18, 2021. Available: https://www.blazerboats.com/5-Advantages-of-Adding-Twin-Outboards-to-Your-Boat-1-10618.html.

[5] A. Lida, “Surfing 101: Fins,” *Everyday California*, Jan. 28, 2021. Available: https://www.everydaycalifornia.com/blogs/everyday-thoughts/surfing-101-fins.

[6] “14.4 Archimedes’ Principle and Buoyancy | University Physics Volume 1,” *State University of New York*, 2024. Available: https://courses.lumenlearning.com/suny-osuniversityphysics/chapter/14-4-archimedes-principle-and-buoyancy/#:~:text=This%20weight%20is%20supported%20by,fluid%20displaced%20by%20the%20object.&text=FB%3Dwfl%2C,mathematician%20and%20inventor%20Archimedes%20(ca.

[7] A. Sorensen, “Marine Control Systems - Propulsion and Motion Control of Ships and Ocean Structures,” *Department of Marine Technology - Norwegian University of Science and Technology*, 2013. https://folk.ntnu.no/assor/publications/marcyb.pdf

[8] A. Zucconi, “The Mathematics of Catenary,” *Alan Zucconi*, Dec. 13, 2020. Available: https://www.alanzucconi.com/2020/12/13/catenary-1/.

[9] B. Disisto, “Will this be our biggest ever river catch? | Updates,” *The Ocean Cleanup*, Apr. 17, 2024. Available: https://theoceancleanup.com/updates/the-ocean-cleanup-makes-biggest-ever-river-catch-in-guatemala/.

[10] “Barges for Sale,” Sun Machinery Corp., 2024. Available: https://www.sunmachinery.com/barges_for_sale.html.

[11] “Butyl Tape: The Ultimate Guide,” *General Sealants*, Inc., Mar. 25, 2022. Available: https://www.generalsealants.com/butyl-tape-the-ultimate-guide/.

[12] “46 CFR Part 3 -- Designation of Oceanographic Research Vessels*,” Code of Federal Regulations*, Apr. 23, 2024. https://www.ecfr.gov/current/title-46/part-3.

[13] “’Circular Explorer’ - by oeoo & Holcim,” *One Earth - One Ocean e. V.*, 2024. Available: https://oneearth-oneocean.com/en/the-solution/circular-explorer-by-oeoo-holcim/.

[14] “Clean Sea Solutions | Waterfront cleanup solutions,” *Clean Sea Solutions*, 2024. Available: https://www.cleanseasolutions.no.

[15] “Dashboard,” *The Ocean Cleanup*, 2024. Available: https://theoceancleanup.com/dashboard/.

[16] D. Padilla-Vasquez, “Protect Our Planet from Plastic Pollution: 5 Things to Know,” *unfoundation.org*, May 31, 2023. Available: https://unfoundation.org/blog/post/protect-our-planet-from-plastic-pollution-5-things-to-know/.

[17] D. Sukanan, “Discarded fishing nets are a menace to corals and marine life,” *Sustainability Times*, Jul. 02, 2021. Available: https://www.sustainability-times.com/environmental-protection/discarded-fishing-nets-are-a-menace-to-corals-and-marine-life/.

[18] E. Joner, “Brushless Motor Power and Efficiency Calculations,” *Tyto Robotics*, Sep. 23, 2023. Available: https://www.tytorobotics.com/blogs/articles/brushless-motor-power-and-efficiency-analysis.

[19] “Final SeaClear demonstration: Dubrovnik - SEACLEAR,” *SEACLEAR*, Oct. 23, 2023. Available: https://seaclear-project.eu/news/news/116-final-seaclear-demonstration-dubrovnik.

[20] “Galvanic Corrosion - AMPP,” *AMPP*. Available: https://www.ampp.org/technical-research/impact/corrosion-basics/group-1/galvanic-corrosion.

[21] “Geometry Definitions,” *Glenn Research Center | NASA,* 2023. Available: https://www.grc.nasa.gov/www/k-12/VirtualAero/BottleRocket/airplane/geom.html.

[22] G. Tarjan, “Catamaran Stability | Luxury Catamaran Long Island, New York,” *Aeroyacht LTD*, Apr. 24, 2024. Available: https://aeroyacht.com/catamaran-learning-center-2/catamaran-stability/.

[23] H. Leung, “Southeast Asia Pushes Back Against Global Garbage Trade,” *TIME*, Jun. 03, 2019. Available: https://time.com/5598032/southeast-asia-plastic-waste-malaysia-philippines/.

[24] “HAWK HOBBY Underwater Thruster MAX 24V 1080W Brushless Motor,” *Amazon.com*. Available: https://www.amazon.com/HAWK-HOBBY-Underwater-Brushless-Propeller/dp/B0B5Q56HZP/ref=pd_ci_mcx_mh_mcx_views_0?pd_rd_w=E1krW&content-id=amzn1.sym.8b590b55-908d-4829-9f90-4c8752768e8b%3Aamzn1.symc.40e6a10e-cbc4-4fa5-81e3-4435ff64d03b&pf_rd_p=8b590b55-908d-4829-9f90-4c8752768e8b&pf_rd_r=S3C28YJ4NH2QQ6CR4C8A&pd_rd_wg=rczJW&pd_rd_r=52dc483f-76c2-4472-abd2-a1b7acaa32ea&pd_rd_i=B0B5Q56HZP.

[25] “How does plastic get into the ocean? – life’s a beach UK,” *Life’s a Beach*, Aug. 2023. Available: https://www.lifesabeach.org/how-does-plastic-get-into-the-ocean/.

[26] “How Much Does Injection Molding Cost? | Rex Plastics Mold Manufacturer,” *Rex Plastics*, Jul. 15, 2013. Available: https://rexplastics.com/plastic-injection-molds/how-much-do-plastic-injection-molds-cost.

[27] H. Palmer, “Fleet,” *Maersk Supply Service*, 2024. Available: https://www.maersksupplyservice.com/fleet/.

[28] H. Ritchie and M. Roser, “Where does the plastic in our oceans come from?,” *Our World in Data*, Mar. 2024, Available: https://ourworldindata.org/ocean-plastics.

[29] I. Giskes, “Tackling Ghost Gear in Mexico Waters,” *Ocean Conservancy*, Feb. 11, 2022. Available: https://oceanconservancy.org/blog/2022/02/11/tackling-ghost-gear-mexico-waters/.

[30] “Interceptor Original | Rivers,” *The Ocean Cleanup*, Jan. 26, 2021. Available: https://theoceancleanup.com/rivers/interceptor-original/.

[31] “Jellyfishbot a solution for water cleaning, depollution & preservation,” *IADYS*, 2024. Available: https://www.iadys.com/jellyfishbot/.

[32] J. Rojas, “Plastic Waste is Exponentially Filling our Oceans, but where are the Robots?” in *2018 IEEE Region 10 Humanitarian Technology Conference* (R10-HTC), Dec. 2018, pp. 1–6. doi: 10.1109/R10-HTC.2018.8629805. Available: https://ieeexplore.ieee.org/document/8629805.

[33] K. R. Zavadil and N. R. Armstrong, “Surface chemistries of lithium: Detailed characterization of the reactions with O2 and H2O using XPS, EELS, AND microgravimetry,” *Surface Science*, vol. 230, no. 1, pp. 47–60, May 1990, doi: 10.1016/0039-6028(90)90015-Z.

[34] K. Verhagen, “System 03: A Beginner’s Guide | Updates,” *The Ocean Cleanup*, Aug. 31, 2023. Available: https://theoceancleanup.com/updates/system-03-a-beginners-guide/.

[35] “Media Gallery,” *The Ocean Cleanup*, 2024. Available: https://theoceancleanup.com/media-gallery/.

[36] M. Eriksen et al., “Plastic Pollution in the World’s Oceans: More than 5 Trillion Plastic Pieces Weighing over 250,000 Tons Afloat at Sea,” *PLOS ONE*, vol. 9, no. 12, p. e111913, Dec. 2014, doi: 10.1371/journal.pone.0111913. Available: https://journals.plos.org/plosone/article?id=10.1371/journal.pone.0111913.

[37] M. Koppe, “An underwater robot to clean up coastal areas,” *CNRS News*, Jan. 23, 2023. Available: https://news.cnrs.fr/articles/an-underwater-robot-to-clean-up-coastal-areas.

[38] N. Zolotova, A. Kosyreva, D. Dzhalilova, N. Fokichev, and O. Makarova, “Harmful effects of the microplastic pollution on animal health: a literature review,” *PeerJ*, vol. 10, p. e13503, Jun. 2022, doi: 10.7717/peerj.13503.

[39] “Our Work | IUCN,” *International Union for Conservation of Nature*, 2023. Available: https://www.iucn.org/our-work.

[40] “Outboard Motor Height: Easiest Way to Find Correct Height & Height Adjustment Tips,” *ePropulsion*, Aug. 16, 2023. Available: https://www.epropulsion.com/post/outboard-motor-height/.

[41] “Plastics - Initiatives,” *World Wildlife Fund*, 2024. Available: https://www.worldwildlife.org/initiatives/plastics

[42] “Plastics in the Ocean,” *Ocean Conservancy*, Jan. 11, 2024. Available: https://oceanconservancy.org/trash-free-seas/plastics-in-the-ocean/.

[43] P. Thevenot, “Press release - 6th anniversary of the Jellyfishbot,” *IADYS*, Feb. 07, 2023. Available: https://www.iadys.com/pr-6-years-18collaborators-80-jellyfishbot-later/.

[44] R. Blair, C. Chow, G. Demanche, and O. Simon, “Underwater Filmography Using Robots,” *WPI Major Qualifying Project*, 2024.

[45] “Shape Effects on Drag,” *Glenn Research Center | NASA*, 2023. Available: https://www1.grc.nasa.gov/beginners-guide-to-aeronautics/shape-effects-on-drag/.

[46] “Standard Test Conditions (STC) of a Photovoltaic Panel,” *Alternative Energy Tutorials*, May 07, 2022. Available: https://www.alternative-energy-tutorials.com/photovoltaics/standard-test-conditions.html.

[47] “The Great Pacific Garbage Patch,” *The Ocean Cleanup*, 2024. Available: https://theoceancleanup.com/great-pacific-garbage-patch/.

[48] “Tugboats for Sale,” *Sun Machinery Corp.*, 2024. Available: https://www.sunmachinery.com/tugboats%20for%20sale.html.

[49] “Types of Marine Corrosion,” *Boat U.S.*, 2022. Available: https://www.boatus.com/expert-advice/expert-advice-archive/2012/july/types-of-marine-corrosion.

[50] U. N. Environment, “Marine litter,” UNEP - *UN Environment Program*, Aug. 18, 2017. Available: http://www.unep.org/topics/ocean-seas-and-coasts/regional-seas-programme/marine-litter.

[51] T. Walker, A. Goodman, and C. Brown, “How to Remove Abandoned ‘Ghost’ Fishing Gear from the Ocean,” *Marine Technology News*, Aug. 19, 2020. Available: https://www.marinetechnologynews.com/news/remove-abandoned-ghost-fishing-604138.

[52] “WasteShark Specs,” *RanMarine*, 2023. Available: https://www.ranmarine.io/products/wasteshark/

[53] “What is MQTT? - MQTT Protocol Explained - AWS,” *Amazon Web Services*, Inc., 2024. Available: https://aws.amazon.com/what-is/mqtt/.

[54] “What is OpenPlotter? — OpenPlotter 3 documentation,” *OpenPlotter*, 2024. https://openplotter.readthedocs.io/en/latest/description/what_is_openplotter.html.

Appendix A: Net Optimization Code

```
# -*- coding: utf-8 -*-
from scipy.optimize import fsolve
import numpy as np
import matplotlib.pyplot as plt

def equation_to_solve(a, L, x):
    return L - a * np.sinh(x / a)

def solve_for_a(L, x):
    initial_guess = 1.0  # Initial guess for the value of a
    a_solution = (fsolve(equation_to_solve, initial_guess, args=(L, x)))/2
    return a_solution[0]

min_rope_length = 3
max_rope_length = 12
plt.close()

# Lists:
# x_values = [];
# for i in np.arange(1.0,12.0,0.1):
#     x_values.append(i)
x_values = {}
Lines = {}
for j in range (min_rope_length,max_rope_length,2):
    Lines['L_'+str(j)] = []
    x_values['x_'+str(j)] = []
    for i in np.arange(1.0,float(j),0.1):
        x_values['x_'+str(j)].append(i)
        a_solution = solve_for_a(j, i)
        theta = (np.pi/2)-np.arctan((j/2)/a_solution)
        Travel = 1/(np.cos(theta)) # actual distance traveled with course corrections for per
straightline distance unit
        if Travel < 5:
            Lines['L_'+str(j)].append(abs(Travel/(i)))
        else:
            Lines['L_'+str(j)].append(0)

min_coef = min(Lines['L_'+str(max_rope_length - 1)])
min_point = np.extract(Lines['L_'+str(max_rope_length - 1)] == min_coef,
np.arange(len(Lines['L_'+str(max_rope_length - 1)])))
min_sep = round(x_values['x_'+str(max_rope_length-1)][int(min_point)], 3)
#min_sep = round(np.interp(min_coef,x_values['x_'+str(max_rope_length -
1)],Lines['L_'+str(max_rope_length - 1)],8.0,9.0),4)

# Optimal Constants:
```

```
L = max_rope_length - 1  # Total lenth of rope in meters
x = min_sep  # Distance between robots in meters (effective sweep length)

a_solution = solve_for_a(L, x)
theta = (np.pi/2)-np.arctan((L/2)/a_solution)
Travel = 1/(np.cos(theta))

print("Optimal Rope Length: " + str(L) + " m")
print("Solution for Power Consumption Coefficient: " +str(min_coef) + " 1/m")
print("Solution for Robot Separation: " + str(min_sep) + " m")
print("Solution for a:", a_solution)
print("Solution for theta: " + str(theta*(180/np.pi)) + " degrees")
print("Solution for Travel: " + str(Travel) + " m/m")

#Plotting
plt.xlabel('Distance Between Robots (m)')
plt.ylabel('Separation Parameter (1/m)')
plt.title('Distance Between Robots vs Separation Parameter')

for j in range(min_rope_length,max_rope_length,2):
    plt.plot(x_values['x_'+str(j)],Lines['L_'+str(j)],label = 'L_'+str(j)+'m')

plt.plot([0,min_sep],[min_coef, min_coef],'--',color='k') #horizontal line to optimum
plt.plot([min_sep,min_sep],[0, min_coef],'--',color='k') #verticle line to optimum
plt.annotate('(x='+str(min_sep)+', y='+str(round(min_coef,3))+')', (min_sep, min_coef),
size=14, xytext=(4.5,0.05))
plt.plot(min_sep, min_coef, 'o',color='k')
plt.xlim((0,11))
plt.ylim((0,1))
plt.xticks(np.arange(1,12,step=1))
plt.legend()
plt.show()
```

Appendix B: Robot Operational Code

B-1: Raspberry Pi Operation

```
import pigpio
import paho.mqtt.client as mqtt
 # Create a Pi object
pi = pigpio.pi()
 # Replace these with the actual GPIO pin numbers
GPIO_PIN_LEFT = 27 #actually right
GPIO_PIN_RIGHT = 17 #actually left
 # Set up the GPIO pins for output and start PWM
pi.set_mode(GPIO_PIN_LEFT, pigpio.OUTPUT)
pi.set_mode(GPIO_PIN_RIGHT, pigpio.OUTPUT)
 # Define the pulse width modulation ranges, 4.7, 50, half speed: 33, 45
MIN_PWM = 33
MAX_PWM = 45
 # MQTT setup
MQTT_BROKER = "your_mqtt_broker"
MQTT_PORT = 1883
MQTT_TOPIC = "your_topic"
 # Define the MQTT callback function
def on_message(client, userdata, message):
    msg = str(message.payload.decode("utf-8"))
    if msg == 'w':  # Forward
        pi.set_PWM_dutycycle(GPIO_PIN_LEFT, MIN_PWM)
        pi.set_PWM_dutycycle(GPIO_PIN_RIGHT, MAX_PWM)
    elif msg == 's':
        pi.set_PWM_dutycycle(GPIO_PIN_LEFT, MAX_PWM)
```

```
        pi.set_PWM_dutycycle(GPIO_PIN_RIGHT, MIN_PWM)
    elif msg == 'd':  # Turn left
        pi.set_PWM_dutycycle(GPIO_PIN_LEFT, MAX_PWM)
        pi.set_PWM_dutycycle(GPIO_PIN_RIGHT, MAX_PWM)
    elif msg == 'e':  # Turn left&forward
        pi.set_PWM_dutycycle(GPIO_PIN_LEFT, 128)
        pi.set_PWM_dutycycle(GPIO_PIN_RIGHT, MAX_PWM)
    elif msg == 'a':  # Turn right
        pi.set_PWM_dutycycle(GPIO_PIN_LEFT, MIN_PWM)
        pi.set_PWM_dutycycle(GPIO_PIN_RIGHT, MIN_PWM)
    elif msg == 'a':  # Turn right&forward
        pi.set_PWM_dutycycle(GPIO_PIN_LEFT, MIN_PWM)
        pi.set_PWM_dutycycle(GPIO_PIN_RIGHT, 128)
 # Create a MQTT client
client = mqtt.Client()
client.on_message = on_message
client.connect(MQTT_BROKER, MQTT_PORT)
client.subscribe(MQTT_TOPIC)
client.loop_start()
 # Clean up on exit
pi.stop()
```

B-2: Water Sensor Data

```
import pigpio
import paho.mqtt.client as mqtt
import time
# Initialize the MQTT client
mqtt_client = mqtt.Client()
# Set up MQTT broker details
mqtt_broker = "192.168.10.189"
mqtt_port = 1883
mqtt_topic = "Leak"
# Connect to the MQTT broker
mqtt_client.connect(mqtt_broker, mqtt_port)
# Initialize pigpio
pi = pigpio.pi()
SENSOR_GPIO = 10
pi.set_mode(SENSOR_GPIO, pigpio.INPUT)

try:
    sensor_state = pi.read(SENSOR_GPIO)
    if sensor_state == 1:
        print("Water detected")
        # Publish a message to the MQTT topic
        mqtt_client.publish(mqtt_topic, "Water detected")
    else:
        print("No Water Detected")
except Exception as e:
    print(f"An error occurred while reading the sensor: {e}")
finally:
    # Clean up
    pi.stop()
    mqtt_client.disconnect()
```

B-3: PID Implementation

```
from simple_pid import PID
import pigpio
# Create a Pi object
pi = pigpio.pi()
# Replace these with the actual GPIO pin numbers
GPIO_PIN_LEFT = 27  # Actually on the right side
GPIO_PIN_RIGHT = 17  # Actually on the left side
# Define the pulse width modulation ranges
MIN_PWM = 4.7
MAX_PWM = 50
def set_motor_speeds(left_speed, right_speed):
    # Map the speeds to the PWM range
    left_pwm = map_speed_to_pwm(left_speed, 'left')  # Speed increases with
decreasing PWM
    right_pwm = map_speed_to_pwm(right_speed, 'right')  # Speed increases with
increasing PWM

    # Set the PWM duty cycle for each motor
    pi.set_PWM_dutycycle(GPIO_PIN_LEFT, left_pwm)
    pi.set_PWM_dutycycle(GPIO_PIN_RIGHT, right_pwm)

def map_speed_to_pwm(speed, motor):
    if motor =='left':
        return 33 - (speed * (33 - MIN_PWM) / 2)
    elif motor == 'right':
        return (45 + speed * (MAX_PWM - 45) / 2)

def get_current_heading():
    with open("heading1_data.txt", "r") as file:
        heading_value = file.read().strip()
        if heading_value.replace('.', '', 1).isdigit():
            return float(heading_value)

def get_desired_heading():
    with open("heading_data.txt", "r") as file:
        heading_value = str(file.read().strip())
        if heading_value.replace('.', '', 1).isdigit():
            return float(heading_value)
```

```
desired_heading = get_desired_heading()
pid_left = PID(1, 0.1, 0.05, setpoint=desired_heading)
pid_right = PID(1, 0.1, 0.05, setpoint=desired_heading)

base_speed = 0  # Replace with your actual base speed

while True:
    current_heading = get_current_heading()
    control_left = pid_left(current_heading)
    control_right = pid_right(current_heading)
    left_motor_speed = base_speed + control_left
    right_motor_speed = base_speed + control_right
    set_motor_speeds(left_motor_speed, right_motor_speed)
```

B-4: GPS Data

```
#! /usr/bin/python

import time

import smbus

import signal

import sys

import paho.mqtt.client as mqtt

mqtt_broker = "your_mqtt_broker_ip"

mqtt_port = 1883

mqtt_topic = "robot1/gps"

BUS = None

address = 0x42

gpsReadInterval = 0.03

client = mqtt.Client()

client.connect(mqtt_broker, mqtt_port, 60)


 def connectBus():

    global BUS

    BUS = smbus.SMBus(1)

def parseResponse(gpsLine):

  if(gpsLine.count(36) == 1):                    # Check #1, make sure '$' doesnt appear
twice

    if len(gpsLine) < 84:                        # Check #2, 83 is maximun NMEA sentenace
length.

        CharError = 0;

        for c in gpsLine:                        # Check #3, Make sure that only readiable
ASCII charaters and Carriage Return are seen.

            if (c < 32 or c > 122) and  c != 13:
```

```
            CharError+=1
        if (CharError == 0):#    Only proceed if there are no errors.
            gpsChars = ''.join(chr(c) for c in gpsLine)
            if (gpsChars.find('txbuf') == -1):          # Check #4, skip txbuff allocation error
                gpsStr, chkSum = gpsChars.split('*',2)  # Check #5 only split twice to avoid
unpack error
                gpsComponents = gpsStr.split(',')
                chkVal = 0
                for ch in gpsStr[1:]: # Remove the $ and do a manual checksum on the rest of
the NMEA sentence
                    chkVal ^= ord(ch)
                if (chkVal == int(chkSum, 16)): # Compare the calculated checksum with the
one in the NMEA sentence
                    if gpsComponents[0] == "$GNRMC":
                        status = gpsComponents[2]
                        if status == 'A':  # Data is valid
                            latitude = float(gpsComponents[3])
                            longitude = float(gpsComponents[5])
                            speed_over_ground = float(gpsComponents[7])
                            return latitude, longitude, speed_over_ground
                return None
def handle_ctrl_c(signal, frame):
        sys.exit(130)
#This will capture exit when using Ctrl-C
signal.signal(signal.SIGINT, handle_ctrl_c)
def readGPS():
    c = None
    response = []
```

```
    try:
        while True: # Newline, or bad char.
            c = BUS.read_byte(address)
            if c == 255:
                return False
            elif c == 10:
                break
            else:
                response.append(c)
        parseResponse(response)
    except IOError:
        connectBus()
    except Exception as e:
        print (e)
connectBus()

while True:
    gps_data = readGPS()
    if gps_data is not None:
        client.publish(mqtt_topic, gps_data)
    time.sleep(gpsReadInterval)
```

B-5: GPS Calculations

```
from math import radians, sin, cos, sqrt, atan2

#Haversine formula to calculate the distance between two sets of coordinates:

def calculate_distance(lat1, lon1, lat2, lon2):
    # Convert coordinates to radians
    lat1, lon1, lat2, lon2 = map(radians, [lat1, lon1, lat2, lon2])

    # Calculate differences
    dlon = lon2 - lon1
    dlat = lat2 - lat1

    # Haversine formula
    a = sin(dlat/2)**2 + cos(lat1) * cos(lat2) * sin(dlon/2)**2
    c = 2 * atan2(sqrt(a), sqrt(1-a))

    # Radius of earth in kilometers. Use 3956 for miles
    radius = 6371000.0

    # Calculate and return distance
    distance_m = radius * c
    return distance_m
```

B-6: Heading Data

```
import sys

import time

import math

import IMU

import datetime

import os

RAD_TO_DEG = 57.29578

M_PI = 3.14159265358979323846

G_GAIN = 0.070          # [deg/s/LSB]  If you change the dps for gyro, you need to update this value accordingly

AA =  0.40              # Complementary filter constant

MAG_LPF_FACTOR = 0.4    # Low pass filter constant magnetometer

ACC_LPF_FACTOR = 0.4    # Low pass filter constant for accelerometer

ACC_MEDIANTABLESIZE = 9         # Median filter table size for accelerometer. Higher = smoother but a longer delay

MAG_MEDIANTABLESIZE = 9         # Median filter table size for magnetometer. Higher = smoother but a longer delay


################## Compass Calibration values ############

# Use calibrateBerryIMU.py to get calibration values

# Calibrating the compass isnt mandatory, however a calibrated

# compass will result in a more accurate heading value.


magXmin =  0

magYmin =  0

magZmin =  0

magXmax =  0
```

magYmax = 0

magZmax = 0

'''

Here is an example:

magXmin = -1748

magYmin = -1025

magZmin = -1876

magXmax = 959

magYmax = 1651

magZmax = 708

Dont use the above values, these are just an example.

'''

################ END Calibration offsets ##################

#Kalman filter variables

Q_angle = 0.02

Q_gyro = 0.0015

R_angle = 0.005

y_bias = 0.0

x_bias = 0.0

XP_00 = 0.0

XP_01 = 0.0

XP_10 = 0.0

XP_11 = 0.0

YP_00 = 0.0

YP_01 = 0.0

YP_10 = 0.0

```
YP_11 = 0.0
KFangleX = 0.0
KFangleY = 0.0

def kalmanFilterY ( accAngle, gyroRate, DT):
    y=0.0
    S=0.0

    global KFangleY
    global Q_angle
    global Q_gyro
    global y_bias
    global YP_00
    global YP_01
    global YP_10
    global YP_11

    KFangleY = KFangleY + DT * (gyroRate - y_bias)

    YP_00 = YP_00 + ( - DT * (YP_10 + YP_01) + Q_angle * DT )
    YP_01 = YP_01 + ( - DT * YP_11 )
    YP_10 = YP_10 + ( - DT * YP_11 )
    YP_11 = YP_11 + ( + Q_gyro * DT )

    y = accAngle - KFangleY
    S = YP_00 + R_angle
    K_0 = YP_00 / S
```

```
    K_1 = YP_10 / S

    KFangleY = KFangleY + ( K_0 * y )
    y_bias = y_bias + ( K_1 * y )

    YP_00 = YP_00 - ( K_0 * YP_00 )
    YP_01 = YP_01 - ( K_0 * YP_01 )
    YP_10 = YP_10 - ( K_1 * YP_00 )
    YP_11 = YP_11 - ( K_1 * YP_01 )

    return KFangleY

def kalmanFilterX ( accAngle, gyroRate, DT):
    x=0.0
    S=0.0

    global KFangleX
    global Q_angle
    global Q_gyro
    global x_bias
    global XP_00
    global XP_01
    global XP_10
    global XP_11

    KFangleX = KFangleX + DT * (gyroRate - x_bias)
```

```
    XP_00 = XP_00 + ( - DT * (XP_10 + XP_01) + Q_angle * DT )
    XP_01 = XP_01 + ( - DT * XP_11 )
    XP_10 = XP_10 + ( - DT * XP_11 )
    XP_11 = XP_11 + ( + Q_gyro * DT )

    x = accAngle - KFangleX
    S = XP_00 + R_angle
    K_0 = XP_00 / S
    K_1 = XP_10 / S

    KFangleX = KFangleX + ( K_0 * x )
    x_bias = x_bias + ( K_1 * x )

    XP_00 = XP_00 - ( K_0 * XP_00 )
    XP_01 = XP_01 - ( K_0 * XP_01 )
    XP_10 = XP_10 - ( K_1 * XP_00 )
    XP_11 = XP_11 - ( K_1 * XP_01 )

    return KFangleX
gyroXangle = 0.0
gyroYangle = 0.0
gyroZangle = 0.0
CFangleX = 0.0
CFangleY = 0.0
CFangleXFiltered = 0.0
CFangleYFiltered = 0.0
kalmanX = 0.0
```

```
kalmanY = 0.0
oldXMagRawValue = 0
oldYMagRawValue = 0
oldZMagRawValue = 0
oldXAccRawValue = 0
oldYAccRawValue = 0
oldZAccRawValue = 0

a = datetime.datetime.now()

#Setup the tables for the mdeian filter. Fill them all with '1' so we dont get devide by zero error
acc_medianTable1X = [1] * ACC_MEDIANTABLESIZE
acc_medianTable1Y = [1] * ACC_MEDIANTABLESIZE
acc_medianTable1Z = [1] * ACC_MEDIANTABLESIZE
acc_medianTable2X = [1] * ACC_MEDIANTABLESIZE
acc_medianTable2Y = [1] * ACC_MEDIANTABLESIZE
acc_medianTable2Z = [1] * ACC_MEDIANTABLESIZE
mag_medianTable1X = [1] * MAG_MEDIANTABLESIZE
mag_medianTable1Y = [1] * MAG_MEDIANTABLESIZE
mag_medianTable1Z = [1] * MAG_MEDIANTABLESIZE
mag_medianTable2X = [1] * MAG_MEDIANTABLESIZE
mag_medianTable2Y = [1] * MAG_MEDIANTABLESIZE
mag_medianTable2Z = [1] * MAG_MEDIANTABLESIZE

IMU.detectIMU()     #Detect if BerryIMU is connected.
if(IMU.BerryIMUversion == 99):
```

```
    print(" No BerryIMU found... exiting ")
    sys.exit()
IMU.initIMU()       #Initialise the accelerometer, gyroscope and compass
while True:
    #Read the accelerometer,gyroscope and magnetometer values
    ACCx = IMU.readACCx()
    ACCy = IMU.readACCy()
    ACCz = IMU.readACCz()
    GYRx = IMU.readGYRx()
    GYRy = IMU.readGYRy()
    GYRz = IMU.readGYRz()
    MAGx = IMU.readMAGx()
    MAGy = IMU.readMAGy()
    MAGz = IMU.readMAGz()

    #Apply compass calibration
    MAGx -= (magXmin + magXmax) /2
    MAGy -= (magYmin + magYmax) /2
    MAGz -= (magZmin + magZmax) /2

    ##Calculate loop Period(LP). How long between Gyro Reads
    b = datetime.datetime.now() - a
    a = datetime.datetime.now()
    LP = b.microseconds/(1000000*1.0)
    outputString = "Loop Time %5.2f " % ( LP )
```

```
    ################################################
    #### Apply low pass filter ####
    ################################################
    MAGx =  MAGx  * MAG_LPF_FACTOR + oldXMagRawValue*(1 -
MAG_LPF_FACTOR);
    MAGy =  MAGy  * MAG_LPF_FACTOR + oldYMagRawValue*(1 -
MAG_LPF_FACTOR);
    MAGz =  MAGz  * MAG_LPF_FACTOR + oldZMagRawValue*(1 -
MAG_LPF_FACTOR);
    ACCx =  ACCx  * ACC_LPF_FACTOR + oldXAccRawValue*(1 -
ACC_LPF_FACTOR);
    ACCy =  ACCy  * ACC_LPF_FACTOR + oldYAccRawValue*(1 - ACC_LPF_FACTOR);
    ACCz =  ACCz  * ACC_LPF_FACTOR + oldZAccRawValue*(1 - ACC_LPF_FACTOR);

    oldXMagRawValue = MAGx
    oldYMagRawValue = MAGy
    oldZMagRawValue = MAGz
    oldXAccRawValue = ACCx
    oldYAccRawValue = ACCy
    oldZAccRawValue = ACCz

    ################################################
    #### Median filter for accelerometer ####
    ################################################
    # cycle the table
    for x in range (ACC_MEDIANTABLESIZE-1,0,-1 ):
        acc_medianTable1X[x] = acc_medianTable1X[x-1]
        acc_medianTable1Y[x] = acc_medianTable1Y[x-1]
```

```
    acc_medianTable1Z[x] = acc_medianTable1Z[x-1]

# Insert the lates values
acc_medianTable1X[0] = ACCx
acc_medianTable1Y[0] = ACCy
acc_medianTable1Z[0] = ACCz

# Copy the tables
acc_medianTable2X = acc_medianTable1X[:]
acc_medianTable2Y = acc_medianTable1Y[:]
acc_medianTable2Z = acc_medianTable1Z[:]

# Sort table 2
acc_medianTable2X.sort()
acc_medianTable2Y.sort()
acc_medianTable2Z.sort()

# The middle value is the value we are interested in
ACCx = acc_medianTable2X[int(ACC_MEDIANTABLESIZE/2)];
ACCy = acc_medianTable2Y[int(ACC_MEDIANTABLESIZE/2)];
ACCz = acc_medianTable2Z[int(ACC_MEDIANTABLESIZE/2)];

##########################################
#### Median filter for magnetometer ####
##########################################
# cycle the table
for x in range (MAG_MEDIANTABLESIZE-1,0,-1 ):
```

```
    mag_medianTable1X[x] = mag_medianTable1X[x-1]
    mag_medianTable1Y[x] = mag_medianTable1Y[x-1]
    mag_medianTable1Z[x] = mag_medianTable1Z[x-1]

# Insert the latest values
mag_medianTable1X[0] = MAGx
mag_medianTable1Y[0] = MAGy
mag_medianTable1Z[0] = MAGz

# Copy the tables
mag_medianTable2X = mag_medianTable1X[:]
mag_medianTable2Y = mag_medianTable1Y[:]
mag_medianTable2Z = mag_medianTable1Z[:]

# Sort table 2
mag_medianTable2X.sort()
mag_medianTable2Y.sort()
mag_medianTable2Z.sort()

# The middle value is the value we are interested in
MAGx = mag_medianTable2X[int(MAG_MEDIANTABLESIZE/2)];
MAGy = mag_medianTable2Y[int(MAG_MEDIANTABLESIZE/2)];
MAGz = mag_medianTable2Z[int(MAG_MEDIANTABLESIZE/2)];
#Convert Gyro raw to degrees per second
rate_gyr_x =  GYRx * G_GAIN
rate_gyr_y =  GYRy * G_GAIN
rate_gyr_z =  GYRz * G_GAIN
```

```
#Calculate the angles from the gyro.
gyroXangle+=rate_gyr_x*LP
gyroYangle+=rate_gyr_y*LP
gyroZangle+=rate_gyr_z*LP
#Convert Accelerometer values to degrees
AccXangle =  (math.atan2(ACCy,ACCz)*RAD_TO_DEG)
AccYangle =  (math.atan2(ACCz,ACCx)+M_PI)*RAD_TO_DEG

#Change the rotation value of the accelerometer to -/+ 180 and
#move the Y axis '0' point to up.  This makes it easier to read.
if AccYangle > 90:
   AccYangle -= 270.0
else:
   AccYangle += 90.0

#Complementary filter used to combine the accelerometer and gyro values.
CFangleX=AA*(CFangleX+rate_gyr_x*LP) +(1 - AA) * AccXangle
CFangleY=AA*(CFangleY+rate_gyr_y*LP) +(1 - AA) * AccYangle

#Kalman filter used to combine the accelerometer and gyro values.
kalmanY = kalmanFilterY(AccYangle, rate_gyr_y,LP)
kalmanX = kalmanFilterX(AccXangle, rate_gyr_x,LP)

#Calculate heading
heading = 180 * math.atan2(MAGy,MAGx)/M_PI

#Only have our heading between 0 and 360
```

```
    if heading < 0:
        heading += 360

################################################################
####################Tilt compensated heading#####################
################################################################
    #Normalize accelerometer raw values.
    accXnorm = ACCx/math.sqrt(ACCx * ACCx + ACCy * ACCy + ACCz * ACCz)
    accYnorm = ACCy/math.sqrt(ACCx * ACCx + ACCy * ACCy + ACCz * ACCz)



    #Calculate pitch and roll
    pitch = math.asin(accXnorm)
    roll = -math.asin(accYnorm/math.cos(pitch))


    #Calculate the new tilt compensated values
    #The compass and accelerometer are orientated differently on the the BerryIMUv1, v2 and v3.
    #This needs to be taken into consideration when performing the calculations
    #X compensation
    if(IMU.BerryIMUversion == 1 or IMU.BerryIMUversion == 3):            #LSM9DS0 and (LSM6DSL & LIS2MDL)
        magXcomp = MAGx*math.cos(pitch)+MAGz*math.sin(pitch)
    else:                                                #LSM9DS1
        magXcomp = MAGx*math.cos(pitch)-MAGz*math.sin(pitch)


    #Y compensation
```

```
    if(IMU.BerryIMUversion == 1 or IMU.BerryIMUversion == 3):            #LSM9DS0 and (LSM6DSL & LIS2MDL)
        magYcomp = MAGx*math.sin(roll)*math.sin(pitch)+MAGy*math.cos(roll)-MAGz*math.sin(roll)*math.cos(pitch)
    else:                                                               #LSM9DS1
        magYcomp = MAGx*math.sin(roll)*math.sin(pitch)+MAGy*math.cos(roll)+MAGz*math.sin(roll)*math.cos(pitch)


    #Calculate tilt compensated heading
    tiltCompensatedHeading = 180 * math.atan2(magYcomp,magXcomp)/M_PI


    if tiltCompensatedHeading < 0:
        tiltCompensatedHeading += 360



  ######################## END Tilt Compensation ########################


    if 1:                       #Change to '0' to stop showing the angles from the accelerometer
        outputString += "#  ACCX Angle %5.2f ACCY Angle %5.2f  #  " % (AccXangle, AccYangle)


    if 1:                       #Change to '0' to stop  showing the angles from the gyro
        outputString +="\t# GRYX Angle %5.2f  GYRY Angle %5.2f  GYRZ Angle %5.2f # " % (gyroXangle,gyroYangle,gyroZangle)


    if 1:                       #Change to '0' to stop  showing the angles from the complementary filter
        outputString +="\t#  CFangleX Angle %5.2f   CFangleY Angle %5.2f  #" % (CFangleX,CFangleY)
```

```
    if 1:                   #Change to '0' to stop  showing the heading
        outputString +="\t# HEADING %5.2f  tiltCompensatedHeading %5.2f #" %
(heading,tiltCompensatedHeading)

    if 1:                   #Change to '0' to stop  showing the angles from the Kalman filter
        outputString +="# kalmanX %5.2f   kalmanY %5.2f #" % (kalmanX,kalmanY)
        # Write heading to a file
        with open("heading_data.txt", "w") as file:
            file.write(str(heading))
    print(outputString)
    #slow program down a bit, makes the output more readable
    time.sleep(0.03)
##Heading Publish
import paho.mqtt.client as mqtt
import time
mqtt_broker = "your_broker_ip"
mqtt_port = 1883
mqtt_topic = "heading"

mqtt_client = mqtt.Client()
mqtt_client.connect(mqtt_broker, mqtt_port)

def publish_heading(heading):
    mqtt_client.publish(mqtt_topic, str(heading))

while True:
```

```
# Read heading from file
with open("heading_data.txt", "r") as file:
    heading_value = float(file.read().strip())

# Perform calculations with the heading value
# For example, let's double the heading value
#modified_heading = heading_value * 2

# Publish modified heading to MQTT topic
#publish_heading(modified_heading)
publish_heading(heading_value)

time.sleep(1)  # Adjust sleep time as needed
```

```
##Heading Subscribe
import paho.mqtt.client as mqtt
import time
import math

mqtt_broker = "your_broker_ip"
mqtt_port = 1883
mqtt_topic = "heading"

mqtt_client = mqtt.Client()
mqtt_client.connect(mqtt_broker, mqtt_port)

def publish_heading(heading):
    mqtt_client.publish(mqtt_topic, str(heading))

while True:
    # Read heading from file
    with open("heading_data.txt", "r") as file:
        heading_value = float(file.read().strip())

    # Perform calculations with the heading value
    # For example, let's double the heading value
    #modified_heading = heading_value * 2

    # Publish modified heading to MQTT topic
    #publish_heading(modified_heading)
    publish_heading(heading_value)
```

```
def on_message(client, userdata, msg):
    received_heading = float(msg.payload.decode())
    own_heading = heading_value()
    print("Received Heading:", received_heading)
    print("Own Heading:", own_heading)
    if abs(received_heading - own_heading) < 10:  # Adjust the threshold as needed
        print("Headings are close.")
    else:
        print("Headings are not close.")

# Initialize MQTT Client
mqtt_client = mqtt.Client()

# Set up MQTT callbacks
mqtt_client.on_message = on_message

# Connect to MQTT Broker
mqtt_client.connect(mqtt_broker, mqtt_port)

# Subscribe to MQTT topic
mqtt_client.subscribe(mqtt_topic)

# Start the MQTT loop
mqtt_client.loop_forever()

time.sleep(0.03)  # Adjust sleep time as needed
```

Appendix C: Interview Notes

C-1: Clean Blue Sea – 09/29/23

Questions:

1. What is the development status of FRED?
    a. Is the robot still being developed?
    b. Will it become a commercial product?
    c. What does the sensor fleet look like on FRED? What kinds of information does it collect and how is it used?
2. How do the two smaller Fred's determine what locations need cleaning up? Is it based off of density? Do they use sonar?
    a. How do the robots communicate with each other? The operator?
3. How did you determine your method of trash collection? How do you compare it to the likes of Ocean Cleanup?
    a. How does the robot know when to turn on the conveyor belt?
4. Is FRED capable of capturing fishing nets or only standard plastic trash?
    a. Do you know anything about the dynamics of fishing nets in the ocean?
    b. Were other collection methods (not a conveyor belt) considered or tested?
5. How effective are your sonar fish deterrents?
    a. How does this system work? What kind of tech does it use?
    b. Does it only work on certain kinds of fish? Or is it more general?
6. What challenges have you encountered while prototyping and testing FRED?
    a. Any difficulties regarding encountering wildlife?
    b. What does the conveyor belt use to pull in trash?
    c. How effective are the solar panels at keeping the system operational?
    d. Has FRED encountered open ocean conditions? How did it fair?

Notes:

- Tim Perry, Chief engineer in 2019
- Given Presentation
    - All electric vessel
    - FRED
        - Was originally supposed to be a pretty big bot
        - Uses solar panels
    - Developing smaller scale
        - Potential Swarming
    - Previous Projects
        - San Diego State
            - Fiberglass/plastic wood holes
        - USD
            - Solar Powered Convey Belt Vehicle

        - Flight Controller
    - 16 Foot Prototype
        - Catarman Hull Styled Project
        - Solar Charged Controller, remote
        - Car Batteries
    - PixHawk System and ardupilot
        - GPS Waypoint Commands
        - Semi-autonomous aviation
- Fred
    - Development Challenges
        - Development Costs: Way more expected than anticipated
    - Grants:
        - Most of the grants should be for non-profit orgs
        - Outside gov grants, get people to pay for gyers
        - Not a lot of big pockets of trash, small clusters within arenas
            - Had trouble getting these large vessels
        - Partner with the scientific community
            - Assess ocean help
            - What datapoint are most valuable to oceanographers
    - Developing Micro FRED
        - Small 3D platform
        - Shifting to ROS
        - Having computer vision to
        - Hydrographic sensing
            - Offering sensor readings to companies offers more values and allows companies to provide funding, pick up trash along the way
            - Develop a 3D map for the surface level
                - Allows the vessel to have a deep map
            - Pick up debris and finding the location of where the hotspots would be much more valuable
            - Navigation software needed
                - Add as many sensors as possible and data functionality, preferably
        - Develop partnerships
            - SDSU: Living Labs (MOCLLAB)
            - Ecotourism groups would be interested in paying to learn about the problem
            - Education Missions
                - Teach more about marine debris crisis in SD

- Micro FRED Scope
    - Still in the design phase
    - Waterproof requries Epoxy to
        - 85% of buoyancy force
        - PVC Pipes are easier and provides a lot more volume compared to weight
        - Using these catapult holes
        - Simulation Program
            - Including ROS
        - Focused on, teaching it how to navigate and for its navigation software
    - Vision
        - ZEDX Camera
        - Jets and Nano Camera
            - Around $150
        - Stereoscopic
        - Sensor Fleet Location
            - RGK GPS, GPS coordinates
            - Aren't as accurate but internal sensors internal gyroscopes, accelerometer, and magnetometers
        - Underwater sonar
            - Hydrographic scanning
                - Point Clouds of elevation
                    - High spots
            - Looking at the map and comparing at it's the one it already knows to see that between the scans
            - Ultrasonic sensors and live sensors
                - The choppiness of the water and reflectivity can affect the data
                - Machine vision is a much more reliable choice to find itemse with smaller vessels
            - Software stabilization Integration
                - Nothing as of right now
                -
        - Start the Software as soon as possible (at least from CBS)
        -

        - Fish sonar deterrent is not used and have and not found an off the shelf option to do that
            - Noises inside the propellers act as a sonic sensor to deter wildlife away from the vessel
            - Challenges with the nets are that animals or their habitat could be entangled or damaged
    - Clariy FRED Scope
        - Testing out hydrographic scanning functionality
    - Swarm FRED Scrope
    - Conveyer belt collector method
        - Most logical
        - In terms of surface debris, seems to be the most effective
        - Ended the debris into a bin for easier swapping
        - Continuously operation or turned on manually
            - Constantly but powered is much more efficient if there were some sort of sensors
        - Funnel system into the conveyer
    - How to prioritize, such as trash density
        - Based on visual judgements and word of mouth where they find hotspots to focus on
    - Fishing net exist at every different level such as depth of buyoancy, how do they determine and does it cause problems with the covneyer belt
        - Primarily operated around the Bay
        - Commercial fishing nets are much deeper into the ocean
        - Vessels have gotten caught in the fishing nets themselves
        - Not recommended with conveyer belt system
        - Recommends cutting the nets somehow
    - Going through initial prototype, have they gone other methods
        - Focused on conveyer belts unfortunately
            - Cleats on the belt and especially the angles
        - Swarming would be used to push the nets towards another larger vessel to collect
        - Breaking down into smaller chunks for net
    - Wildlife difficulties/considerations
        - Have not encountered as it was away due to the sonar of the propellers
    - Solar Powered FRED, has it been affective in keeping its duration
        - Successful
        - 4 Control Panels
            - 400 Watts each

        - Never riding them with full powers
        - Typically run for 3 hours but only have used 75% as of experimenting
    - Testing out in Open Sea conditions
        - 16 –Foot Sail boats so they stay away from sea-state conditions and fear getting swarmed

C-2: GreenSea IQ – 09/29/23

Questions:

Thank you for agreeing to meet with us, we are very excited about a possible collaboration between our team and GreenSea IQ. Do you mind if we record this meeting for our records?

To start, we'd like to give some more information about our project and why we reached out to your company specifically. We are continuing two years of research and design on an autonomous ocean clean-up robot, specifically tasked to retrieve abandoned fishing nets. This is a collaborative effort between the Mechanical Engineering and Robotics Engineering departments here at WPI. Our goal for this year is to design and test the feasibility of a robotic swarm approach to retrieving tangled and discarded fishing nets left in the ocean. A large part of this depends on fast and accurate communication between the robots through a sophisticated software system. During our preliminary research, we found GreenSea IQ and your OPENSEA platform for controlling naval robotics, which is why we reached out.

1. Would you mind introducing yourself, explaining your position and role within the company?
2. Is there any possibility we could use OPENSEA software for our project?
3. What do you mean when you say OPENSEA is open source? Can we integrate it with ROS2?
    a. Open source typically means free…
        i. If somehow not, how much would that be worth?
4. What programming language does it use? Does it use Python? C++?
    a. If it's neither and proprietary, how hard is it to integrate it with other programs?
    b. The website stated that it is adaptable and can be integrated into different systems, specifically what type of systems?
5. May we please use OPENSEA to develop our autonomous cleaning robot? For free?
6. Does it only work with industry standard ROVs? Or can it work with ones created from the ground up?
    a. If so, can a model of the created ROV be imported into the simulator?
7. Why isn't any of the documentation available online? (Don't actually ask this)
8. Can machine learning be integrated into the application?
    a. If so, is that done through the app natively or can it connect to another application such as PyTorch?
9. What is the bandwidth of the communication systems? Can it stream wireless video at water level?
    a. If so, how far is the average range and what is the bitrate?

10. GreenSea IQ's website shows multiple systems that operate just off the coastline. What is the maximum range of your current robotic systems? What is the limiting factor for that range?
    a. Does it require a nearby mother ship?

Points

- Machine learning integration
    - Keep things separate as much as possible
    - Architecture oriented like ROS
        - Build applications independently
        - Passed along communications to greater systems
    - Net detection can be done on our side
        - Interface can be taken care of by them
- Simulation Software going with OPENSEA
    - Additional models can be added but depends on fidelity
        - Designed to be a training tool for operators
        - If for vehicle dynamics, does a good job on it but requires a lot of data to Whitebox simulate it due to constraints required
    - Find the achievable goals first before using the simulation software
- Swarm Approach
    - Using OPENSEA to operate the machine learning application
    - Don't need to know all the capabilities of the system or set of vehicles
    - GAZIBO route would be a fresh start to use
    - Would provide resources
        - Focus on the per system and the autonomous behavior
        - Basic license
        - Controller systems
            - Cost associated with it
- Communication Hardware Recommendation
    - For a small vessel, RF Comms that is IV Based would be preferred
- General Pricing for Support
    - *Dillin will get back to us with this

C-3: Net Your Problem – 10/02/23

Questions:

- Where do most of the nets you recycle come from? (Corporations? Self-collection?)
    - Collect nets directly from fishing companies themselves
    - Take a dragger in which is how they work in MA
    - Blue Harvest
    - A lot more difficult to recyscle thing in the ocean because they are foul
- How are fishing nets removed from the water?
    - Are many of the nets you work with retrieved from the ocean with no known previous user?
        - A lot of the nets retrieved are self-reported
        - Fishermen themselves who grapple for their lost gear
        - Ghost gear project (Caitlin gave us the women's contact information)
    - What is the state of the fishing net once you receive them? Is there a point in which the nets cannot be recycled?
        - The gear would have holes too big, with the fishing being done, but cannot be reused for another fishermen as it is undesirable
        - State usually comes clean
        - When it is too dirty, the recyclers will not take it
    - Where in the water are fishing nets typically found? (Surface? Subsurface?)
        - Hard for judgement, they don't usually run into nets with such a small dragger fleet
        - Very random between surface and ground floor
        - Draggers specifically are the ones that lose nets and they often sink down
        - Gill nets are most common \/
        - Nets made up of nylon
            - Usually made up of pieces, wrapped up, tangled.
        - Never seen a net floating in the North Atlantic
        - Divers encountering Gille nets
        - Human waste is much more prominent
    - How often are nets returned or found with weights or buoys still attached?
        - She doesn't accept any nets with weights or buoys, they are extremely heavy and difficult to remove by hand
        - Needs excavator to move nets with chains/buoys, even her forklift isn't strong enough for those.
- What volume of nets are you able to recycle every year?

    - As a company, they recycle is collected to be 1 million pounds since 2017
    - She personally has 75,000 lbs at their warehouse, with not all of that can be recycled
    -
- What do you know about ghost gear and its contribution to wildlife endangerment?
- How are fishing companies managing their waste?
    - Most fishermen or fishing companies try to rescue lost nets
    - Nets cost $30,000 apiece which most fishermen can risk losing
    - She estimated that 90% of all gear lost in North America is accidental, either due to the net getting caught on something or adverse weather.
    - Nets retrieved directly from the ocean are harder to recycle do to organic contaminants and fouling.
    - Nets are often stored on ships or shipyards for extended periods of time before being recycled
- What regulations currently exist to prevent fishing net disposal in the ocean?
- Is it possible to automate the net recycling process? How difficult are the nets to manipulate?
    - Cannot see a way for this to be automated with completely hands-off human assistance
    - Shredding can be very difficult from her experience and might require manual labor
    - Plastix could be technologically improved with better systems to shred net ropes
    - Would be good to see a way to melt down mixed plastics together
        - Proven difficulty with different melting points

<u>Notess</u>

- Caitlin
    - Started w/ghost gear off cape cod
- Dangle grapples off boats to collect ghost gear, find those locations through sonar
- In NA, the common practice is that many nets that ended up as ghost gear is accidental due to the high prices of fishing nets (around $30,000)
    - Around Asian waters, is more of a practice to leave the nets behind
- Grapple
    - 2-4-foot-long metal prongs with a barb that is used to drag behind the boat
    - Can be based off of sonar
    - Grappling is a skill, usually have a more experienced operator controlling the grapple on ghost gear missions.

Appendix D: Bill Of Materials

Sub-System	Name	Part Description	Part Number	Vendor	Unit Cost	Quantity	Total Cost
Electronics	Raspberry Pi CPU	Raspberry pi 4 - 4 gb of ram	B07TC2BK1X	Amazon	62	2	124
	Gyroscope IMU	BerryGPS-IMU GPS and 10DOF for Raspberry Pi - accelerometer, gyroscope, magnetometer and barometric/Altitude sensor	B072MNBC9M	Amazon	71	2	142
	Camera	Raspberry Pi Camera Module V2-8 Megapixel,1080p (RPI-CAM-V2)	B01ER2SKFS	Amazon	19.99	2	39.98
	Voltage Regulator	PlusRoc Waterproof 12V/24V to 5V Converter DC-DC Step Down Module Power Adapte (Micro USB Connector)	B09DGFR24W	Amazon	10.99	2	21.98
	Sonar	RS485 750cm Ultrasonic level sensor	101991041	Digikey	21.9	2	43.8
	Water Sensor	Simple Water Detection Sensor with Digital Output	4965	Adafruit	1.95	6	11.7
	Brushless Motor ESC	Readytosky Bidirectional 40A Brushless ESC 2-6S UBEC 3A 5V	B08HWQ58QX	Amazon	20.99	4	83.96
	DC Brushless Motor	Underwater Thruster MAX 24V 1080W Brushless Motor with 3-Blade Nylon Propeller	B0B5Q56HZP	Amazon	112.99	4	451.96
	Battery Charger	TANKPOW 750mA Battery Charger,12V Car Battery Charger	B08C41W3N9	Amazon	16.98	1	16.98
	Lead Acid Battery	Lead Acid 12V 18Ah	B0B3MHJXLF	Amazon	35	2	70
	Wire Sealing Grommets	1/2" IP68 Strain Relief Nylon Cord Grip Waterproof NPT Cable Glands (10pk)	B092ZLR67B	Amazon	8.99	1	8.99
	Electronics Double-Sided Tape	Double Sided Tape 3M Tape - 1/4 in * 15.62 FT	B0BJV3YFP6	Amazon	7.38	1	7.38
	1-4 Wire Splitters	1 in 4 Out Quick Terminal Block Electrical Connector for 24-12 AWG (10pk)	B0B28GNVGZ	Amazon	12.73	1	12.73
	On/Off Switches	Waterproof Toggle Switch 30A 12VDC/15A with Weatherproof Cover (5pk)	B0BJ2XJ4JR	Amazon	11.68	1	11.68
	Battery Strap	30in x 1in Velcro Strap (4pk)	B09QSY9B7J	Amazon	11.68	1	11.68
	Wifi Router	WAVLINK AC1200 WiFi Router, 5GHz+2.4GHz Dual Band WiFi 5 Router with 4x5dBi Antennas, 10/100Mbps WAN/LAN	B0C6D9WV5K	Amazon	23.98	1	23.98
	Wifi Transmitter and Reciever	Anjielo Smart WiFi Point-to-Point Access with 20DBi High-Gain Antenna, 2.4G WiFi 2600ft Bridge	B09WMBD1S7	Amazon	59.98	2	119.96
	GPS Booster	Bingfu Waterproof GPS Navigation Antenna with SMA Male Connector	B07R7RC96G	Amazon	8.99	2	17.98
Structure	Robot Side Panels	0-001 Aluminum Side Panels (0.187" Thick 5052 H32 Aluminum)	Custom	Xometry	36.25	4	145
	Robot Motor Mounts	ABS mount to hold each motor	Custom	Makerspace	0	4	0
	Robot Sealing Brackets	0-007 Front Panel Mount ABS Sealing Bracket	Custom	Makerspace	0	4	0
	Robot Sealing Brackets	0-008 Hatch Panel Mount ABS Sealing Bracket	Custom	Makerspace	0	4	0
	Robot Sealing Brackets	0-009 Back Panel Mount ABS Sealing Bracket	Custom	Makerspace	0	4	0
	Robot Sealing Brackets	0-010 Bottom Panel Mount ABS Sealing Bracket	Custom	Makerspace	0	4	0
	ABS 3D Printer Filament	ABS Filament 1.75mm Red, 1kg Accuracy +/- 0.03mm	B09DKQHL67	Amazon	23.36	1	23.36
	Sealing Tape	1/4 in. x 40 ft. Butyl Rubber Sealant Tape	457389	Home Depot	5.25	2	10.5
	Gasket Material	Oil-Resistant Buna-N, Adhesive-Back, 1/4" x 36", 3/16" Thick	8525T137	McMaster-Carr	4.69	3	14.07
	Rubber Sheet	12"x12" Neoprene Rubber Sheet (1/64" thick and 50A durometer)	1370N31	McMaster-Carr	10.86	1	10.86
	Polycarbonate Siding 24x48x0.03	Front Panel + 2 Back Panel + 2 Hatch Panel	15582	Online Metals	27.99	2	55.98
	Polycarbonate Siding 24x48x0.04	Front Panel + Back Foil	NA	ME Dept	0	4	0
	1x1 80-20	4 - 18" lengths of 1"x1" 80-20 Rail	NA	ME Dept	0	2	0
	2x1 80-20	2 - 18" lengths of 2"x1" 80-20 Rail	NA	ME Dept	0	3	0
	2x1 80-20	6 - 18" lengths of 2"x1" 80-20 Rail (sold as 3')	47065T107	McMaster-Carr	25.96	3	77.88
	1.5in 1/4-20	Mounting for hatch gasket mounts (10pk)	98164A222	McMaster-Carr	10.63	2	21.26
	14mm M4	Mounting hardware for thrusters (25pk)	92290A150	McMaster-Carr	8.59	1	8.59
	1/4 Threaded Inserts	Brass 1/4 Threaded Inserts for hatch panel (10pk)	93362A806	McMaster-Carr	12.33	1	12.33
	80-20 Angle Bracket	Bracket Fastener for Standard 8mm Slot	B0B2ZXPGHD	Amazon	8.99	1	8.99
	1.0in 1/4-20	315 Stainless 1/4-20 Button Head 1.0in Long (25pk)	98164A214	McMaster-Carr	11.7	2	23.4
	7/8in 1/4-20	316 Stainless 1/4-20 Button Head 7/8in Long (25pk)	98164A519	McMaster-Carr	11.29	6	67.74
	5/8in 1/4-20	316 Stainless 1/4-20 Button Head 5/8in Long (25pk)	98164A212	McMaster-Carr	9.28	5	46.4
	3/8in 1/4-20	316 Stainless 1/4-20 Button Head 3/8in Long (25pk)	98164A209	McMaster-Carr	14.41	7	100.87
	1/4in Sealing Washers	Galvanized Steel Washers with Neoprene Seal 1/4in ID (100pk)	94708A214	McMaster-Carr	6.56	1	6.56
	Flex Seal	Zinc-Plated Alloy Steel 1/4-20 Button Head and Slot Nut 1/2in Long (4pk)	47065T139	McMaster-Carr	3.05	9	27.45
	1/4-20 Slot Nut	25pk of 1/4-20 slot nuts	47065T905	McMaster-Carr	7.83	5	39.15
	1/4-20 Lock Nut	50pk of 1/4-20 lock nuts	90715A125	McMaster-Carr	8.95	3	26.85
Floatation	PVC Floats	4in Sch40 PVC Side Floats (5ft per robot)	193879	Home Depot	4.1	10	41
	ABS Floats	2in Sch40 ABS Side Floats (16in per robot)	193801	Home Depot	2.2	3	6.6
	PVC Cement + Primer	Adhesive to attach PVC components	187100	Home Depot	13.23	1	13.23
	ABS Cement	Adhesive to attach ABS components	888718	Home Depot	7.87	1	7.87
	Silicone Caulking	Advanced Silicone 2 10.1 oz. Clear Kitchen and Bath Caulk	469296	Home Depot	10.98	1	10.98
	Flex Seal	Gorilla Waterproof Patch & Seal Tape 4" x 10' Black (1pk)	1003542193	Home Depot	15.91	1	15.91
	Flex Seal	Gorilla Waterproof Patch & Seal Tape 4" x 10' Black (1pk)	B07HSKRYQW	Amazon	14.97	1	14.97
	Rust-Oleum Red Spray Paint	12 oz. Custom Spray 5-in-1 Gloss Sunrise Red Spray Paint	1008934138	Home Depot	7.98	3	23.94
	ABS Flanges	Solid ABS flanges for float support	Custom	Makerspace	4.875	8	39
	ABS Saddle Connectors (w/ Pipe)	0-003 Sadle Connector printed in ABS	Custom	Makerspace	0	8	0
	ABS Saddle Clamps	0-004 Sadle Clamp printed in ABS	Custom	Makerspace	0	8	0
	PVC End Caps	4in Sch40 PVC Caps	4880K58	McMaster-Carr	10.64	8	85.12
Net	Golfing Net (10ft x 7ft)	Black Nylon Golf Netting with Rope Rings (10ft x 7ft)	B0BX3K638T	Amazon	29.99	1	29.99
	Net Bouys	2.5in Round Bouy with 7oz Positive Bouyancy	FL-113	Nets & More	1.508	24	36.192
	Latch Mounting Plate	0-013 Mounting plate for latch mechanism	NA	SendCutSend	10	2	20
	Latch Top Plate	0-019 Top plate for clamping locking gear	NA	SendCutSend	5	2	10
	Latch Locking Gear	0-016 Locking gear for latch mechanism	NA	Makerspace	0	2	0
	Latch Pinion Gear	0-017 Pinion gear for latch mechanism	NA	Makerspace	0	2	0
	Locking Gear Spacers	0-015 0.1875in thick spacers for locking gear	NA	Makerspace	0	4	0
	Pinion Spacer	0-018 0.1875 thick spacer for pinion gear	NA	Makerspace	0	2	0
	Latch Lock	0-014 Capture Mechanism for locking gear	NA	Makerspace	0	2	0
	Latch Mounting Plate Spacers	0.5inOD 0.25inID aluminum spacer (0.75in tall) for latch plate (pack of 5)	B07K34NZ2K	Amazon	4.26	2	8.52
						Total	2311.302

Appendix E: CAD Part Drawings

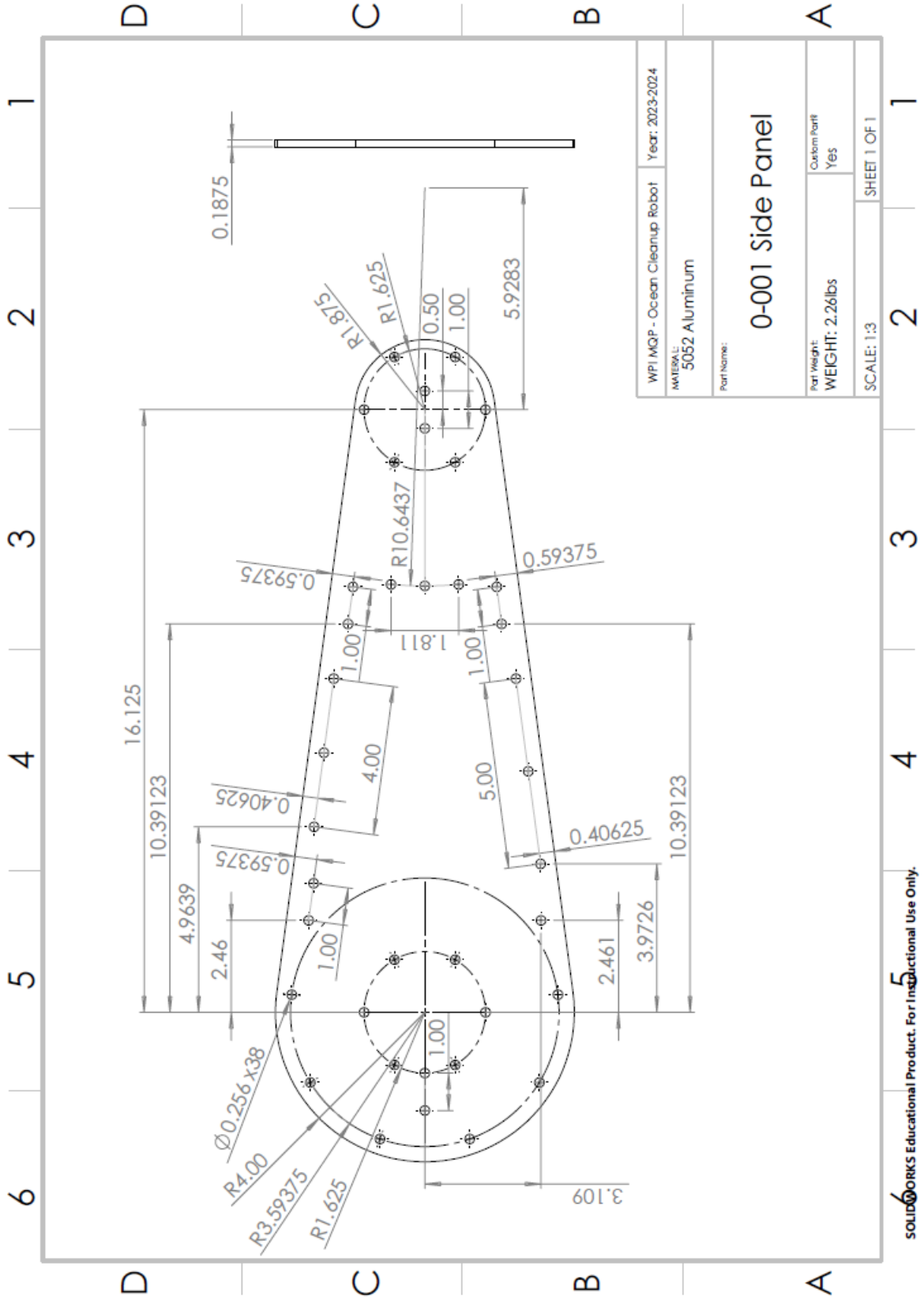

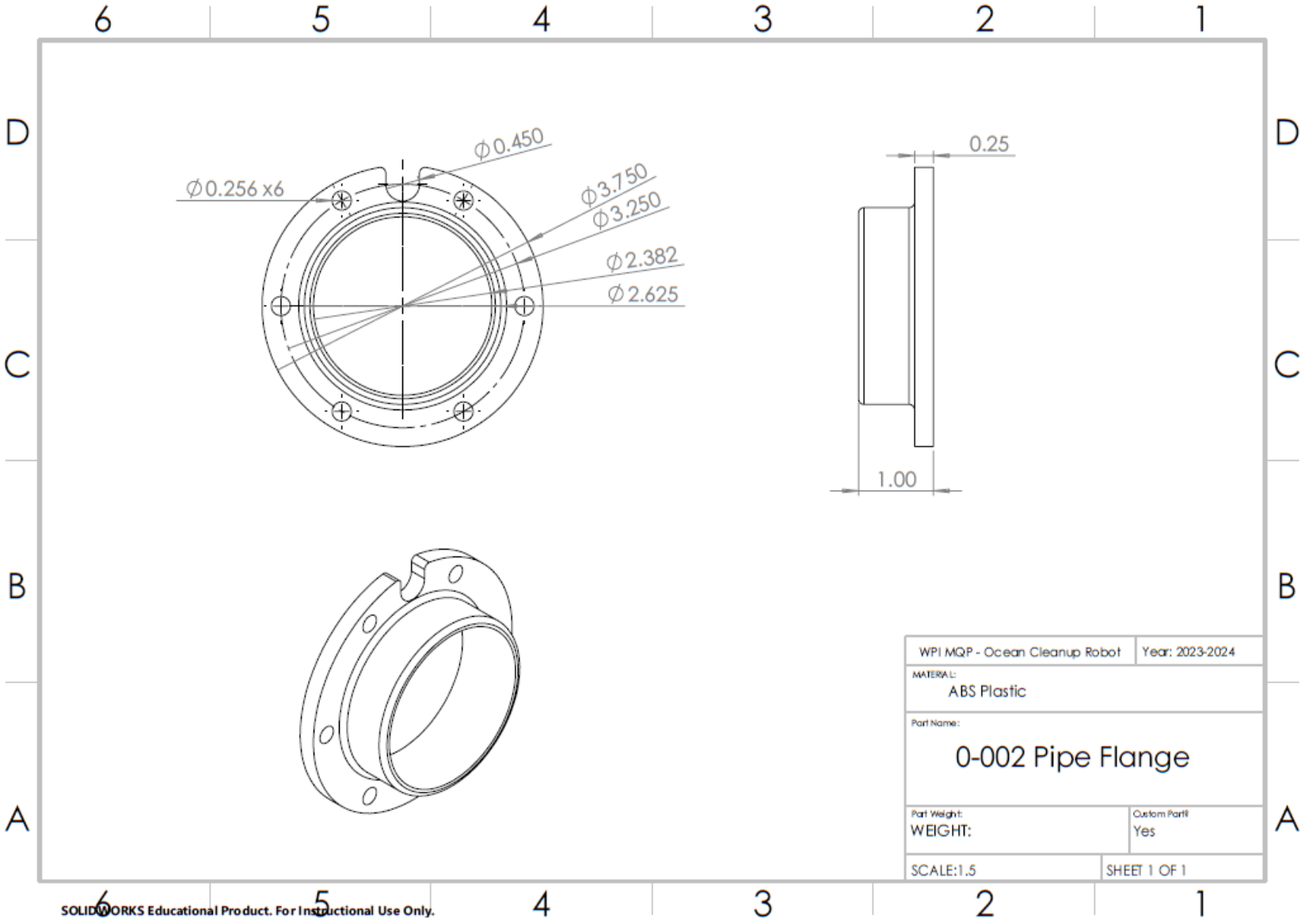
6
5
4
3
2
1
D
C
B
A
⌀0.450
⌀0.256 x6
⌀3.750
⌀3.250
⌀2.382
⌀2.625
0.25
1.00
WPI MQP - Ocean Cleanup Robot
Year: 2023-2024
MATERIAL:
ABS Plastic
Part Name:
0-002 Pipe Flange
Part Weight:
WEIGHT:
Custom Part#
Yes
SCALE:1.5
SHEET 1 OF 1
SOLIDWORKS Educational Product. For Instructional Use Only.

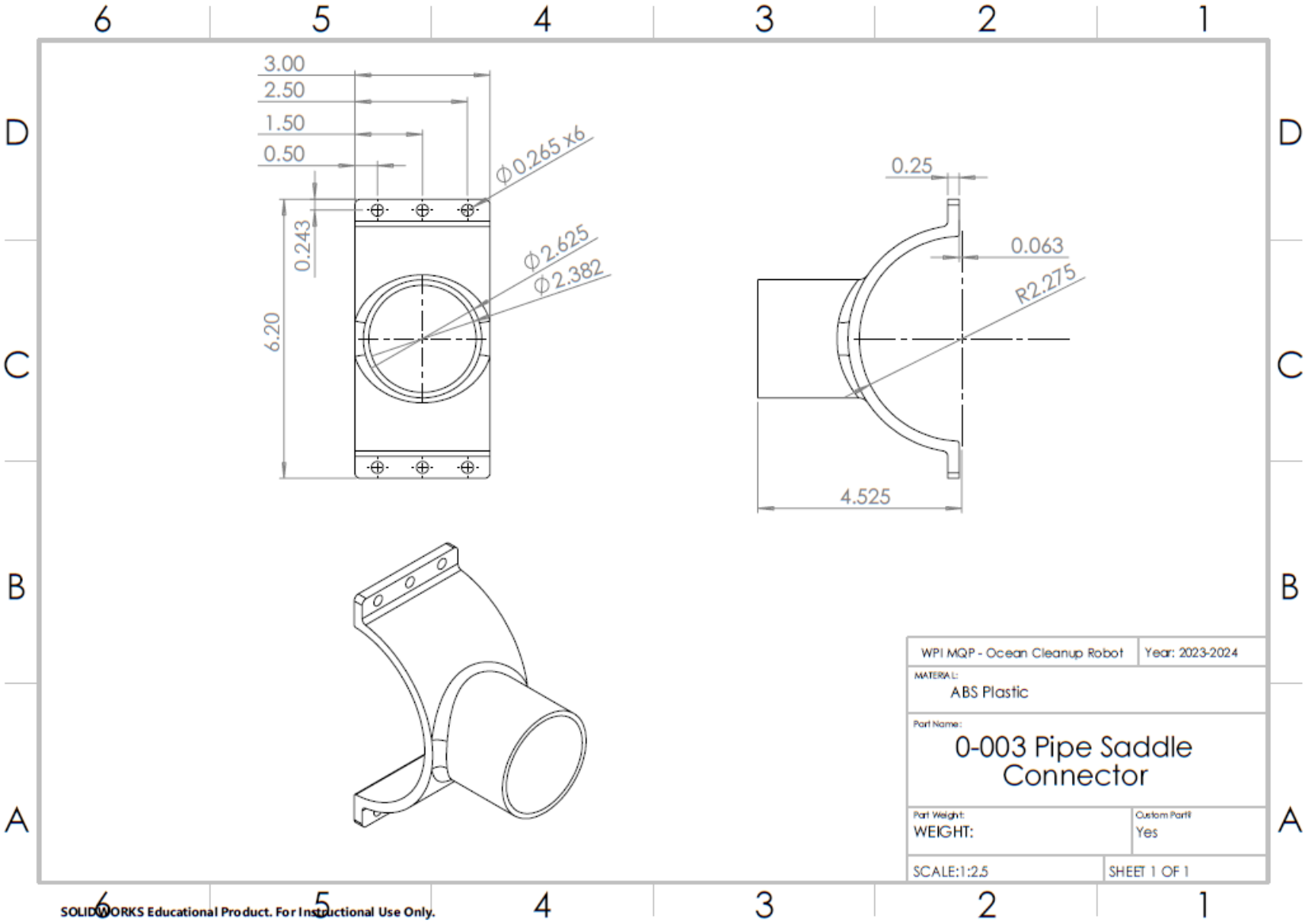
3.00
2.50
1.50
0.50
Φ0.265 x6
0.243
Φ2.625
Φ2.382
6.20
0.25
0.063
R2.275
4.525
WPI MQP - Ocean Cleanup Robot
Year: 2023-2024
MATERIAL:
ABS Plastic
Part Name:
0-003 Pipe Saddle Connector
Part Weight:
WEIGHT:
Custom Part?
Yes
SCALE:1:2.5
SHEET 1 OF 1
SOLIDWORKS Educational Product. For Instructional Use Only.

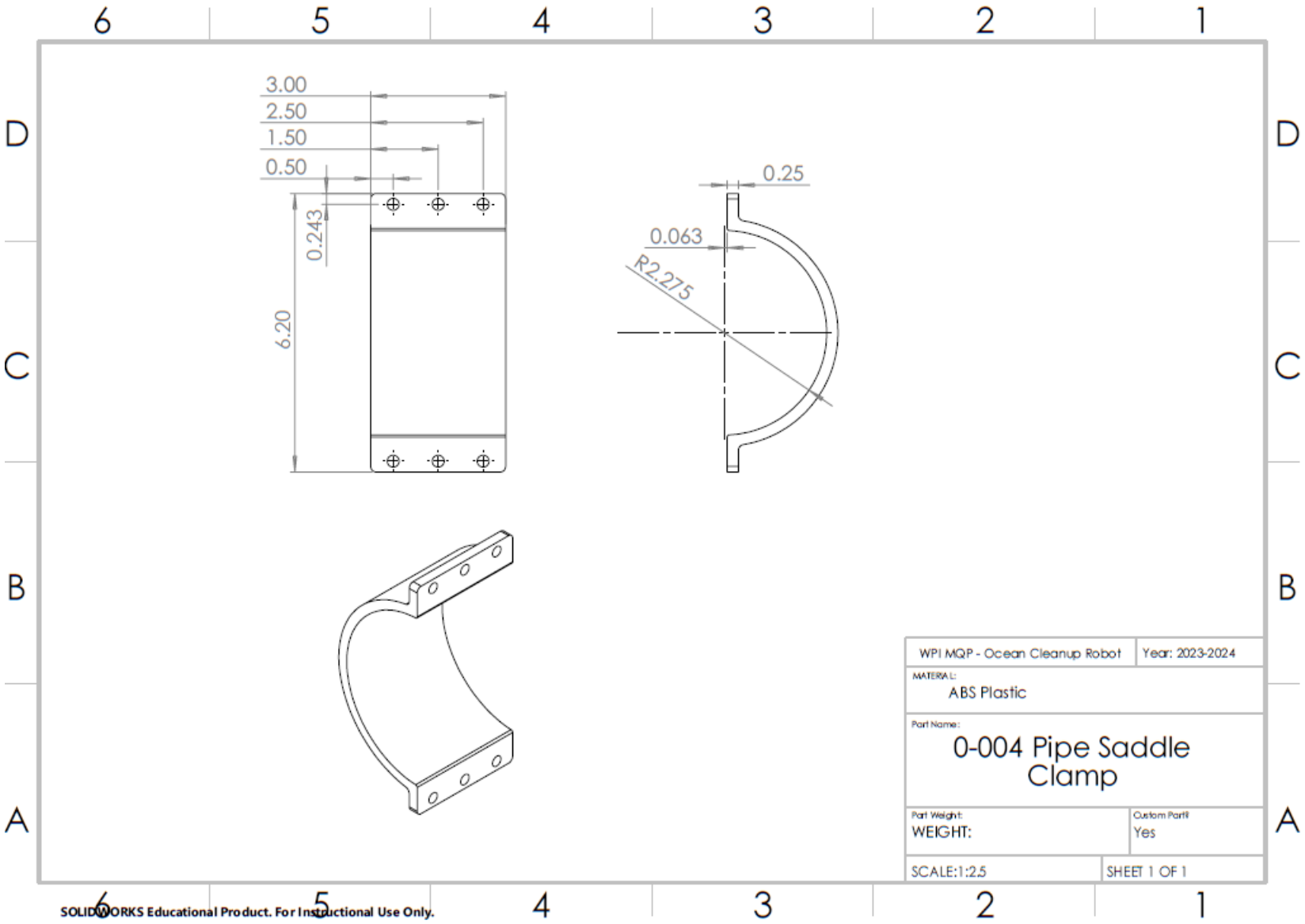
3.00
2.50
1.50
0.50
0.243
6.20
0.25
0.063
R2.275
WPI MQP - Ocean Cleanup Robot
Year: 2023-2024
MATERIAL:
ABS Plastic
Part Name:
0-004 Pipe Saddle Clamp
Part Weight:
WEIGHT:
Custom Part?
Yes
SCALE:1:2.5
SHEET 1 OF 1
SOLIDWORKS Educational Product. For Instructional Use Only.

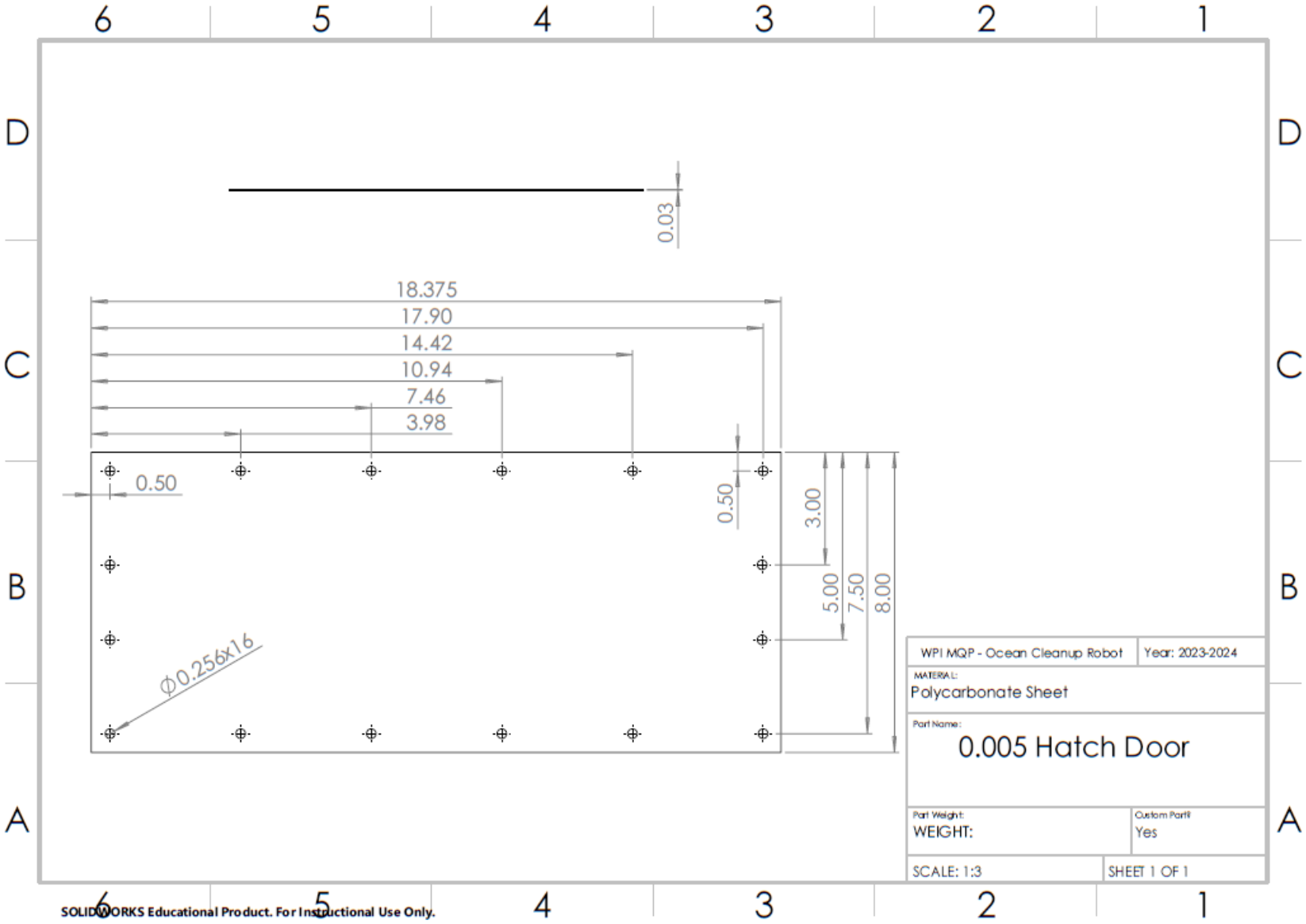
6
5
4
3
2
1
D
C
B
A
0.03
18.375
17.90
14.42
10.94
7.46
3.98
0.50
0.50
3.00
5.00
7.50
8.00
Ø0.256x16
WPI MQP - Ocean Cleanup Robot
Year: 2023-2024
MATERIAL:
Polycarbonate Sheet
Part Name:
0.005 Hatch Door
Part Weight:
WEIGHT:
Custom Part?
Yes
SCALE: 1:3
SHEET 1 OF 1
SOLIDWORKS Educational Product. For Instructional Use Only.

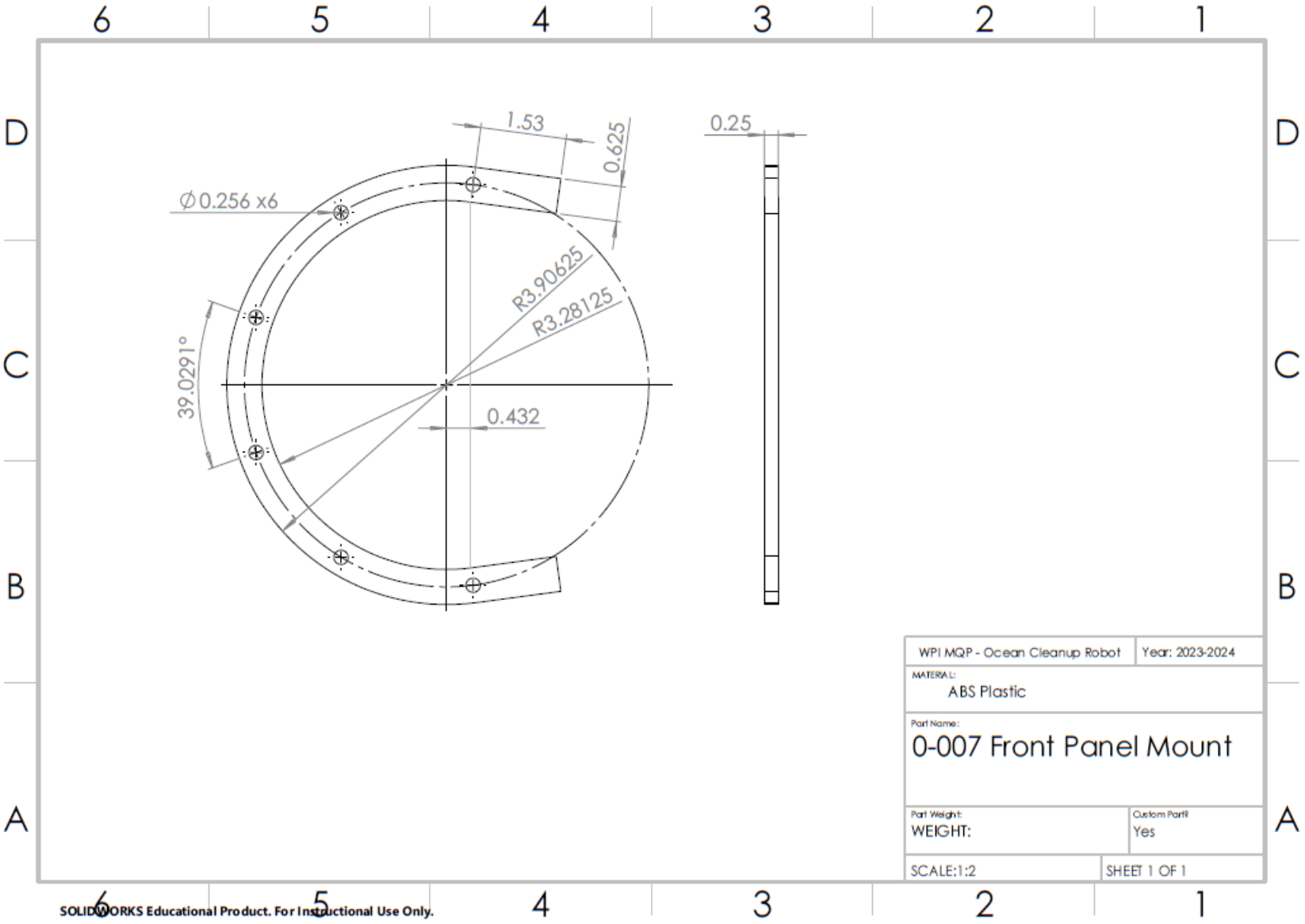
1.53
0.625
0.25
∅0.256 x6
R3.90625
R3.28125
39.0291°
0.432
WPI MQP - Ocean Cleanup Robot
Year: 2023-2024
MATERIAL:
ABS Plastic
Part Name:
0-007 Front Panel Mount
Part Weight:
WEIGHT:
Custom Part?
Yes
SCALE:1:2
SHEET 1 OF 1
SOLIDWORKS Educational Product. For Instructional Use Only.

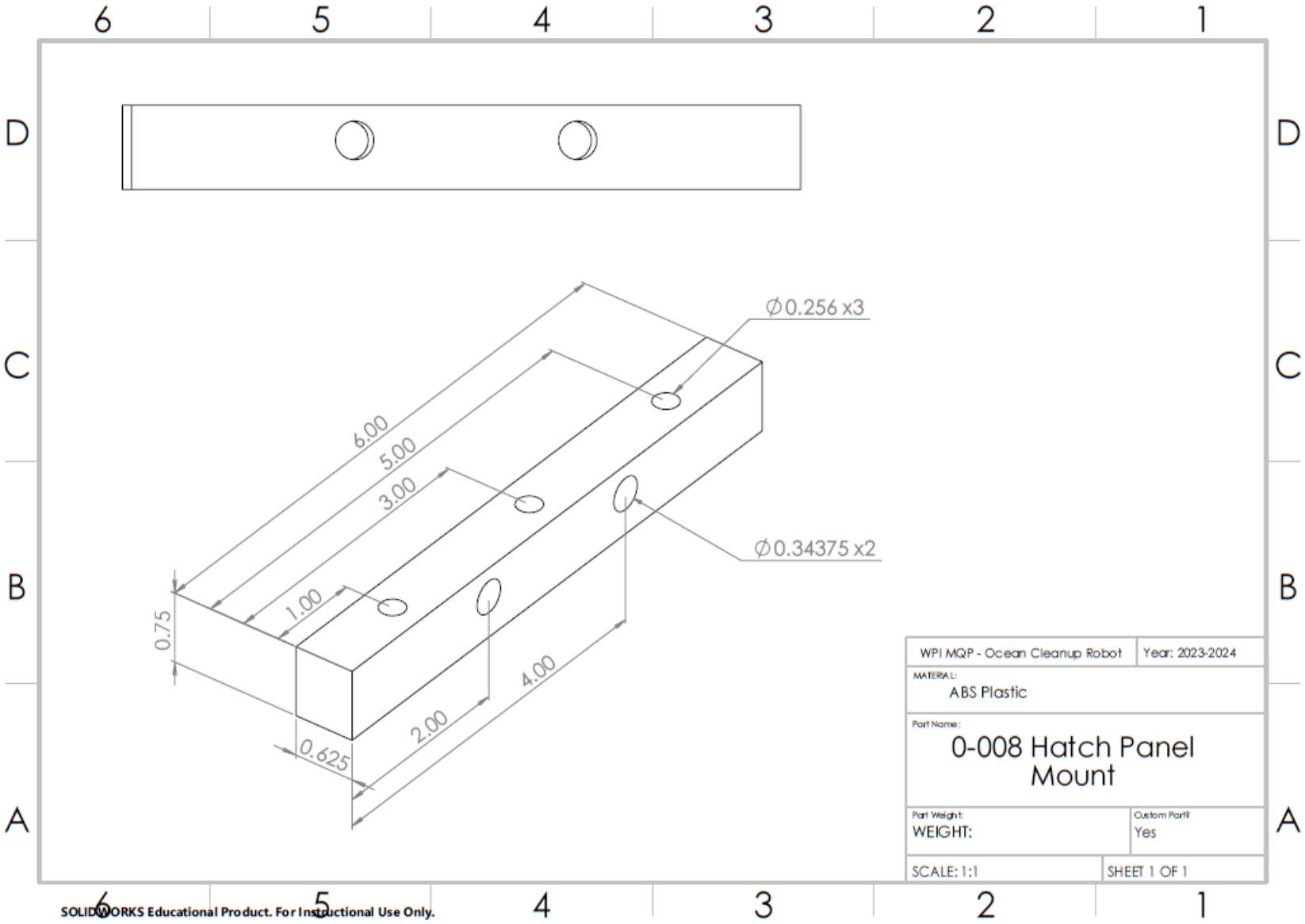
6
5
4
3
2
1
D
C
B
A
Ø0.256 x3
Ø0.34375 x2
6.00
5.00
3.00
1.00
0.75
0.625
2.00
4.00
WPI MQP - Ocean Cleanup Robot
Year: 2023-2024
MATERIAL:
ABS Plastic
Part Name:
0-008 Hatch Panel Mount
Part Weight:
WEIGHT:
Custom Part?
Yes
SCALE: 1:1
SHEET 1 OF 1
SOLIDWORKS Educational Product. For Instructional Use Only.

WPI MQP - Ocean Cleanup Robot
Year: 2023-2024
MATERIAL:
ABS Plastic
Part Name:
0-009 Back Panel Mount
Part Weight:
WEIGHT:
Custom Part?
Yes
SCALE: 1:2
SHEET 1 OF 1
R10.6437
R10.9562
R10.3312
0.625
15.145°
0.25
SOLIDWORKS Educational Product. For Instructional Use Only.

WPI MQP - Ocean Cleanup Robot
Year: 2023-2024
MATERIAL:
ABS Plastic
Part Name:
0-010 Bottom Panel Mount
Part Weight:
WEIGHT:
Custom Part?
Yes
SCALE: 1:1.5
SHEET 1 OF 1
Ø0.256 x3
1.00
3.50
6.00
7.00
0.25
0.625
SOLIDWORKS Educational Product. For Instructional Use Only.

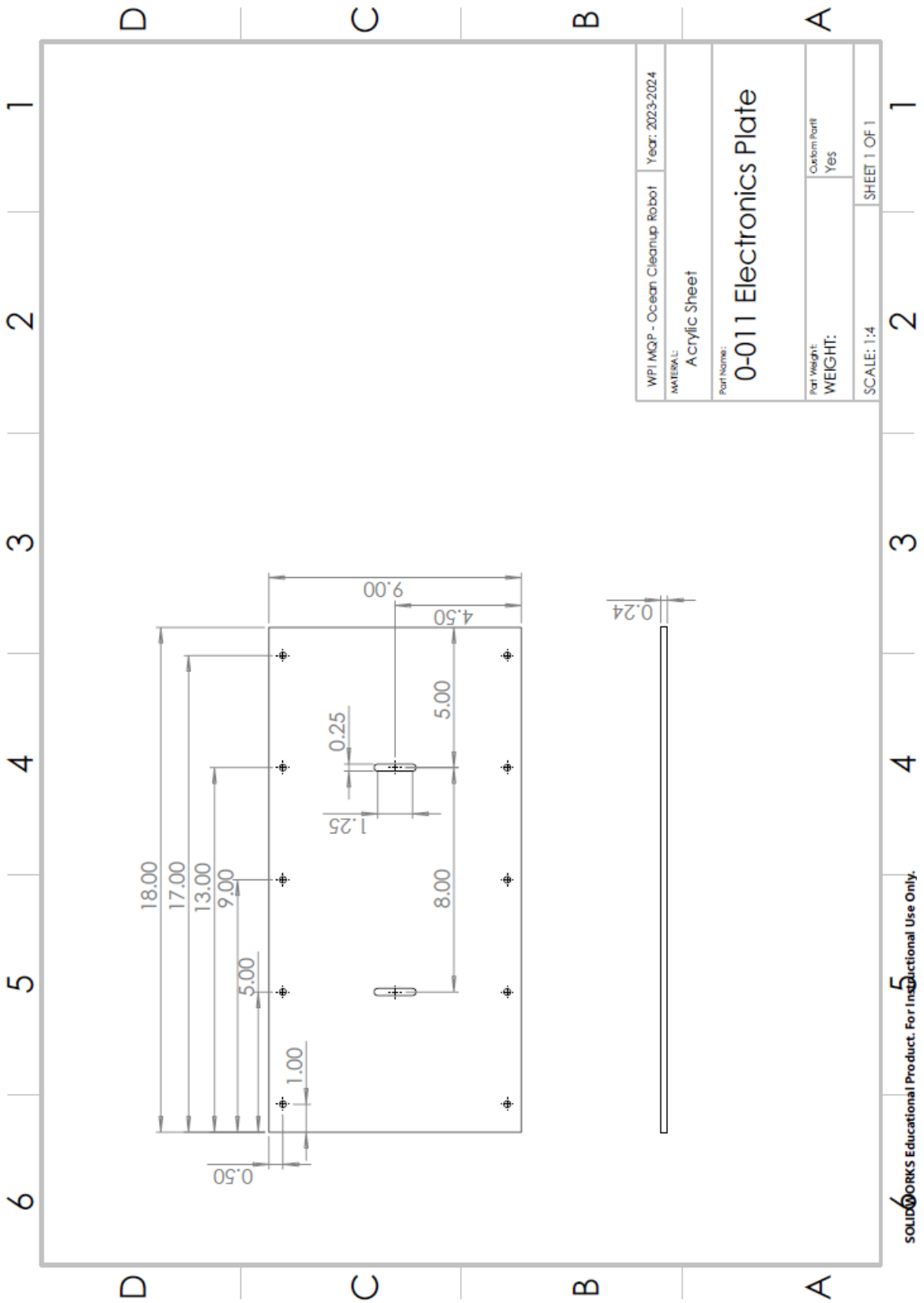
WPI MQP - Ocean Cleanup Robot
Year: 2023-2024
MATERIAL:
Acrylic Sheet
Part Name:
0-011 Electronics Plate
Part Weight:
WEIGHT:
Custom Part?
Yes
SCALE: 1:4
SHEET 1 OF 1
9.00
4.50
5.00
0.25
1.25
8.00
18.00
17.00
13.00
9.00
5.00
1.00
0.50
0.24
SOLIDWORKS Educational Product. For Instructional Use Only.

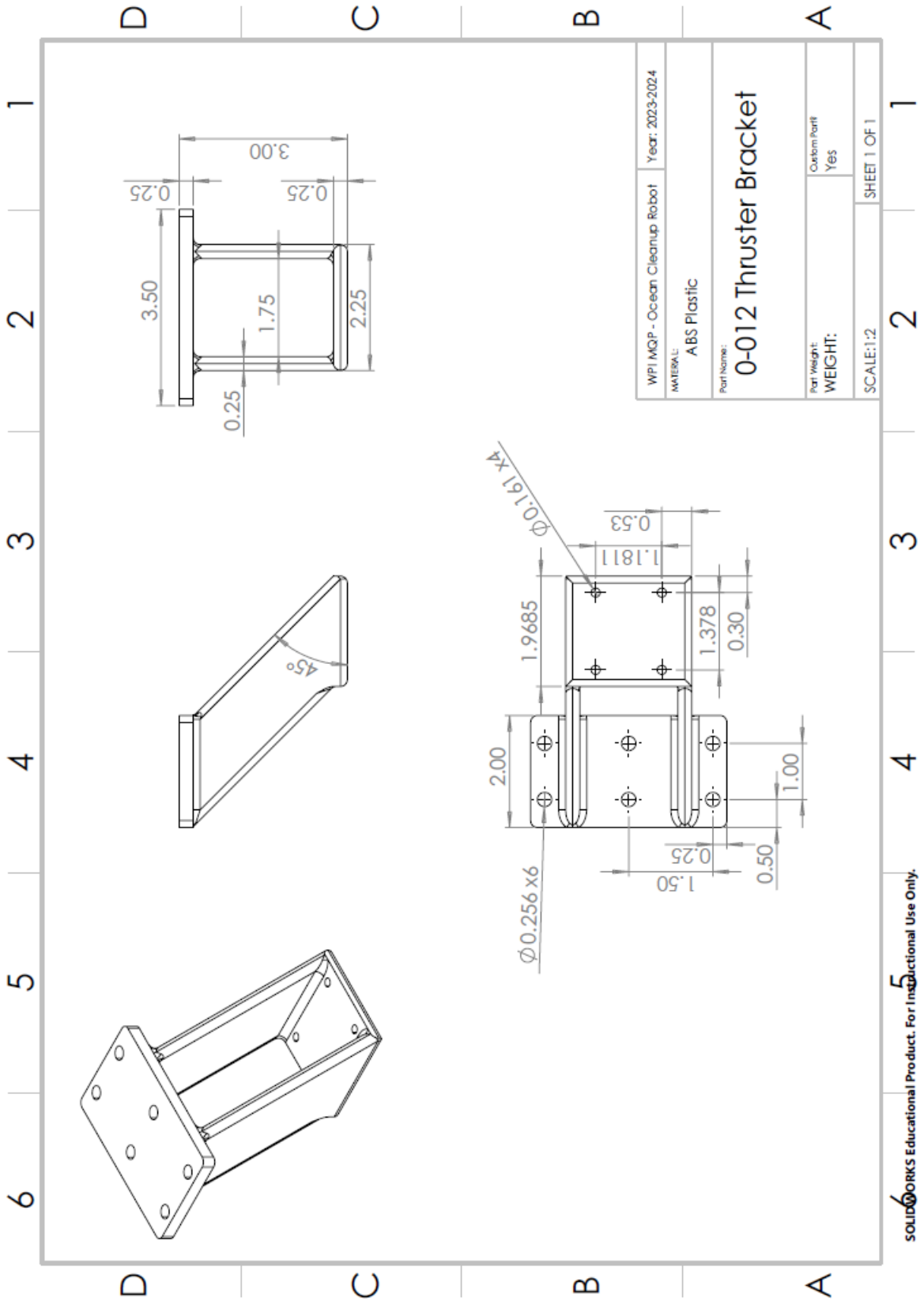
WPI MQP - Ocean Cleanup Robot
Year: 2023-2024
MATERIAL:
ABS Plastic
Part Name:
0-012 Thruster Bracket
Part Weight:
WEIGHT:
Custom Part#
Yes
SCALE:1:2
SHEET 1 OF 1
3.00
0.25
0.25
3.50
1.75
2.25
0.25
45°
4x Ø0.191
0.53
1.1811
1.9685
1.378
0.30
2.00
1.00
0.25
1.50
0.50
Ø0.256 x6
SOLIDWORKS Educational Product. For Instructional Use Only.

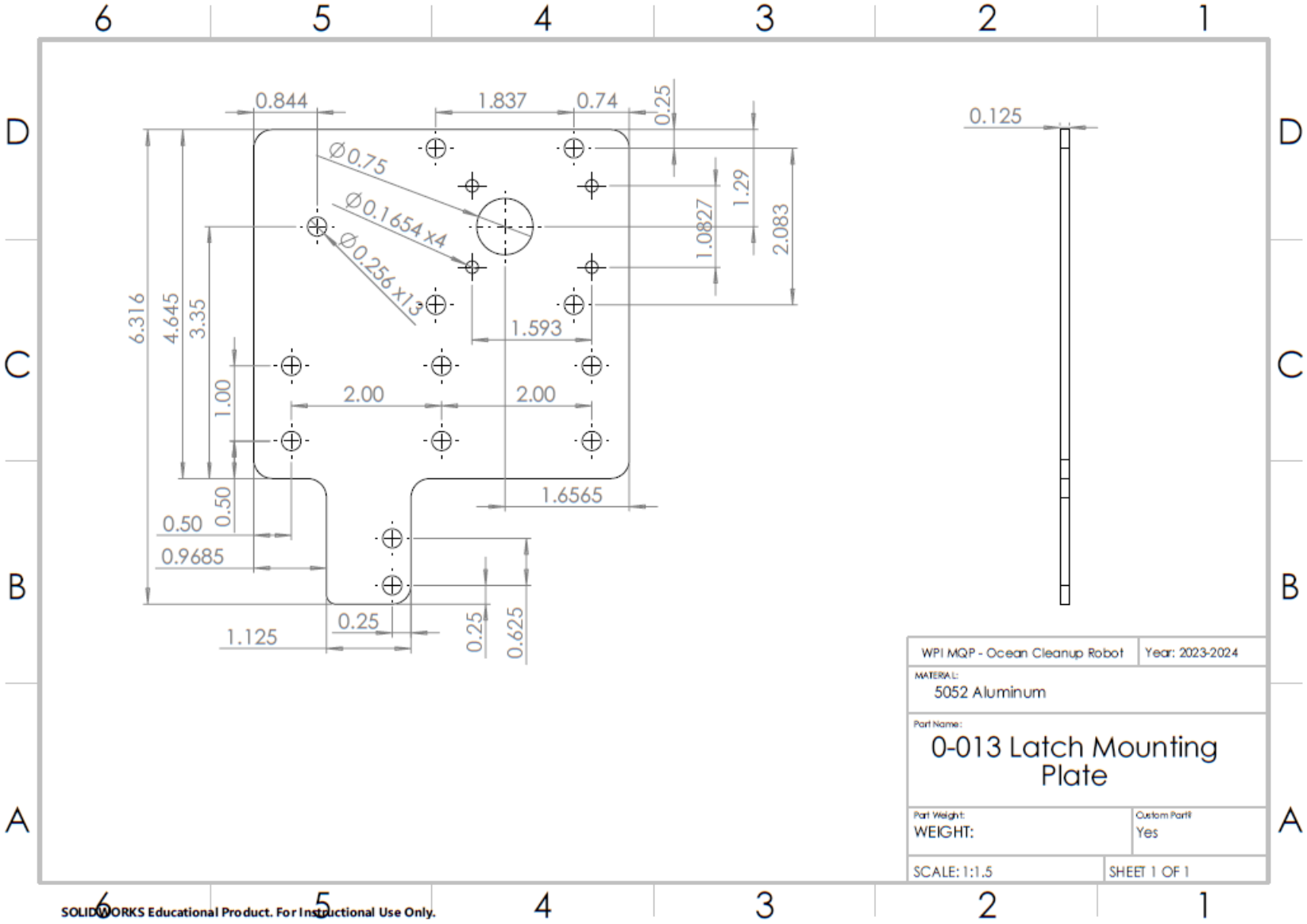
0.844
1.837
0.74
0.25
Ø0.75
Ø0.1654 x4
Ø0.256 x13
1.29
1.0827
2.083
6.316
4.645
3.35
1.00
0.50
0.50
1.593
2.00
2.00
1.6565
0.9685
0.25
1.125
0.25
0.625
0.125
WPI MQP - Ocean Cleanup Robot
Year: 2023-2024
MATERIAL:
5052 Aluminum
Part Name:
0-013 Latch Mounting Plate
Part Weight:
WEIGHT:
Custom Part?
Yes
SCALE: 1:1.5
SHEET 1 OF 1
SOLIDWORKS Educational Product. For Instructional Use Only.

1.125
0.625
0.25
1.125
0.875
Ø0.256 x2
0.75
0.625
Ø0.25
Ø0.25
WPI MQP - Ocean Cleanup Robot
Year: 2023-2024
MATERIAL:
ABS Plastic
Part Name:
0-014 Latch Lock
Part Weight:
WEIGHT:
Custom Part?
Yes
SCALE:2:1
SHEET 1 OF 1
SOLIDWORKS Educational Product. For Instructional Use Only.

WPI MQP - Ocean Cleanup Robot
Year: 2023-2024
MATERIAL:
ABS Plastic
Part Name:
0-015 Gear Spacer
Part Weight:
WEIGHT:
Custom Part?
Yes
SCALE:2:1
SHEET 1 OF 1
0.1875
Φ0.256
Φ0.15
SOLIDWORKS Educational Product. For Instructional Use Only.

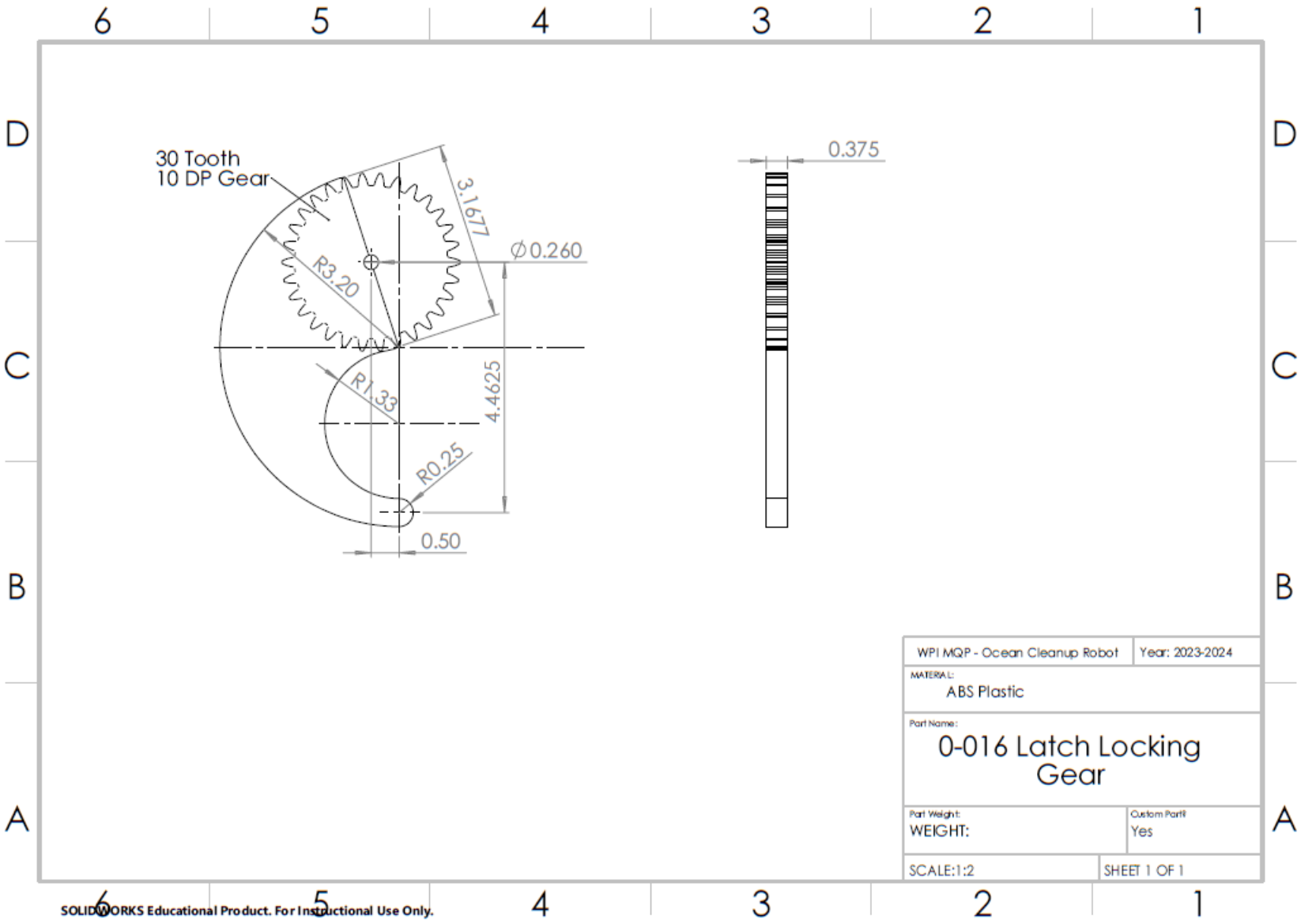
30 Tooth
10 DP Gear
3.1677
∅0.260
R3.20
R1.33
4.4625
R0.25
0.50
0.375
WPI MQP - Ocean Cleanup Robot
Year: 2023-2024
MATERIAL:
ABS Plastic
Part Name:
0-016 Latch Locking Gear
Part Weight:
WEIGHT:
Custom Part?
Yes
SCALE:1:2
SHEET 1 OF 1
SOLIDWORKS Educational Product. For Instructional Use Only.

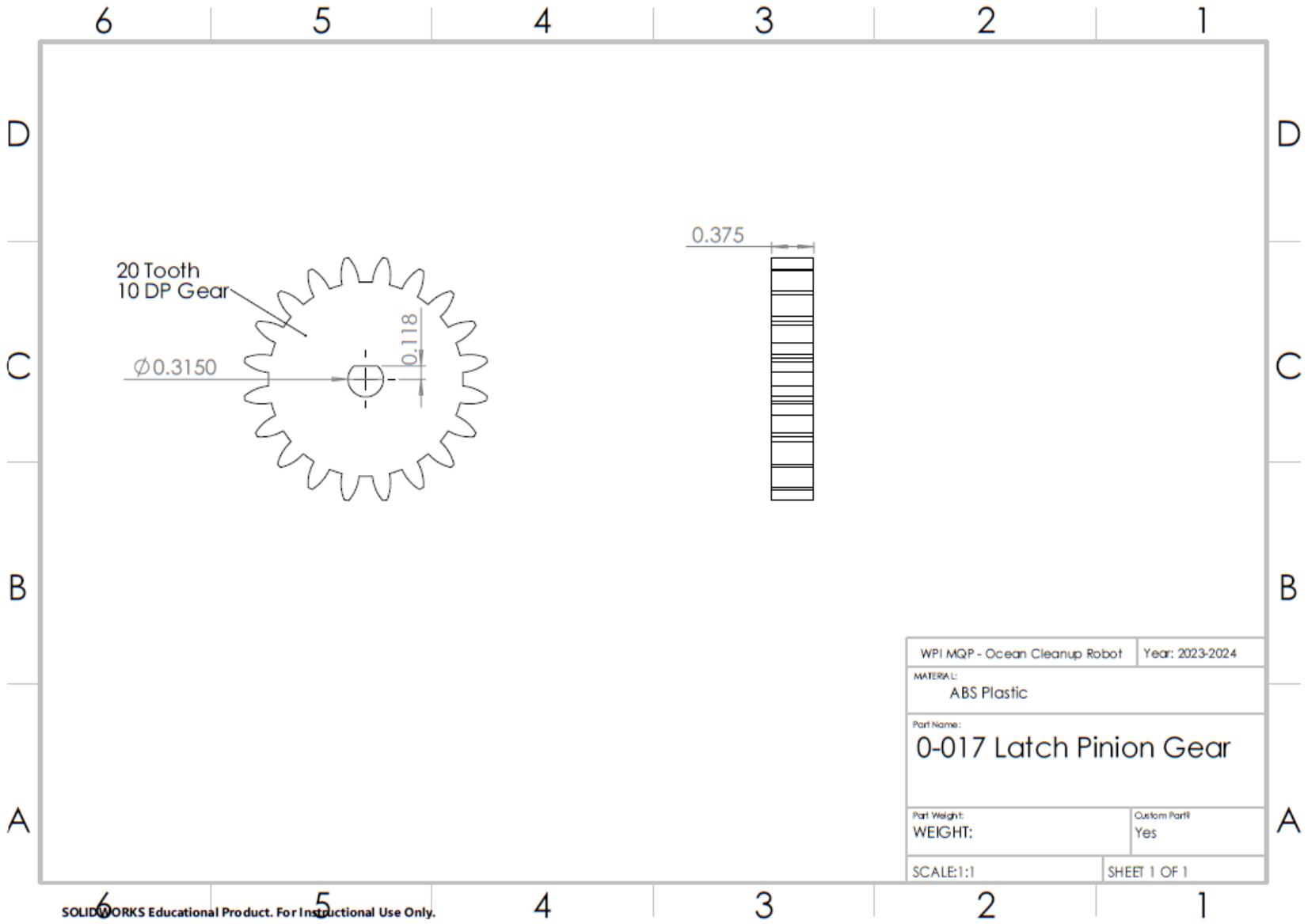
6
5
4
3
2
1
D
C
B
A
20 Tooth
10 DP Gear
∅0.3150
0.118
0.375
WPI MQP - Ocean Cleanup Robot
Year: 2023-2024
MATERIAL:
ABS Plastic
Part Name:
0-017 Latch Pinion Gear
Part Weight:
WEIGHT:
Custom Part?
Yes
SCALE:1:1
SHEET 1 OF 1
SOLIDWORKS Educational Product. For Instructional Use Only.

WPI MQP - Ocean Cleanup Robot
Year: 2023-2024
MATERIAL:
ABS Plastic
Part Name:
0-018 Pinion Spacer
Part Weight:
WEIGHT:
Custom Part?
Yes
SCALE:2:1
SHEET 1 OF 1
0.1875
Φ0.98A
Φ0.33465
SOLIDWORKS Educational Product. For Instructional Use Only.

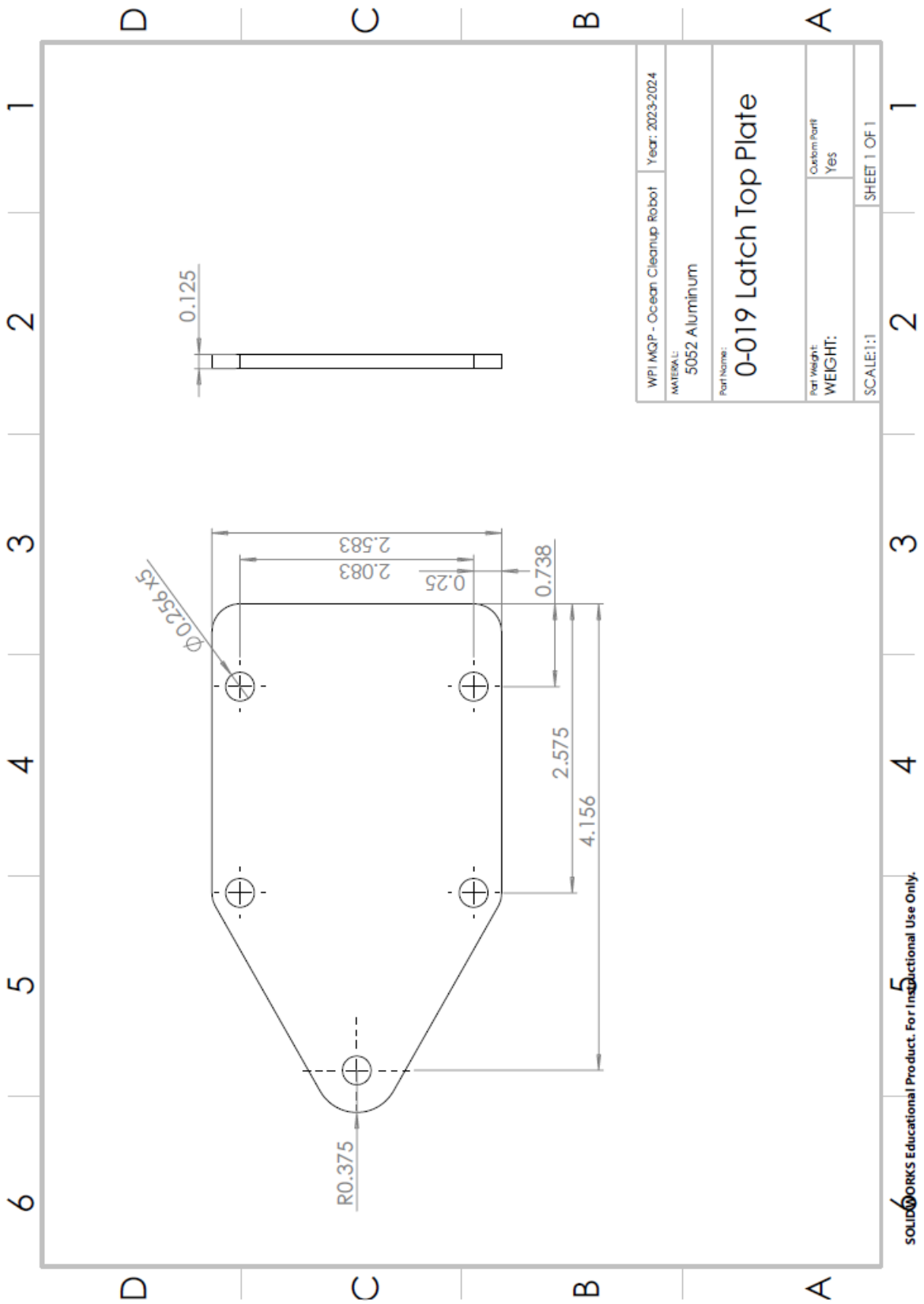
0.125
2.583
2.083
0.25
0.738
Ø0.256 x5
2.575
4.156
R0.375
WPI MQP - Ocean Cleanup Robot
Year: 2023-2024
MATERIAL:
5052 Aluminum
Part Name:
0-019 Latch Top Plate
Part Weight:
WEIGHT:
Custom Part?
Yes
SCALE:1:1
SHEET 1 OF 1
SOLIDWORKS Educational Product. For Instructional Use Only.

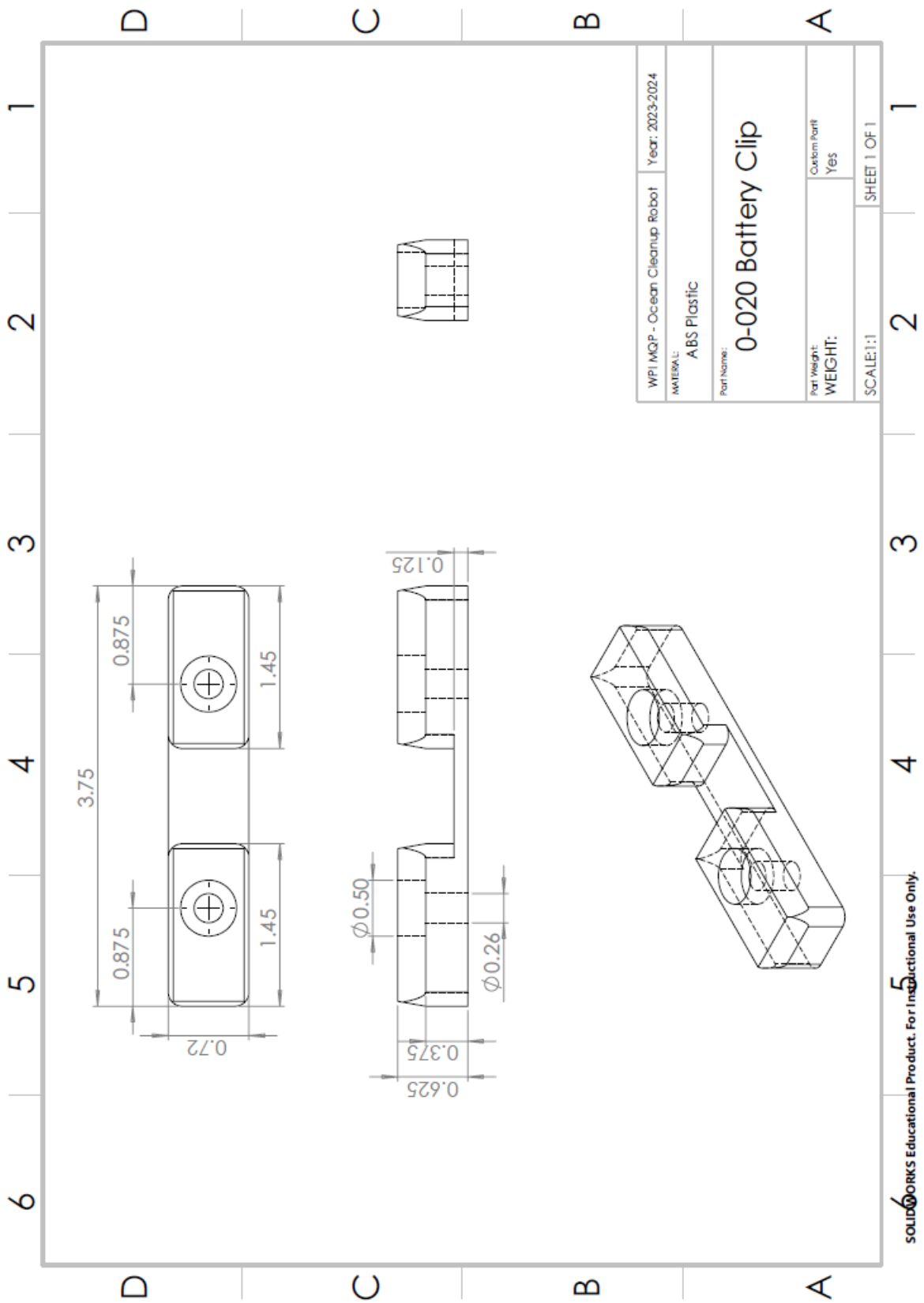
WPI MQP - Ocean Cleanup Robot
Year: 2023-2024
MATERIAL:
ABS Plastic
Part Name:
0-020 Battery Clip
Part Weight:
WEIGHT:
Custom Part?
Yes
SCALE:1:1
SHEET 1 OF 1
3.75
0.875
0.875
1.45
1.45
0.72
0.125
Ø0.50
Ø0.26
0.375
0.625
SOLIDWORKS Educational Product. For Instructional Use Only.

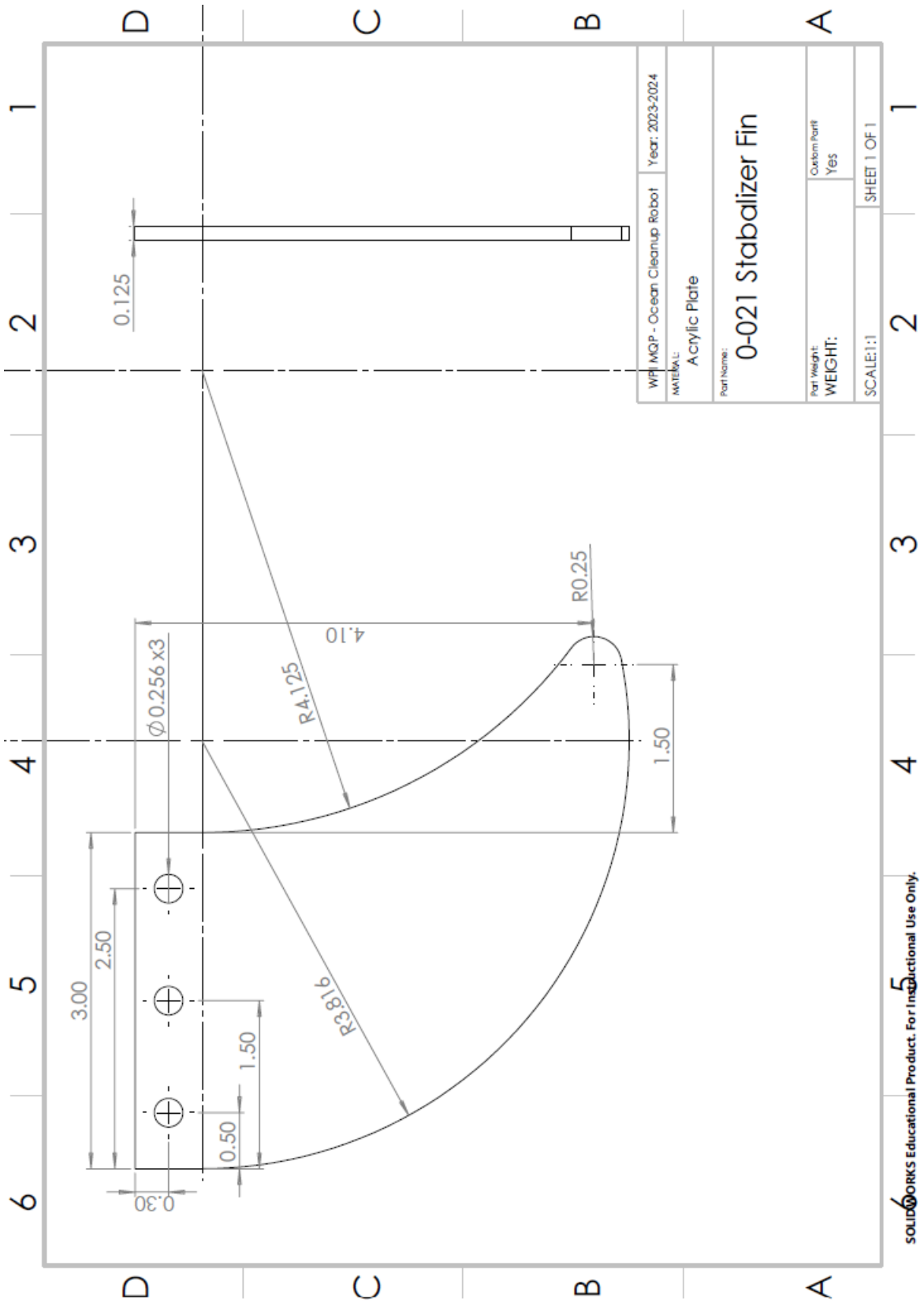
WPI MQP - Ocean Cleanup Robot
Year: 2023-2024
MATERIAL:
Acrylic Plate
Part Name:
0-021 Stabalizer Fin
Part Weight:
WEIGHT:
Custom Part?
Yes
SCALE:1:1
SHEET 1 OF 1
0.125
R0.25
4.10
R4.125
1.50
Ø0.256 x3
3.00
2.50
R3.816
1.50
0.50
0.30
SOLIDWORKS Educational Product. For Instructional Use Only.

0.125
3.00
2.50
1.50
0.50
ϕ0.256 x03
0.30
0.60
WPI MQP - Ocean Cleanup Robot
Year: 2023-2024
MATERIAL:
Acrylic Sheet
Part Name:
0-022 Clamp Spacer
Part Weight:
WEIGHT:
Custom Part?
Yes
SCALE:2:1
SHEET 1 OF 1
SOLIDWORKS Educational Product. For Instructional Use Only.

WPI MQP - Ocean Cleanup Robot
Year: 2023-2024
MATERIAL:
ABS Plastic
Part Name:
1-003 NOM 2in SCH 40
ABS Pipe
Part Weight:
WEIGHT:
Custom Part?
No
SCALE: 1:2
SHEET 1 OF 1
4.00
Φ2.375
Φ2.072
SOLIDWORKS Educational Product. For Instructional Use Only.

30.00
Ø4.50
Ø4.029
WPI MQP - Ocean Cleanup Robot
Year: 2023-2024
MATERIAL:
PVC Plastic
Part Name:
1-004 NOM 4in SCH 40
PVC Pipe
Part Weight:
WEIGHT:
Custom Part?
No
SCALE:1:10
SHEET 1 OF 1
SOLIDWORKS Educational Product. For Instructional Use Only.

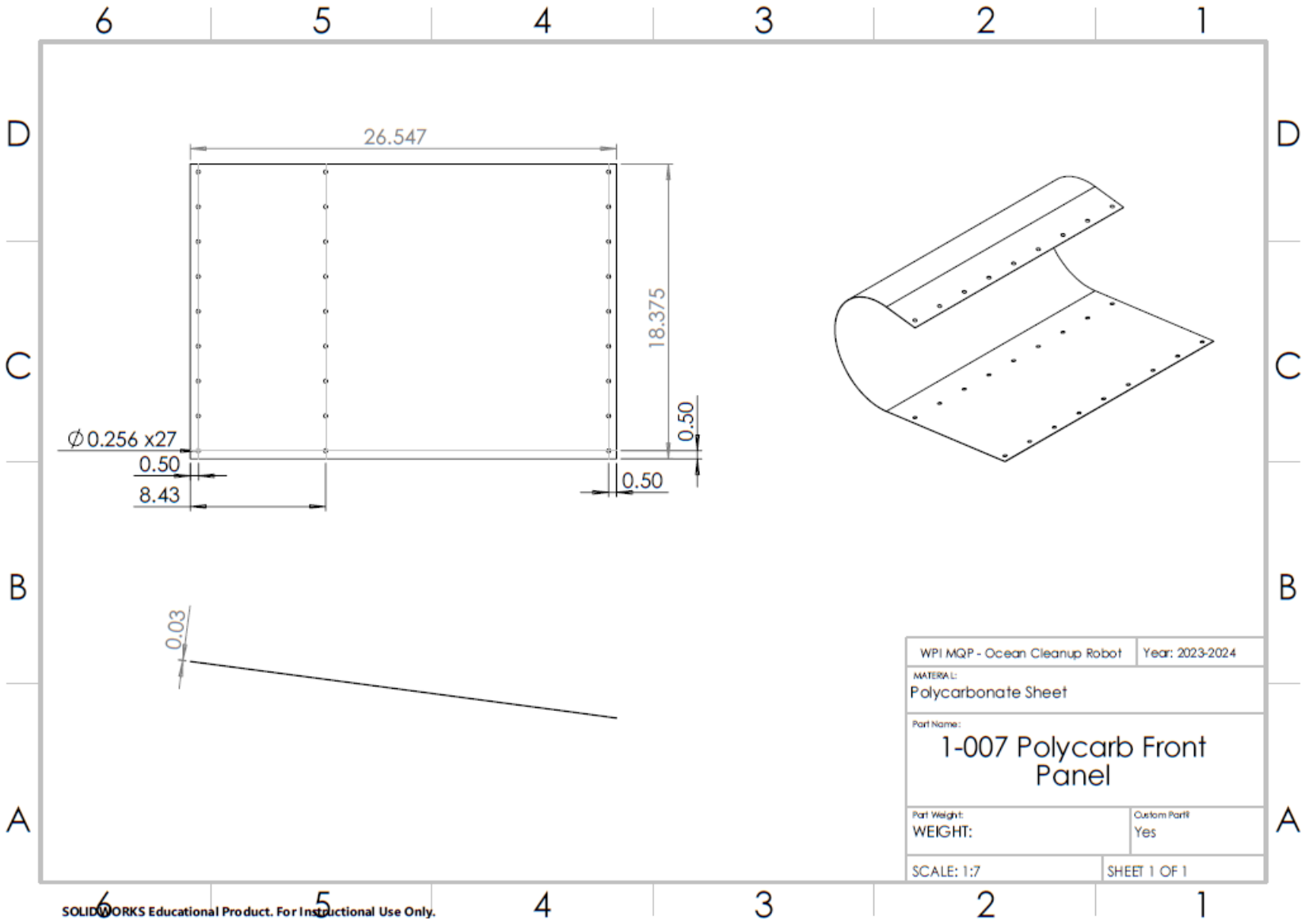
26.547
18.375
0.50
Ø0.256 x27
0.50
8.43
0.50
0.03
WPI MQP - Ocean Cleanup Robot
Year: 2023-2024
MATERIAL:
Polycarbonate Sheet
Part Name:
1-007 Polycarb Front Panel
Part Weight:
WEIGHT:
Custom Part?
Yes
SCALE: 1:7
SHEET 1 OF 1
SOLIDWORKS Educational Product. For Instructional Use Only.

WPI MQP - Ocean Cleanup Robot
Year: 2023-2024
MATERIAL:
Polycarbonate Sheet
Part Name:
1-008 Polycarb Back Panel
Part Weight:
WEIGHT:
Custom Part?
Yes
SCALE: 1:4
SHEET 1 OF 1
0.03
Ø0.256 x18
0.50
18.00
0.50
0.50
4.69
SOLIDWORKS Educational Product. For Instructional Use Only.

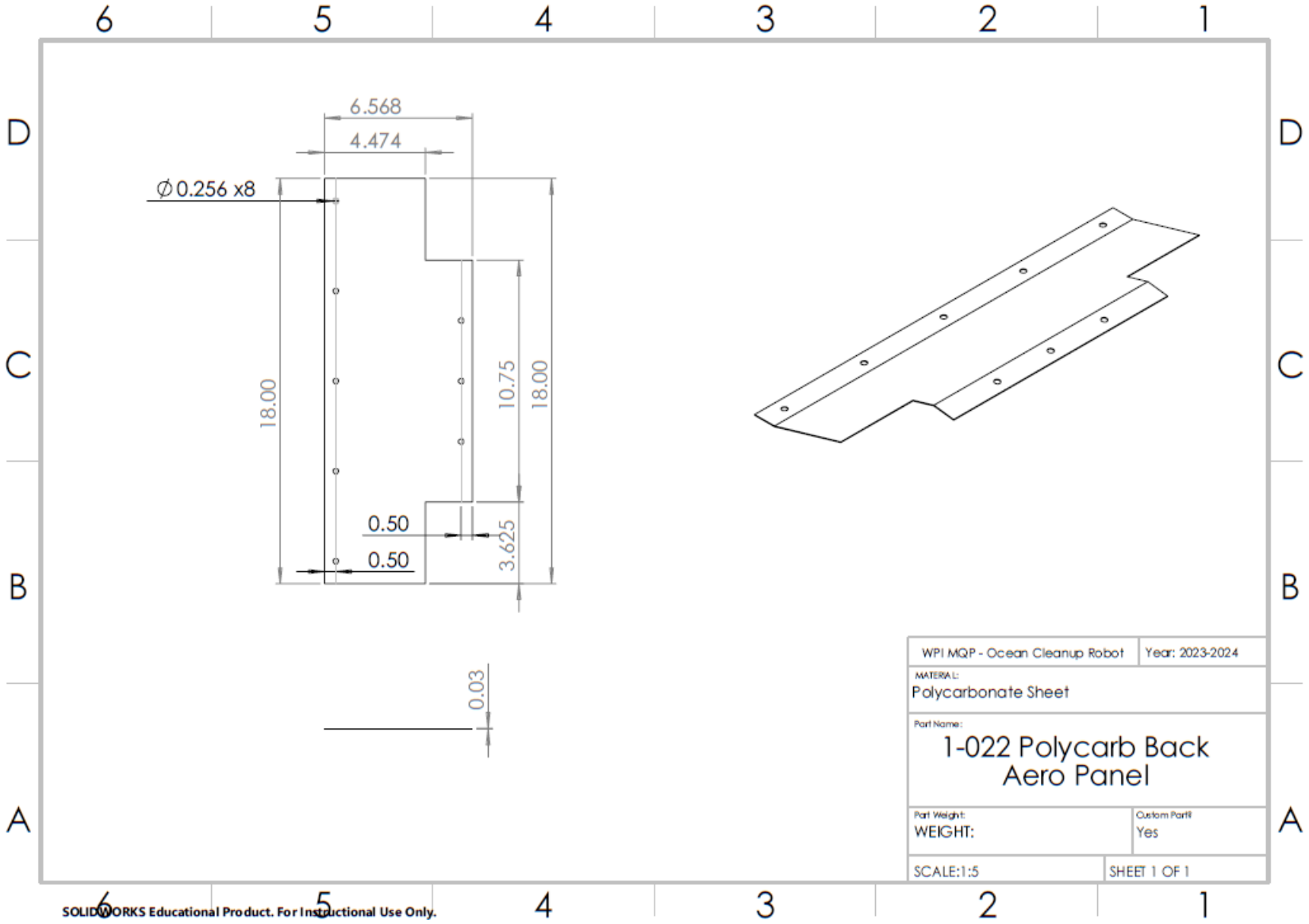
6.568
4.474
∅0.256 x8
18.00
10.75
18.00
0.50
0.50
3.625
0.03
WPI MQP - Ocean Cleanup Robot
Year: 2023-2024
MATERIAL:
Polycarbonate Sheet
Part Name:
1-022 Polycarb Back Aero Panel
Part Weight:
WEIGHT:
Custom Part?
Yes
SCALE:1:5
SHEET 1 OF 1
SOLIDWORKS Educational Product. For Instructional Use Only.

WPI MQP - Ocean Cleanup Robot
Year: 2023-2024
MATERIAL:
Polycarbonate Sheet
Part Name:
1-023 Polycarb Top Aero Plate
Part Weight:
WEIGHT:
Custom Part?
Yes
SCALE:1:2
SHEET 1 OF 1
1.00
1.00
0.50
6.561
Φ0.256 x4
4.875
0.50
0.03
SOLIDWORKS Educational Product. For Instructional Use Only.

Appendix F: Testing/Showcase Videos

All videos made during testing at the WPI pool and Lake Quinsigamond can be found in the following YouTube playlist.

https://www.youtube.com/playlist?list=PLpnt9k5azQSd18ZkP5zOOp6qlucLSuCHa